Whole transcriptome profiling of compartmentalized motoneurons

~

Globale Transkriptomanalyse von kompartimentierten Motoneuronen

Doctoral thesis for a doctoral degree

at the Graduate School of Life Sciences,

Julius-Maximilians-Universität Würzburg,

Section Neuroscience

submitted by

Lena Saal

from

Schweinfurt

Würzburg 2016

Submitted on:……………………………………………………………………

Members of the *Promotionskomitee*:

Chairperson: Prof. Dr. Paul Pauli

Primary Supervisor: Prof. Dr. Michael Sendtner

Supervisor (Second): Prof. Dr. Erich Buchner

Supervisor (Third): Prof. Dr. Utz Fischer

Date of Public Defence:………………………………………………….

Date of Receipt of Certificates:………………………………………

Table of contents

Abbreviations

3'UTR	3' untranslated region
ALS	Amyotrophic lateral sclerosis
BDNF	Brain-derived neurotrophic factor
cDNA	complementary DNA
CNTF	Ciliary neurotrophic factor
DMEM	Dulbecco's modified essential medium
DNA	Desoxyribonucleic acid
dNTPs	Desoxyribonucleosidtriphosphates
DRG	Dorsal root ganglia
DTT	Dithiothreitol
ES cells	Embryonic stem cells
fALS	Familiar amyotrohpic lateral sclerosis
FPKM	Fragments per kilobase of exon per million fragments
FUS	Fused in sarcoma
GAPDH	Glyceraldehyde-3-phosphate dehydrogenase
GO	Gene ontology
HBRR	Human brain reference RNA
HBSS	Hanks' balanced salt solution
HEK	Human embryonic kidney
hiPS cells	Human induced pluripotent stem cells
hnRNP R	heterogeneous nuclear ribonucleoprotein R
iCLIP	individual-nucleotide resolution crosslinking and immunoprecipitation
iPS cells	Induced pluripotent stem cells
kd	Knockdown
kDa	Kilodalton
KEGG	Kyoto Encyclopedia of Genes and Genomes
MALBAC	Multiple annealing and looping-based amplification cycles
MHC	Major histocompatibility complex
miRNA	MicroRNA
mRNA	messenger ribonucleic acid
NADPH	Nicotineamide adenine dinucleotide phosphate
NLS	Nuclear localization signal
nt	Nucleotides
PBS	Phosphate buffered saline
PCR	Polymerase chain reaction
PORN	Poly-DL-ornithine hydrobromide
qPCR	quantitative polymerase chain reaction
RBP	RNA-binding protein
RGG	Arginine and glycine rich domain
RNA	ribonucleic acid
RNA-Seq	RNA sequencing

Abbreviations

RNP	Ribonucleoprotein
ROS	Reactive oxygen species
RRM	RNA recognition motif
rRNA	ribosomal ribonucleic acid
sALS	sporadic amyotrophic lateral sclerosis
SMA	Spinal muscular atrophy
SMN	Survival of motor neuron
snRNP	Small nucear ribonucleoprotein particle
SOD1	Superoxide dismutase 1
TDP-43	TAR DNA-binding protein-43
TTX	Tetrodotoxin

Summary

Spinal muscular atrophy and amyotrophic lateral sclerosis are the two most common devastating motoneuron diseases. The mechanisms leading to motoneuron degeneration are not resolved so far, although different hypotheses have been built on existing data. One possible mechanism is disturbed axonal transport of RNAs in the affected motoneurons. The underlying question of this study was therefore to characterize changes in transcript levels of distinct RNAs in cell culture models of spinal muscular atrophy and amyotrophic lateral sclerosis, especially in the axonal compartment of primary motoneurons.

To investigate this in detail we first established compartmentalized cultures of primary mouse motoneurons. Subsequently, total RNA of both compartments was extracted separately and either linearly amplified and subjected to microarray profiling or whole transcriptome amplification followed by RNA-Sequencing was performed. To make the whole transcriptome amplification method suitable for compartmentalized cultures, we adapted a double-random priming strategy. First, we applied this method for initial optimization onto serial dilutions of spinal cord RNA and later on to the compartmentalized motoneurons.

Analysis of the data obtained from wildtype cultures already revealed interesting results. First, the RNA composition of axons turned out to be highly similar to the somatodendritic compartment. Second, axons seem to be particularly enriched for transcripts related to protein synthesis and energy production. In a next step we repeated the experiments by using knockdown cultures. The proteins depleted hereby are Smn, Tdp-43 and hnRNP R. Another experiment was performed by knocking down the non-coding RNA 7SK, the main interacting RNA of hnRNP R. Depletion of Smn led to a vast number of deregulated transcripts in the axonal and somatodendritic compartment. Transcripts downregulated in the axons upon Smn depletion were especially enriched for GOterms related to RNA processing and encode proteins located in neuron projections including axons and growth cones. Strinkingly, among the upregulated transcripts in the somatodendritic compartment we mainly found MHC class I transcripts suggesting a potential neuroprotective role. In contrast, although knockdown of Tdp-43 also revealed a large number of

downregulated transcripts in the axonal compartment, these transcripts were mainly associated with functions in transcriptional regulation and RNA splicing. For the hnRNP R knockdown our results were again different. Here, we observed downregulated transcripts in the axonal compartment mainly associated with regulation of synaptic transmission and nerve impulses. Interestingly, a comparison between deregulated transcripts in the axonal compartment of both hnRNP R and 7SK knockdown presented a significant overlap of several transcripts suggesting some common mechanism for both knockdowns.

Thus, our data indicate that a loss of disease-associated proteins involved in axonal RNA transport causes distinct transcriptome alterations in motor axons.

Zusammenfassung

Spinale Muskelatrophie und Amyotrophe Lateralsklerose zählen zu den beiden häufigsten und schwersten Motoneuronerkrankungen. Der zugrunde liegende Mechanismus beider Krankheiten ist bis heute nicht geklärt, dennoch werden verschiedene Theorien diskutiert. Ein möglicher Grund ist ein gestörter axonaler Transport von RNAs in den betroffenen Motoneuronen. Daraus folgernd ergab sich die zugrunde liegende Frage dieser Arbeit, ob Veränderungen in den Transkriptleveln bestimmter RNAs unter krankheitsähnlichen Bedingungen vor allem im axonalen Kompartiment von primären Maus-Motoneuronen beobachtet werden können.

Um die Fragestellung genauer zu untersuchen, etablierten wir zuerst kompartimentierte Kulturen von primären Motoneuronen. Darauffolgend haben wir die totale RNA aus beiden Kompartimenten separat extrahiert und entweder diese linear amplifiziert und zur Microarrayanalyse gegeben oder wir führten eine Amplifikation des kompletten Transkriptoms mit anschließender RNA-Sequenzierung durch. Um die Amplifikation des kompletten Transkriptoms auch für die kompartimentierten Kulturen geeignet zu machen, verwendeten wir eine double-random priming Strategie und haben diese entsprechend angepasst. Zuerst wendeten wir die Methode an Serienverdünnungen von RNA aus dem Rückenmark an, um die Methode zu optimisieren. Später benutzten wir die Methode ebenfalls für kompartimentierte Motoneurone.

Schon die Analyse der Wildtyp-Daten lieferte interessante Ergebnisse. Erstens, die Zusammensetzung der RNA in Axonen war höchst ähnlich zu der im somatodendritischen Kompartiment. Zweitens, in Axonen scheinen speziell Transkripte angereichert zu sein, welche mit Proteinsynthese und Energieproduktion in Verbindung stehen. In einem nächsten Schritt wurden dann die Experimente unter Verwendung von Knockdown-Kulturen wiederholt. Die Proteine, die dabei vermindert wurden waren Smn, Tdp-43 und hnRNP R. Ein weiteres Experiment wurde durchgeführt indem die nicht-codierende RNA 7SK verringert wurde. Die Depletion von Smn führte zu einer hohen Anzahl an deregulierten Transkripten sowohl im axonalen, als auch im somatodendritischen Kompartiment. Transkripte, die im

axonalen Kompartiment nach Smn Depletion verringert waren, waren überwiegend für GOTerms angereichert, welche mit RNA Prozessierung in Verbindung stehen oder welche Proteine codieren, die in neuronalen Fortsätzen, einschließlich Axon und Wachstumskegel lokalisiert sind. Bemerkenswert ist, dass wir unter den hochregulierten Transkripten im somatodendritischen Kompartiment überwiegend MHC Klasse I Transkripte gefunden haben. Dies könnte eine mögliche neuroprotektive Rolle dieser Transkripte annehmen lassen. Im Gegensatz zu den Ergebnissen beim Smn Knockdown fanden wir beim Tdp-43 Knockdown ebenfalls eine große Anzahl an herunterregulierten Transkripten im axonalen Kompartiment, diese sind allerdings überwiegend mit Funktionen in der Transkriptionsregulierung und beim RNA Splicing assoziiert. Die Ergebnisse des hnRNP R Knockdowns waren ebenfalls unterschiedlich. Bei diesem fanden wir die herunteregulierten Transkripte im axonalen Kompartiment überwiegend mit einer Regulierung der synaptischen Übertragung sowie mit Nervenimpulsen assoziiert. Interessanterweise zeigte ein Vergleich der deregulierten Transkripte sowohl im axonalen Kompartiment vom hnRNP R Knockdown, als auch vom 7SK Knockdown eine signifikante Übereinstimmung mehrerer Transkripte. Dies lässt einen teilweise gemeinsamen Mechanismus für beide Genprodukte vermuten.

Somit deuten unsere Daten darauf hin, dass ein Verlust von krankheitsassoziierten Proteinen, die eine Rolle beim axonalen RNA-Transport spielen, zu verschiedenen Transkriptomveränderungen in Axonen von Motoneuronen führt.

1 Introduction

1.1 Motoneuron diseases

Motoneuron diseases are serious and so far incurable forms of progressive neurodegeneration with two major variants. The first one is known as amyotrophic lateral sclerosis (ALS), the second is spinal muscular atrophy (SMA). Both diseases are leading to death within few years and no effective treatment exists so far. There are major differences with respect to heredity and the types of motoneurons affected by each disease.

1.1.1 Amyotrophic lateral sclerosis (ALS)

Amyotrophic lateral sclerosis (ALS) was first described by Charcot in 1874. The disease has an incidence of approximately 2 per 100000 individuals per year and accounts therefore for the most prevalent degenerative motoneuron disease affecting the upper as well as the lower motoneurons. Despite some exceptions the disease mostly starts at an age of 50-60, more commonly affecting men than women (Sendtner 2014). The average survival is estimated to be approximately 3 years from symptom onset, although some milder forms of the disease exist (Chen et al., 2013). 90% of ALS patients are suffering from a sporadic form of the disease (sALS) while only 5-10% of ALS patients dispose a positive family history (fALS) with a predominant autosomal-dominant inheritance (Andersen and Al-Chalabi 2011). The so far identified genetic defects underlying fALS (Mancuso and Navarro 2015) point to multifactorial pathogenic processes as these defects are quite heterogeneous on a genetic basis.

One common form of fALS relies on an autosomal dominant mutation in the Cu^{2+}/Zn^{2+}-dependent superoxide dismutase 1 (SOD-1) gene and accounts for about 10-20% of fALS (Rosen et al., 1993). To date, more than 50 different mutations have been identified in this gene although there seems to be no correlation between a specific mutation in the SOD-1 gene and disease onset or severity (Andersen and Al-Chalabi 2011). Furthermore there seems to be no difference in the clinical appearance between patients with SOD-1 mutations and sALS patients.

The predominant role of the SOD-1 protein is the detoxification of superoxide radicals from the cell thereby preventing the generation of hydroxyl radicals reacting with a variety of molecules. Interestingly, not only fALS patients with mutations in the SOD-1 gene but patients with ALS in general show elevated markers of free radical damage in their cerebrospinal fluid, serum and urine (Smith et al., 1998, Simpson et al., 2004). Another aspect which should be taken into account is the fact that only the transgenic overexpression of mutant SOD-1 causes severe forms of the disease (Gurney et al., 1994) whereas a knockout of the SOD-1 gene is not leading to any motoneuron disease (Reaume et al., 1996). As furthermore not all identified mutations of SOD-1 in fALS involve a loss of the enzymatic activity of SOD-1 this points to other pathogenic mechanisms. Important to mention are here the findings that mutant SOD-1 also acts on cell types not primarily affected in fALS like microglia and astrocytes. For example, mutant SOD-1 increases NADPH oxidase-mediated superoxide production in microglia (Harraz et al., 2008) leading to a prolonged reactive oxygen species (ROS) production. Astrocytes on the contrary seem to release mutant SOD-1 interacting with chromogranin (Urushitani et al., 2006). Furthermore, chimeric mice expressing mutant SOD-1 only in astrocytes show clear signs of motoneuron degeneration (Clement et al., 2003). Additionally, in cell culture it has been shown that astrocytes expressing mutant SOD-1 exert toxic effects on cocultured embryonic primary mouse motoneurons (Nagai et al., 2007) or human stem cell-derived motoneurons (Di Giorgio et al., 2008). All these findings are therefore leading to the assumption that also non-neuronal cells expressing mutant forms of SOD-1 contribute to the disease by influencing motoneurons negatively.

Another idea which tries to explain the processes in ALS caused by mutant SOD-1 is the idea of mitochondrial dysfunction and disturbed respiratory chain activity. This idea is based on the observation of protein inclusions in motoneurons and other neuronal celltypes. Strikingly, these inclusions do not include TDP-43 protein and thereby differ from inclusions normally observed in the most cases of sALS and other forms of fALS (Maekawa et al., 2009). However, some of these protein aggregates including the mutant SOD-1 protein aggregate with mitochondria could contribute to a possible mitochondria dysfunction. Furthermore an impaired calcium buffering capacity could be observed in mitochondria isolated from neural tissues of SOD-1 mutant mice (Damiano et al., 2006, Grosskreutz et al., 2010). Interestingly, these

observations occurred in a presymptomatic disease stage in mouse models possibly contributing to a defective axonal transport of mitochondria and membrane-bound organelles (De Vos et al., 2007) and therefore leading to the generally observed dying-back axonopathy in ALS.

As mentioned above, fALS caused by mutant SOD-1 is not the only form of ALS displaying protein inclusions. For a long time it was suspected that also alterations in the RNA metabolism can contribute to ALS although this became more concrete only in the last few years. Thus, one of the most important findings supporting this hypothesis was the discovery of TAR DNA-binding protein-43 (TDP-43) as a major component of ubiquitin-positive cellular inclusions (Neumann et al., 2006). These inclusions are mainly located in nuclei and soma of neurons appearing as threads, skeins or compact bodies. As such inclusions have also been found in frontotemporal lobar dementia (Buratti and Baralle 2008), Huntington's disease (Schwab et al., 2008), Alzheimer's disease and dementia with Lewy body inclusions (Higashi et al., 2007) this points to such inclusions as a hallmark for neurodegenerative diseases.

Until today the function of TDP-43 in the cell is not fully understood. Basically, the protein belongs to the hnRNP family (Krecic and Swanson 1999) possessing two RNA recognition motifs (RRM1 and RRM2) and a C-terminal glycine-rich domain. Therefore, TDP-43 resembles many other RNA-binding proteins like fused in sarcoma (FUS) or heterogeneous nuclear ribonucleoprotein R (hnRNP R).

After TDP-43 was identified as a major component of proteinaceous inclusions in ALS and other neurodegenerative diseases the search for possible mutations in the *TDP-43* gene started. Indeed, approximately 4% of patients suffering from fALS and 1.5% of patients with sALS dispose mutations in the *TDP-43* gene (Rutherford et al., 2008, Mackenzie et al., 2010). All of the so far identified mutations associated with fALS are autosomal dominant encoding mostly a missense mutation within the C-terminal domain encoding the glycine-rich domain (Pesiridis et al., 2009). Interestingly, this domain displays a part of the protein which is important for protein-protein interactions and does not play a role in RNA binding.

Even of high interest is the fact that not full-length TDP-43 but a truncated form of the protein, a 20-25 kDa C-terminal fragment, is found in the highly ubiquitinylated and phosphorylated inclusions (Pesiridis et al., 2011). It is still under debate whether the

loss of function of the TDP-43 protein due to the cleavage of the N-terminus is causing the neurodegeneration or whether the clearance of the protein from the nucleus as well as cytoplasmic regions is the trigger for degeneration of neurons, or whether both observations are rather not the cause but a second or third step in the cascade of neurodegeneration.

Although the whole function of the TDP-43 protein is not known so far, many roles have been identified. Several of them are associated with functions in RNA metabolism including direct RNA interactions. One is the implication of TDP-43 in pre-mRNA processing according to its predominant nuclear localization. Possible functions are here the regulation of transcription (Buratti and Baralle 2010), alternative splicing (Buratti et al., 2001) and the processing of micro-RNAs (miRNAs) (Buratti et al., 2010). Likewise a disturbed neurite outgrowth phenotype upon depletion of Tdp-43 could be observed (Fiesel et al., 2011, Fallini et al., 2012) as well as defects in neuromuscular junction establishment (Feiguin et al., 2009) suggesting an important role for TDP-43 in neuronal maintenance. As TDP-43 has been found to interact with several thousand different RNAs, in particular intronic regions, this supports the different nuclear functions of the TDP-43 protein. But several studies also point to other roles as even interactions of TDP-43 with 3' untranslated regions (3' UTRs) and noncoding RNAs (Polymenidou et al., 2011, Sephton et al., 2011, Tollervey et al., 2011, Colombrita et al., 2012) could be identified. In particular the fact that TDP-43 interacts with 3'UTRs of mRNAs as well as the observation of alterations of the expression level of more than 600 mRNAs in the adult mouse brain after depletion of Tdp-43 (Polymenidou et al., 2011) points to a possible role for TDP-43 in the subcellular processing and distribution of distinct mRNAs. As furthermore transcripts associated with important motoneuron functions, like choline acetyl transferase (Polymenidou et al., 2011) histone deacetylase 6 (HDAC6) (Fiesel et al., 2010, Fiesel et al., 2011) and low molecular weight neurofilament (Nfl) (Strong et al., 2007), were found to be altered when Tdp-43 protein is missing in the cell and an axonal localization of the Tdp-43 protein in spinal motoneurons could be observed (Fallini et al., 2012) one question becomes more and more interesting: What is the specific role of Tdp-43 in the subcellular localization of mRNAs in neurons and how are transcript levels altered especially in the axonal compartment upon Tdp-43 depletion?

1.1.2 Spinal muscular atrophy (SMA)

In contrast to ALS affecting people mostly at an age of 50-60, spinal muscular atrophy (SMA) is the most common neurodegenerative disease in children and young adults (Crawford and Pardo 1996), only affecting the lower spinal motoneurons thus causing paralysis as well as muscle atrophies.

But not only the age when the disease starts and the type of motoneurons affected are distinct to ALS. Also the type of heredity shows differences. SMA is an autosomal recessive disease and more than 90% of all cases are caused by deletion or homozygous mutation of the *Survival of Motor Neuron* (*SMN*) gene on chromosome 5q13 leading to loss of function of the gene and the corresponding protein (Lefebvre et al., 1995). Humans possess two copies of the gene on chromosome 5, the telomeric *SMN1* and the centromeric *SMN2* gene. The only difference between the two copies exists in only 5 nucleotides in the 3' region of the gene (Wirth 2000), of which only one mutation resides in the coding region. The latter presents as a translationally silent cytosine to thymidine exchange at position 6 of exon 7 resulting in skipping of exon 7 in the majority of transcripts from the *SMN2* gene. Consequently, more than 80% of the SMN protein resulting from the *SMN2* transcript lack the C-terminal 16 amino acids (Monani et al., 1999). This leads to an unstable corresponding protein (Cho and Dreyfuss 2010) which is not able to self-associate and therefore results in defects in SMN complex formation as well as reduced activity.

In contrast to the human genome, the mouse genome only contains one copy of the *Smn* gene. Gene knockout of Smn in the mouse leads to embryonic lethality (Schrank et al., 1997) being consistent with the ubiquitious expression of the protein and its important role in the assembly of spliceosomes. Interestingly, overexpression of the human *SMN2* gene in mice on a Smn knockout background leads to birth of the mice followed by the development of typical symptoms of SMA (Monani et al., 2000). Also important to notice is hereby the fact that the expression of a high number of *SMN2* copies even completely reverses the SMA phenotype resulting in healthy mice (Monani et al., 2000).

The SMN protein interacts with many different proteins and plays important roles in a variety of cellular processes most of them associated with RNA processing (Kolb et al., 2007, Burghes and Beattie 2009, Li et al., 2014). The best described function of

SMN so far is its role in the biogenesis of spliceosomal small nuclear ribonucleoprotein particles (snRNPS) as well as other RNPs (Battle et al., 2006). The main function of SMN thereby is the mediation of the formation of the Sm core domain of uridine-rich spliceosomal snRNPs consisting of seven Sm proteins. For this purpose SMN is building a complex together with the specific proteins Gemin 2-8 and unrip (Fischer et al., 1997, Liu et al., 1997, Chari et al., 2008). If SMN is deficient in this process, impairment of snRNP assembly (Gabanella et al., 2007, Zhang et al., 2008) as well as altered pre-mRNA splicing can be observed (Zhang et al., 2008, Lotti et al., 2012). Nevertheless, the question whether such splicing defects are directly caused by SMN loss or are reflecting secondary effects as a consequence of cellular dysfunction is not answered so far (Baumer et al., 2009, Garcia et al., 2013).

Besides the findings on the function of the SMN protein in splicing and snRNP assembly and resulting defects upon deficiency of Smn, other interesting hypotheses regarding the etiology of SMA came up. These are based on the observation that the Smn protein is localized in axons of motoneurons (Zhang et al., 2003, Dombert et al., 2014) as well as the identification of several RNA binding proteins interacting with SMN, a quite interesting result regarding the fact that SMN itself is not able to bind mRNAs. Among these RNA binding proteins candidates like hnRNP R and Q (Mourelatos et al., 2001, Rossoll et al., 2002), IMP1 (Fallini et al., 2014), FMRP (Piazzon et al., 2008), HuD (Fallini et al., 2011), FUS (Yamazaki et al., 2012) and TDP-43 (Wang et al., 2002, Tsuiji et al., 2013) were found. Especially the interaction with TDP-43 could be quite interesting for further investigation regarding the possible function of TDP-43 in axonal translocation of mRNAs already discussed above. Therefore it seems quite likely that SMN possesses additional functions in the regulation of mRNA processing and in the subcellular transport of mRNAs into neurites, besides its function in snRNP biogenesis. Further support for this hypothesis is coming from results showing an impairment in the axonal levels of poly(A)-mRNA in general in primary motoneurons upon Smn knockdown, indicating a widespread RNA transport defect (Fallini et al., 2011). Moreover, β-actin mRNA was already identified as a specific candidate translocated by Smn and being reduced in axons of Smn-deficient motoneurons (Rossoll et al., 2003, Glinka et al., 2010). Nevertheless an unbiased approach to identify several RNAs being misregulated in the axons of motoneurons when Smn is missing has not been made so far.

Isolated motoneurons of *Smn-/-;SMN2tg* mice as well as motoneurons of Smn deficient zebrafish already show a clear pathological phenotype in culture. Even though the survival of these motoneurons is normal in cell culture, the cells show an axonal outgrowth defect (McWhorter et al., 2003, Rossoll et al., 2003) detectable especially between days 3 and 7 in culture (Jablonka et al., 2007). Furthermore, growth cones of these motoneurons appear much smaller in size compared to control motoneurons (Rossoll et al., 2003). As also further additional axonal defects are a prominent pathological feature of SMA like defective spontaneous firing (Jablonka et al., 2007) and impaired neurotransmission at neuromuscular junctions in mouse models (Kariya et al., 2008, McGovern et al., 2008, Murray et al., 2008, Kong et al., 2009) as well as patients (Mishra et al., 2004, Swoboda et al., 2005), an unbiased approach could give possible insights into molecular deficiencies causing these symptoms. And maybe one prominent question can be answered: What is the specific role of Smn in the subcellular localization of mRNAs in neurons and how are transcript levels altered especially in the axonal compartment upon Smn depletion?

But during the attempt to find some explanations for the pathology of SMA, even the interaction of Smn with the heterogeneous nuclear ribonucleoprotein R (hnRNP R) requires some closer examination. hnRNP R was identified on the basis of antibodies found in the blood of patients with autoimmune diseases (Hassfeld et al., 1998). The protein consists of 632 amino acids and shows a molecular weight of ~70 kDa. The N-terminus contains, like TDP-43, two RNA recognition motifs (RRM1 and RRM2) and the arginine and glycine rich domain (RGG), common to all hnRNPs, is also located in the C-terminus allowing the recognition of different RNA sequences (Glinka et al., 2010). Furthermore, close to the RGG domain the motive mediating the interaction with Smn is located being quite similar to the motives of other Smn binding proteins (Rossoll et al., 2002).

With 81% sequence identity highly similar to hnRNP R is the cytoplasmically located protein SYNCRIP (synaptotagmin-binding cytoplasmic RNA-interacting protein) also known as hnRNP Q (Mizutani et al., 2000). Due to a missing putative nuclear localization signal (NLS) it is described as the cytoplasmic variant of hnRNP R although no data exist to prove this NLS. The protein sequences of hnRNP R and hnRNP Q are highly homologous and hnRNP Q also contains a Smn binding domain,

similar to the binding domain of the spliceosomal Sm proteins. Likewise to hnRNP R, a mutation of the Smn binding domain in hnRNP Q leads to a defect in Smn binding ability (Mourelatos et al., 2001).

As already pointed out above, Smn and hnRNP R are both localized in axons of motoneurons, besides their nuclear presence (Rossoll et al., 2002, Dombert et al., 2014). hnRNP R binds directly to mRNAs as was already shown specifically for the β-actin mRNA which is reduced upon Smn deficiency (Rossoll et al., 2003, Glinka et al., 2010). Moreover, the interaction of hnRNP R and β-actin mRNA is diminished when the Smn-binding domain of hnRNP R is abolished (Rossoll et al., 2003) suggesting an important role of Smn in the β-actin mRNA translocation. Another interesting fact is the result that a knockdown of hnRNP R leads to a similar axonal phenotype as Smn knockdown. This could be observed not only in isolated motoneurons but also in zebrafish embryos (Glinka et al., 2010). Therefore even here one question remains: What is the specific role of hnRNP R in the subcellular localization of mRNAs in neurons and how are transcript levels altered especially in the axonal compartment upon hnRNP R depletion?

1.2 Axonal RNA transport and axonal transcriptome analysis

One astonishing feature of motoneuron diseases is the often involved impairment of ubiquitious expressed proteins leading to a pathology predominantly affecting motoneurons. But there is no satisfying explanation for this phenomenon so far. One possibility explaining partly this observation is the fact that neurons are highly polarized cells compared to other cell types. A polarization in general leads to a targeting of mRNAs to subcellular domains providing a basis for spatial and temporal control of protein levels in these regions (Martin and Ephrussi 2009). This is important especially for neurons as they extend their cytoplasmic processes for long distances from the cell body into dendrites and axons. Therefore a local regulation of transcript abundance or translation in axons could lead to a rapid and autonomous response to the environment or to injury.

Early ultrastructural studies of rodent hippocampus suggested that axons do not contain any mRNAs or translational machinery at all (Steward and Levy 1982). This report was followed by more studies suggesting a protein synthesis activity in axons

under at least some specific circumstances (Twiss and van Minnen 2006, Jung et al., 2012). Further methodical improvements including advanced nucleic acid detection and reporter systems for visualizing mRNAs and local protein synthesis finally led to the definite observation of mRNAs and translational machineries in axons (Jung et al., 2012). Particularly the improvements in RNA detection allowed the subsequent profiling of axons for their mRNA content revealing a rather unexpected complexity in transcripts localized to axons. The first reports on transcriptomics were based on microarray approaches. Although the experiments were performed in several laboratories and different neuronal cell types were used, hundreds of diverse mRNAs were found in axons (Willis et al., 2007, Taylor et al., 2009, Zivraj et al., 2010, Gumy et al., 2011). Even *in vivo* there is increasing evidence for axonal mRNA localization (Brittis et al., 2002, Sotelo-Silveira et al., 2008, Donnelly et al., 2011, Willis et al., 2011, Ben-Yaakov et al., 2012, Walker et al., 2012, Merianda et al., 2013, Merianda et al., 2013).

But the microarray approaches have some limitations. These include for example the reliance on the existing knowledge about genome sequences, high background levels due to cross-hybridization or a limited range of detection due to background and saturation of signals as well (Wang et al., 2009). Furthermore, it can be quite difficult to compare the expression levels across different experiments, possibly requiring complicated normalization methods. These disadvantages led to further improvements and to the development and establishment of a new method called RNA-Sequencing (RNA-Seq). This method revolutionized transcriptomics even to the single cell level (Saliba et al., 2014). Contrary to microarray approaches, sequence-based methods are directly determining the cDNA sequence and the high-throughput DNA sequencing methods used today allow both mapping and quantifying of the transcriptomes. The common principle of the RNA-Seq method is as follows: a pool of RNA (total or fractionated, whole or poly(A) selected) is reverse transcribed to cDNA fragments containing adaptors at one or both ends. In the following procedure each molecule is sequenced in a high-throughput manner revealing 30-400bp long sequences. These sequences can be obtained from one end (single-end sequencing) or from both ends (pair-end sequencing) (Wang et al., 2009). The advantages of this method are clear. It is a high-thoughput sequencing approach resolving single bases with a low background noise independent of existing genomic

sequences. Furthermore, the required amount of RNA is much less compared to microarrays.

The uncovered complexity of the axonal mRNA content implicates the importance of axonal RNA transport and leads to the question how this transport is happening. So far there is not much known about the mechanisms of axonal RNA transport. mRNAs are transported in RNA-protein complexes containing RNA binding proteins (RBPs) and other proteins. Only a few RBPs have been observed to localize in axons but the exact stoichiometry of RBP and different mRNAs is still not known. But it is clear that several mRNAs are known to be enriched in axons and growth cones (Andreassi et al., 2010, Zivraj et al., 2010, Gumy et al., 2011) and that axonal transport can be regulated through several different impulses (Willis et al., 2007, Taylor et al., 2009, Gumy et al., 2011, Merianda et al., 2013, Merianda et al., 2013). Furthermore one single RBP is able to exert different functions on one mRNA aside of axonal transport such as stabilization (Nielsen et al., 2004, Weidensdorfer et al., 2009).

RBPs have one or more RNA binding domains. These are for example known as RNA recognition motifs (RRMs) or KH domain and are enabling the protein to bind to mRNAs leading to the formation of ribonucleoprotein (RNP) complexes (Glisovic et al., 2008). But in many cases the mRNA binding specificity is not defined by the RNA binding domain alone but through the contribution of multiple domains (Maris et al., 2005). Even the interaction of the RBPs with other proteins in the RNP complex is of high importance bringing additional properties in the posttranscriptional regulation to the RNP complex. One example for the interaction with several other proteins is the zip code binding protein 1 (ZBP1) known for its important role in the transport of β-actin mRNA (Ross et al., 1997). This protein interacts for example with the KH-type splicing regulatory protein (KSRP), Hu-Antigen C (HuC), heterogeneous nuclear ribonucleoprotein E1 (hnRNP E1), E2 (hnRNP E2) and L (hnRNP L) in lysates from rat brain and HEK cells (Snee et al., 2002, Jonson et al., 2007). Besides that, an interaction with hnRNP Q, hnRNP R and Hu-Antigen D (HuD) could also be observed (Atlas et al., 2007, Glinka et al., 2010).

RBPs bind to specific mRNAs by recognizing either primary sequences or secondary structures in the mRNA. Hereby it is important to highlight that the RBP is not only confined to one single sequence or structure but is able to bind multiple different mRNAs. These results were mainly obtained by experiments based on RNA

coimmunoprecipitation (RIP) or cross-linking and immunoprecipitation (CLIP) approaches. Via the RIP assay more than 200 different mRNAs were identified binding to IMP1 (human ortholog of ZBP1) in HEK cells (Jonson et al., 2007), but one disadvantage of traditional RIP is the fact that even mRNAs indirectly bound to the RNP complex are identified leading to misinterpretations of specific interactions (Mili and Steitz 2004). The CLIP approach in contrast resolves direct mRNA-protein interactions in cells or tissues by first cross-linking the protein to its mRNA target before cell lysis. Due to this method over 800 mRNAs were identified to be bound to the fragile X mental retardation protein (FMRP) (Darnell et al., 2011) and more than 6,304 different mRNAs directly bound to Tdp-43 (Polymenidou et al., 2011) in mouse brain. Via individual-nucleotide resolution cross-linking and immunoprecipitation (iCLIP) it was furthermore possible to dissolve the preferred binding clusters of TDP-43 consisting of UG-rich sequences (Tollervey et al., 2011).

The importance of RBPs in neural development and their roles in neurite extension and synaptic plasticity has been shown in several studies (Agnes and Perron 2004, Liu-Yesucevitz et al., 2011). Furthermore, the expression of the RBPs or their availability could effectively determine which mRNAs can localize into axons. Some RBPs including their already known axonal mRNA targets are summarized in Table 1.

Table 1: RNA binding proteins and their respective mRNA targets

RNA binding protein	evidence for axonal mRNA targets (with reference)
CPOB1	kappa-opioid receptor (Bi et al., 2007)
CPEB1	beta-Catenin, EphA1 (Brittis et al., 2002, Kundel et al., 2009)
FMRP	MAP1B (Antar et al., 2005)
GRB7	kappa-opioid receptor (Tsai et al., 2007)
hnRNP R	beta-Actin (Rossoll et al., 2003, Glinka et al., 2010)
hnRNP Q1	RhoA (Xing et al., 2012)
HuD (ELAVL4)	GAP-32, Tau (Atlas et al., 2007, Yoo et al., 2013)
La/SSB	RPL37 (Crosio et al., 2000, van Niekerk et al., 2007)

	beta-Actin, Cofilin1, Calreticulin, eIF2B2, GAP43, MAP1B, RhoA, RPL21, RPS11, SepW1 (Willis et al., 2007, Maher-Laporte and	21
Stau2	DesGroseillers 2010, Kar et al., 2013)	
TDP-43	beta-Actin, MAP1B, RPL37, Tau (Willis et al., 2007, Sephton et al., 2011)	
ZBP1	beta-Actin, GAP-43 (Zhang et al., 2001, Yoo et al., 2013)	

It becomes evident that the interaction between RBP and mRNA target in the axonal compartment is shown only for individual mRNAs. This means approaches giving extensive results for several mRNA targets affected by one RBP are missing so far. Therefore, the aim of this study was to investigate specifically the axonal transcriptome of primary mouse motoneurons and corresponding changes of the axonal RNA content upon depletion of distinct RNA binding proteins and a protein not able to bind mRNAs by itself but known to be part of RNP complexes, respectively.

2 Material and Methods

2.1 Material

2.1.1 Animals

CD-1 mice were maintained as an outbred line and were obtained from Charles River animal facility. They were kept at the animal facilities of the Institute for Clinical Neurobiology at the University Hospital of Wuerzburg providing controlled conditions such as food and water in abundant supply, a 12 hours light/dark cycle, 20-22°C and 55-65% humidity, respectively. Each experiment was performed strictly following the regulations on animal protection of the German Federal and of the Association for Assessment and Accreditation of Laboratory Animal Care, in agreement with the local veterinary authority.

2.1.2 Cell lines

Human Embryonic Kidney 293 cells were used to generate lentiviruses. HEK 293T cells are a highly transfectable derivative where simian virus 40 (SV 40) large T antigen was inserted (DuBridge et al., 1987). This allows episomal replication of transfected plasmids containing the SV40 origin of replication.

2.1.3. Buffers for cell culture

Table 2: Buffers for cell culture

Borate buffer	0.15 M boric acid pH 8.35
Depolarization buffer	30mM KCl
	0.8% NaCl
	2mM CaCl2
10mM Tris HCl pH 9.5	
Poly D-L-ornithine 1X diluted in borate buffer	

2.1.4 Media for cell culture

2.1.4.1 Media for motoneuron cell culture

Table 3: Media for compartmentalized motoneuron cultures

Medium for somatodendritic side	Medium for axonal side
Neurobasal with 1x Glutamax	Neurobasal with 1x Glutamax
2% Horse serum	2% Horse serum
1x B27 supplement	1x B27 supplement
CNTF 5ng/ml	CNTF 5ng/ml
	BDNF 20ng/ml

2.1.4.2 Media for HEK293T cell culture

DMEM with 1x Glutamax

10% fetal bovine serum

1x non essential amino acids

1x penstrep

2.1.5 Chemicals

Chemical	Company
10 U RiboLock RNase inhibitor	Thermo Scientific
100 U Superscript III	Life Technologies
Accuprime *Taq* DNA polymerase	Life Technologies
AMPure XP beads	Beckman Coulter
B-27 supplement	Life Technologies
BDNF	Institute of Clinical Neurobiology
Boric acid	Applichem
Calcium chloride	Merck
CNTF	Institute of Clinical Neurobiology
DMEM	Life Technologies
ERCC RNA spike-in mix 1	Life Technologies
Ethanol	Sigma-Aldrich
Glutamax	Life Technologies
HBRR	Life Technologies
HBSS	Life Technologies
HEPES	Sigma-Aldrich
Horse serum	Linaris
Laminin	Life Technologies

Luminaris HiGreen qPCR Master Mix	Thermo Scientific
Mercaptoethanol	Merck
Micro-90®	Sigma-Aldrich
Non essential amino acids	Invitrogen
Neurobasal	Life Technologies
Penicilin/Streptavidin	Life Technologies
Poly D-L-Ornithine	Sigma-Aldrich
Potassium chloride	Merck
Sodium chloride	Merck
Tris Base	Merck
Trypsin Worthington	Worthington
Trypsin inhibitor	Sigma-Aldrich

2.1.6 Plasmids

Table 4: List of plasmids

Vector	Source
pMD.G VSVG	Addgene (Dull et al., 1998, Zufferey et al., 1998)
pMDLg/pRRE	Addgene (Dull et al., 1998, Zufferey et al., 1998)
pRSV-REV	Addgene (Dull et al., 1998, Zufferey et al., 1998)
pSIH-shTdp43	cloned by Dr. Carsten Drepper
pSIH-shSmn	cloned in this work
pLL3.7-shhnRNP R oligo2	cloned by Dr. Michael Glinka
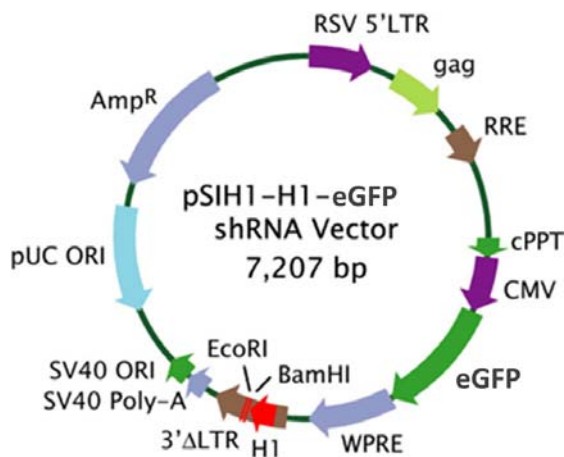
Vektorcard pSIH-eGFP vector

2.1.7 Oligonucleotides

primer name	sequence
MALBAC_primer	GTGAGTGATGGTTGAGGTAGTGTGGAGNNNNNNNN
MALBAC_adapter_1	GTGAGTGATGGTTGAGGTAGTGTGGAG
MALBAC_adapter_2	GAGTGATGGTTGAGGTAGTGTGGAG
MALBAC_adapter_3	CTGTGAGTGATGGTTGAGGTAGTGTGGAG
MALBAC_adapter_4	TCTGTGAGTGATGGTTGAGGTAGTGTGGAG

primer name	forward sequence	reverse sequence
7SK	AGGACGACCTTCCCCGAATA	GCGCCTCATTTGGATGTGTC
Actn4	ATCCAGGAGGCCCTCATCTT	GCATCTCGGGTGAGGATCTG
Ank3	GATTTTATTTACGCCTCTAACTTCTG	TTCTTTCTTTCTCTCTCTCTCTCTC
Apc	TGCATGAATGAAGCTGACG	GCAGCCAACTCACCTCAAAT
Apoe	GGGCAAACCTGATGGAGAA	GCCAGAGAGGTGCTTGAGAC
Atxn2	GCAGTGGAGGATGTTTTGGA	AAAGCGGTAATAGCAGCAAGAA
Axl	CCATCTCCACGTGGTTTCCA	ATACCCACCCATCGTCTGA
Cacna1b	CCCGATCAGGACCACT	CTCATCAACTGGAACCCTC
Cald1	AGGGTTGGCTTGAGGGTTT	TCGGGGGTAGATGACTTGTG
Cdk1	GAAGTGTGGCCAGAAGTCGA	TGAGAGCAAATCCAAGCCGT
Chga	TGAGGAAAAGAAGGAAGAGGAG	GAGAAGGTGAGGGGCAAAG
Clasp1	TTCCTTTCTCTGCCACCTTT	AAACCCAAAACAAACAACACC
Cpsf3	GTGGACGGGAAAACAGCA	GGAGTCTGGGAGGCAAGG
Csrp1	GGGTATCTGGCTTTTTGTGG	CCTGCTTTGCTCTATTGGTCT
Cyc1	TGAAGCGGCATAAGTGGT	ACTGAGGGCTGAAGGAAGA
Dcx	TCCAGTCAGCAAAGGTAAGG	CAGTCCAAGAGAGAACAGCAA
Erc2	CCCGAGACCCTTGTTTGATA	CATGCCCAGTGATAGTTTCG
Fus	TTGATGACCCACCTTCTGCT	ACCTCCTCCATAGCCTCCAC
Gapdh	GCAAATTCAACGGCACA	CACCAGTAGACTCCACGAC
Gphn	TCAAGGCTGTCTGCTTCTTT	ATTTCCCCCAGTTTGTTTGT
Gria1	TGAGTGCCACATGCCACTAG	AGCTCGTCCATTGCCAATGA
Gria2	CTGCTGATAACAGGGGTGGG	GTGCTGGAGGATTGCTCAGT
Grin3a	GACCCTACTCCCCACTCCTG	GCACACACACGGAAATGAAG
Igf1r	TAACGAATGCTGTGCCTACC	CAAGAAACTGAAAGACCAAACC
Igfbp2	GCAGTAAACCCCAGCCAGT	ACCACCCTTCCCCTCTCTAA
Itgav	AACTCAAGCAGAAGGGAGCC	CATCCCGAAGATAGGCGACC
Lgals1	AATCCTCGCTTCAATGCCCA	GTCAGCCTGGTCAAAGGTGA
Malat1	TGCAGTGTGCCAATGTTTCG	AGTCTGCTGTTTCCTGCTCC
Mapt	GCTTCCTTCCCTCTAATCCA	TACCACCTCCACCCTCATC
Mettl9	TTTCTTTGTAGTGTGTAAGGGAGTG	TTGCTTTGTCTGGGAATGAG
Mt3	GTCCTACTGGTGGTTCCTGC	ACACTTCTCACATCCGGCAG
Mycbp2	CGTTTCCCCTTTATTTTGGTT	TGATTCTTTTTCTTCTTTTGCTTG
Myh9	AGAAGACCAAGACACGGCTG	AGATGGTCTTCTCCTCGGCT
Nefl	GAGGGAGAGGAAGAGGAAGG	GGTTGGTTGGTGATGAGGTT
Negr1	GCTATACCCTGTGGTCCTGC	TCAGTGAAGCTGTGAACCCC

Nes	TCTGAGTGGGGTAGATGGAGA	AGAAGAAAGGGGGCGTTG
Pclo	GCTTAGAGGAGAGCAAAGGAAA	ACGGTAACACGCACAGAAGA
Plk2	CTGCTGGACTGCTGGAAC	GCTGCTCTGATTGTAGCCTTT
Pls3	ATGCTGCCCTTGACATTCC	CAAAGAACACTCATCTCCACACA
Ppfia3	CGAAGAAGAGGACAGGAAGAAA	TAGCGGACGGAGAAGGAAG
Prmt2	ACATCCACACTCACCCGTTC	TCAAGGACACCACTGACACAA
Rprl3	GGCCCCTGAGAAGGTCTG	GCTGGCCGTGAGTCTGTT
Scn2a1	TCTCTCTCTCTCTCTCTCTTTCTCT	TCTTTATTCTTTTGGCTTCATTG
Sh2d3c	CAGAGCACCACAGGGACAC	AACAGGGAACCTCAGCAAAA
Shisa5	CCAGTAGCAGGGACACCAA	CAGAAACACCAATCAACACAAAG
Sparc	GTACCTGTCCCACACTGAGC	CCATTCCTCCAGGGCAATGT
Spp1	GGTCAACTAAAGAAGAGGCAAAA	CAGGAAGAACAGAAGCAAAGTG
Stat1	GCTGAGCACTGCTGGTAGAA	CTAGTCCTGGTGCTTGGGTG
Syn3	TGACCCCTTTAGCCACACTT	TGCCAATGTCTTCCTGTTTTT
Synj1	CGTGCTTGTTGGGGTTCTA	CTTGCTAATGGGGAGTGGAT
Thbs1	CGCCTTCCGCATTGAGAATG	CATCTGCCTCAAGGAAGCCA
Tnc	CGTCCAAGCAGACCACAC	CCAGAACCACCCAAGAGAAG
Tpm1	GCTTACCGTGAAACCCCTTC	CCGATTGTCTCCAACATCAGT
Trpm7	TGTTCAATGGGTGTTTCCTG	CACTGCTCCTTCCAAATAAAAA
Tuba1a	GAGGGGGAGGAAGAAGGAG	GCTTGGGTCTCTGTCAAATCA
Tuba1b	GAGCAACACCACAGCCATT	CCTTCCACAGAATCCACACC
Tubb2a	ATGTCAGCCACCTTCATTGG	AGCCTCATCTTCACCCTCCT
Tubb4a	GAGGAGGCTGAAGAGGAGGT	TTGGAGAGACAGTGGGGTTT
Tubb5	CTTTCAGTCAGCAGGGCTTT	GGGAGTGTTCAGAGACCAAGA
Tubb6	TCTTCCGGCCTGACAACTTC	AGACAGTCGCAATGCTCACA
Ubqln2	GGCTAGGCAAGTTCAGTTAAAA	CTCTTCATGGGAGAAGCTGA

primer name	forward sequence	reverse sequence
Smn shRNA oligo (Zhang et al., 2008)	GATCCGAAGAATGCCACAACTCCCTCAAGAGGGGGAGTTGTGGCATTCTTCTTTTTG	AATTCCAAAAAGAAGAATGCCACAACTCCCCTCTTGAGGGAGTTGTGGCATTCTTCG

2.1.8 Commercial kits

Table 5: List of commercial kits

Name	Company
Arcturus PicoPure RNA Isolation Kit	Life Technologies
Endofree Plasmid Maxi Kit	Qiagen
NEBNext Multiplex Oligos for Illumina (Index primer Set 1)	NEB
NEBNext Ultra DNA Library Prep Kit for Illumina	NEB
QIAEX II Gel Extraction Kit	Qiagen
RNeasy Mini Kit	Qiagen
RiboAmp HS Plus Amplification Kit	Life Technologies
Turbo DNA-free kit	Ambion

2.1.9 Software

Table 6: Software

Name	Reference
ApE- A plasmid	Editor v2.0.36 2003-2009 by M. Wayne Davis
GraphPad Prism 4.02	1992-2004 GraphPad Software, Inc., San Diego, California, USA
Microsoft Office 2010	1985-2003 Microsoft Corporation
Oligo 6.71	1989-2005 Wojciech Rychlik; Molecular Biology Insights, Inc., 8685 U.S. Highway 24 West Cascade, CO 80809, USA

2.2 Methods

2.2.1 Isolation of embryonic primary mouse motoneurons

Primary motoneurons from lumbar spinal cord served as a model to understand the molecular mechanism in motoneuron diseases.

Spinal cord tissue from E12.5 mouse embryos was isolated and motoneurons were cultured as described previously (Wiese et al., 2010). In brief, lumbar spinal cords were dissected, processed thoroughly by removing dorsal root ganglia (DRGs) and meninges, collected in 180 µl of HBSS and stored on ice. The tissues were subsequently digested with 0.1% trypsine for 15 min at 37°C. Trypsin digestion was stopped by adding 0.1% trypsin inhibitor. Afterwards the tissue was triturated mechanically by pipetting the solution up and down to form a single cell suspension. To enrich the motoneurons from the mixed population of cells, p75^{NTR} antibody (clone: MLR2) was used. For this step cells were plated onto a 10 cm Nunclon^{TM} Δ surface dish previously coated with tris buffer solution containing p75^{NTR} for 2h.Cells were washed two times with Neurobasal media to remove unspecific binding of cells to the antibody and eluted with 2 ml depolarization buffer. 8 ml of Neurobasal media (life technologies), containing 500 µM GlutaMAX (life technologies), 2% heat inactivated horse serum (Linaris) and 2% B27 supplement (life technologies) was directly added and cells were washed off the plate. Enriched motoneurons were counted in a haemocytometer and plated onto poly-DL-ornithine (Sigma-Aldrich) and laminin (life technologies) coated dishes. Cells were cultured for seven days in Neurobasal medium supplemented with 500 µM GlutaMAX, 2% horse serum, 2% B27 supplement as well as the neurotrophic factors BDNF and CNTF. Medium was changed on day 1 and subsequently on every second day.

2.2.2 Primary mouse motoneuron culture with microfluidic chambers

Microfluidic chambers (Xona Microfluidics, SND 150) were washed with 2% Micro-90® concentrated cleaning solution (Sigma-Aldrich, Z281506-1EA) for 30 min in an ultrasonic bath followed by a washing step just with water for 10 min. Thereafter microfluidic chambers were incubated in 70% ethanol for 30 min and dried overnight under a laminar flow. On the next day, sterile chambers were placed on PORN coated dishes and the main channels as well as the microchannels were covered with laminin solution.

Lumbar spinal motoneurons were isolated from E12.5 mouse embryos and enriched via p75-panning (see above) and plated into precoated microfluidic chambers. For Smn knockdown, Tdp-43 knockdown, hnRNP R knockdown, 7SK knockdown and GFP transduced cultures one million motoneurons were directly infected with lentivirus for 10 min at room temperature prior to plating. To achieve a directed growth of the axons through the microchannels of the microfluidic chamber a BDNF gradient (20 ng/ml) was established in the axonal compartment. CNTF (5 ng/ml) was added to both compartments for survival. Motoneurons were grown for 7 days at 37°C and 5% CO_2 in neurobasal medium containing 500 μM GlutaMAX, 2% horse serum, 2% B27 supplement. 50% of culture medium was exchanged on DIV 1 and then every second day.

2.2.3 Generation of Smn knockdown plasmid

shRNA templates were designed according to the user manual of pSIH-H1 shRNA Cloning and Expression Lentivectors Kit. According to this protocol, the two complementary oligonucleotides were synthesized, phosphorylated and annealed before the ligation step. The pSIH vector was linearized with Eco RI/BamHI. shRNA template was ligated into the linearized pSIH lentivector followed by a transformation of the ligation product into chemocompetent E.coli. shRNA lentivector construct plasmid DNA in maxi scale was purified using an Endotoxin-free plasid purification kit from Qiagen.

2.2.4 Production of lentiviruses

Lentiviruses were produced expressing either shRNA against Smn, hnRNP R, Tdp-43 or 7SK, respectively, or a GFP-reporter gene as internal control. For all knockdown constructs used in this study the pSIH-EGFP expression plasmid containing the corresponding shRNA was used. HEK293T cells were used to generate lentiviruses. Cells were transfected with pRRE, pRSV, pMD2.G vectors and expression plasmid using Lipofectamine 2000 (Invitrogen). Supernatants were collected and concentrated by ultracentrifugation (25000 rpm, 90 min, 4°C). Pellets were dissolved in TBS-5 buffer and stored at -80°C until use.

2.2.5 Extraction and purification of total RNA

Total RNA of the somatodendritic and axonal compartment was extracted with the Pico Pure^{TM} RNA Isolation Kit (Life Technologies), according to the manufacturer's protocol. With this kit the RNA is extracted and directly purified. Briefly, after 7DIV both compartments of the microfluidic chambers were washed two times with PBS. Afterwards, total RNA was extracted separately from both compartments with 100μl extraction buffer each, mixed with 70% ethanol and loaded onto a preconditioned purification column. The extract was spun through the column to capture the RNA on the purification column membrane. Subsequently, the column was washed twice with wash buffer and the RNA was eluted in 11μl of a low ionic strength buffer. Following this procedure, the extracted RNA was directly used for linear amplification.

2.2.6 Linear amplification

Linear amplification was done with the RiboAmp® HS^{Plus} Amplification Kit (Life Technologies). The protocol is based on two rounds of amplification. In brief, in round one, purified total cellular RNA was subjected to 1st strand synthesis with an mRNA-specific primer. This step is followed by 2nd strand synthesis with an exogenous primer. The cDNA was then purified on MiraCol^{TM} columns and in vitro transcription was performed. The amplified aRNA was again purified on MiraCol^{TM} columns before round two of amplification was started. In round two amplified antisenseRNA was again subjected to 1st and 2nd strand synthesis and the resulting cDNA was purified

on MiraCol™ columns. At this point of the protocol, the procedure was stopped and the purified cDNA was given to the Microarray Unit in Wuerzburg for further in vitro transcription, biotin-labeling and hybridization on the corresponding microarray chip (Affymetrix Gene Chip ® Mouse Genome 430 2.0 Array, catalog no. 900496).

2.2.7 Bioinformatical analysis microarrays

The microarray data discussed in this thesis have been deposited in NCBI's Gene Expression Omnibus (Edgar et al. 2002) and are accessible through GEO Series accession number GSE59506 insofar as they are published. Data were analyzed using different R/Bioconductor modules (www.bioconductor.org). Resulting signal intensities were normalized by quantile normalization (Bolstad et al. 2003), differentially expressed genes were selected by the bioconductor package Limma (Smyth 2004). Quality as well as comparability of the data sets were tested by density plot and RNA degradation plot. For functional clustering the Database for Annotation, Visualization and Integrated Discovery (DAVID, http://david.abcc.ncifcrf.gov/home.jsp) was used (Huang et al. 2009).

2.2.8 Whole transcriptome amplification

For serial dilution experiments total spinal cord RNA was extracted from day 14 mouse embryos using the RNeasy Mini Kit (Qiagen). For DNA removal the TURBO DNA-free kit (Ambion) was used. Total RNA was prediluted to 1ng/µl, 100 pg/µl and 10 pg/µl. Three replicates each of 5ng (5 µl of 1 ng/µl), 500 pg (5 µl of 100 pg/µl), 50 pg (5 µl of 10 pg/µl) and 10 pg (1 µl of 10 pg/µl) were prepared and reverse transcribed in 20 µl reactions. Reverse transcription mix contained 0.5 mM dNTPs, 10 U RiboLock RNase inhibitor (Thermo Scientific), 100 U Superscript III (Life Technologies), 4 µl 5x First Strand Buffer, 1 µl 0.1 M DTT and 2.5 µM MALBAC primer (Zong et al., 2012). Reverse transcription was performed at 37°C for 10 min followed by an inactivation at 70°C for 15 min. Before subjecting cDNAs to second strand synthesis, single-stranded cDNAs were purified with QIAEX II Gel Extraction Kit (Qiagen) and eluted in 20 µl. 1 µl was removed from eluate, diluted 1:5 with water and reverse transcription efficiency was evaluated by *Gapdh* qPCR. For second strand synthesis, 1.725 µl 50 µM MALBAC primer, 5 µl Accuprime buffer 2, 1 µl

Accuprime and 24.275 µl water were added to 18 µl purified cDNA and the following PCR program was applied: 98°C 5 min, 37°C 2 min, 68°C 40 min. Thereafter, the now double-stranded cDNA was again purified with QIAEX II Gel Extraction Kit, eluted in 20 µl and 3.15 µl 50 µM MALBAC adapter primer mix containing equimolar amounts of each adapter, 5 µl Accuprime buffer 2, 1 µl Accuprime and 21.85 µl water were added to 19 µl purified cDNA. Subsequent PCR program was applied for amplification: 92°C 2 min, 92°C 30 sec, 60°C 1 min, 68°C 1 min. Cycle number was 12 cycles for 5ng, 15 cycles for 50 pg, 18 cycles for 50 pg and 20 cycles for 10 pg. Resulting PCR amplicons were purified using AMPure XP beads. 55µl AMPure XP beads were added to PCR products, mixed and incubated for 5 min at room temperature. Two washes with 200 µl 80% EtOH each were applied. Beads were air-dried for 10 min and amplicons eluted in 50 µl 0.1xTE buffer. Finally, PCR products were size-separated on a 10% polyacrylamide gel followed by gel-staining with SYBR Green I (Life Technologies) for visualization. 1 µl of purified amplicons was diluted 1:5 in water for subsequent *Gapdh* qPCR.

For library preparation, 50 ng of purified DNA was processed using the NEBNext Ultra DNA Library Kit for Illumina (NEB) in conjunction with NEBNext Multiplex Oligos for Illumina (Index Primer Set 1) (NEB). The protocol was performed according to manufacturer's instructions. 10% polyacrylamide gels were routinely run and stained with SYBR Green I for visualization of the libraries. Finally, obtained libraries were pooled and again purified using AMPure XP beads. For single end sequencing, Illumina MiSeq machine was used in combination with the MiSeq Reagent Kit v3 (150 cycles) and 1% spike-in of the phage PhiX control library.

For initial optimization of the method, 40 pg total spinal cord RNA was used. RNA was processed as described above, except the following differences. In total we set up two sets of experiments. The first set was done as following: two different polymerases (Accuprime *Taq* DNA polymerase and strand displacement polymerase *Bst*, Large fragment (NEB)) for second strand synthesis were used as well as two different primer concentrations (0.2 µM or 1.725 µM final concentration) for second strand synthesis were tested. Furthermore, two different adapter primer concentrations (0.2 µM or 3.15 µM final concentration) for final PCR were used. In the second set the following parameters were used: Accuprime *Taq* DNA polymerase for second strand synthesis, three different primer concentrations (1.725 µM, 5 µM

and 10 µM final concentration) for second strand synthesis as well as two different adapter primer concentrations (3.15 µM or 10 µM final concentration) for final PCR. Each experimental set started with six separate reverse transcription reactions parallelly performed with 40 pg each. For purification with the QIAEX II Gel Purification Kit samples were pooled and eluted in a total volume of 120 µl. For second strand synthesis again six different reactions were set up. Each reaction mix contained 19 µl purified cDNA, MALBAC primer at the indicated concentrations, Accuprime *Taq* DNA polymerase or *Bst* DNA polymerase, Large Fragment. For the experiment set with *Bst* DNA polymerase, Large fragment a total volume of 49 µl was set up. The reaction mix contained purified cDNA, MALBAC primer at the indicated concentrations, 5 µl 10x ThermoPol buffer and 0.2 mM dNTPs. Samples were incubated at 98°C for 5 min, subsequently placed on ice and 8 U *Bst* DNA polymerase were added followed by an incubation at 37°C for 2 min, 65°C for 40 min and 80°C for 20 min. After second strand synthesis, identical samples were again pooled and purified using QIAEX II Gel Extraction Kit. Purified cDNAs were eluted in 40 µl. PCR amplification reactions contained 19 µl purified second strand products, Accuprime *Taq* as well as MALBAC adapter 1 at the indicated concentrations. Aliquots of 4.5 µl volume were removed at the indicated cycles during PCR amplification and treated with 10 U exonuclease I (Thermo Scientific). Finally, aliquots were diluted 1:5 with water for *Gapdh* and *Ubqln2* qPCR.

When the protocol was applied to compartmentalized motoneuron cultures, 1 µl of somatodendritic and 10 µl of axonal RNA were used for reverse transcription. Reverse transcription and the subsequent protocol were performed as described above. Somatodendritic samples were amplified for 6 cycles and axonal samples for 18 cycles for final PCR.

2.2.9 QIAEX II purification of DNA

The cDNA purification with QIAEX II Gel Extraction Kit from Qiagen was always done according to the manufacturer's protocol. This kit enables desalting and elevating the concentration of DNA in the solution. In brief, the samples were transferred to a new tube and 3 volumes of buffer QX1 were added to 1 volume of samples. 10 µl of QIAEX II were added, mixed and incubated at room temperature for 10min. The

samples were mixed every 2 min to keep QIAEX II in suspension. Afterwards the samples were centrifuged and the supernatant removed. The pellet was washed twice with 500 µl Buffer PE and air-dried for 12 min. DNA was eluted in 20 µl water after incubation for 5 min at room temperature and following centrifugation.

2.2.10 Sequencing and read mapping

Single-end sequencing was performed on an Illumina MiSeq machine using the MiSeq Reagent Kit v3 (150 cycles) and 1% spike-in of the phage PhiX control library. Obtained reads were demultiplexed and quality assessment was performed using FastQC (http://www.bioinformatics.bebraham.ac.uk/projects/fastqc) version 0.10.1. For trimming of the reads inhouse scripts were used (Supplementary Fig. S1). First, Illumina adapters were removed and only reads which contained the minimal forward MALBAC sequence (5'-GAGTGATGGTTGAGGTAGTGTGGAG-3') were considered for further analysis. In cases detecting the reverse MALBAC sequence (5'-CTCCACACTACCTCAACCATCACTC-   3'), the sequence was trimmed followed by a collapsing of identical reads and removing of 5'- as well as 3'-oligo-octamers. In cases the reverse MALBAC sequence was not detected, only the first 120 nucleotides of the reads were considered followed by collapsing of the reads and removal of the 5'-oligo-octamers.

Trim Galore version 0.4.0 (http://www.bioinformatics.babraham.ac.uk/projects/trim_galore/trim_galore_v0.4.0.zip) was used for the total RNAseq samples and Cutadapt version 1.3 (http://cutadapt.googlecode.com/files/cutadapt-1.3.tar.gz) was used to remove Illumina adapter sequences. Quality threshold was set to 20.

Trimmed reads consisting of a minimum length of 30 nucleotides were mapped to the genome by using the ENSEMBL mouse reference genome (ftp://ftp.ensembl.org/pub/release-75/fasta/mus_musculus/dna/Mus_musculus.GRCm38.75.dna.primary_assembly.fa.gz) with Star version 2.4.0d [https://code.google.com/p/rna-star/ (alignment option used: outSAMstrandFieldintronMotif)]. Reads which mapped to multiple loci were distributed uniformly.

2.2.11 Data analysis

For generation of FPKM values (http://cufflinks.cbcb.umd.edu/) as well as for identification of differentially expressed genes (parameter used: no-effective-length-correction, compatible-hits-norm) the Cufflinks package version 2.2.1 was used. The max-bundle_frags option was set to 5 000 000 for the total RNAseq samples. ENSEMBL mouse genome annotation was used for gene annotation (ftp://ftp.ensembl.org/pub/release-75/gtf/mus_musculus/Mus_musculus.GRCm38.75.gtf.gz).

The CollectRnaSeqMetrics tool of the Picard Suite version 1.125 (http://broadinstitute.github.io/picard/) was used with default settings for coverage plots and quantification of read mappings to rRNAs, intergenic, intronic, UTR and coding regions. rRNA-interval files were downloaded from https://sites.google.com/site/liguowangspublicsite/home/mm10_rRNA.bed.

BAM files were subsampled for saturation analysis using an inhouse script.

For quantification of gene classes all FPKM values of expressed genes (FPKM≥1) were summed within each ENSEMBL type. We noticed that in the ENSEMBL mouse annotation the abundant ribosomal transcript Gm26924 was annotated as 'lincRNA'. Therefore, we included it manually in the gene class 'rRNA'.

We performed unsupervised complete linkage clustering of significantly differentially expressed genes as detected by Cuffdiff on the rows and columns using the Euclidian distance as a similarity metric. As input $\log_2$(FPKM) values were used.

For gene ontology (GO) term analysis as well as Kyoto Encyclopedia of Genes and Genomes (KEGG) the Database for Annotation, Visualization and Integrated Discovery (DAVID, http://david.abcc.ncifcrf.gov/home.jsp) was used (Huang da et al., 2009).

Sequencing data for whole transcriptome amplification have been deposited in NCBI's Gene Expression Omnibus (Edgar et al., 2002) and are accessible through GEO Series accession number GSE66230 insofar as they are published.

2.2.12 Quantitative real-time PCR

Quantitative real time polymerase chain reaction was performed in Lightcycler 1.5 (Roche) using the Luminaris HiGreen qPCR Kit (Thermo Scientific). 2 µl of diluted

cDNA or amplicons were used for evaluation of amplification efficiency. For validation of differentially expressed transcripts purified amplicons were diluted 1:5 in water after whole transcriptome amplification and 2 µl were used for qPCR. As internal control we always used *Gapdh*. qPCR reactions were set up in a total volume of 20 µl containing 1 µM of forward and reverse primer each and 10 µl 2x Luminaris HiGreen qPCR Master Mix. All primers used are listed in the material section.

3 Results

To investigate the axonal transcriptome of primary mouse motoneurons we used two different approaches. In the first approach we established compartmentalized motoneuron cultures and subjected RNA isolated from both compartments to microarray analysis. In the second approach we again used the compartmentalized motoneuron cultures but now in combination with an optimized whole transcriptome amplification method followed by high-throughput sequencing enabling us to do whole transcriptome profiling. As both approaches have not been applied to primary motoneurons so far, we first were interested in the axonal transcriptome of wildtypic motoneurons. Later on we also used knockdown cultures of the two RNA-binding proteins hnRNP R and Tdp-43, the non-coding RNA 7SK as well as Smn for further analysis.

3.1 Compartmentalized motoneuron cultures

The microfluidic chambers used in this study consist of two compartments, each made of two round reservoirs connected by a main channel (Fig. 1). The two main channels are further connected by thinner 150 µm long microchannels. A volume difference of around 50 µl between the somatodendritic compartment and the axonal compartment allows the isolation of the chemical microenvironments due to the high fluidic resistance of the microchannels.
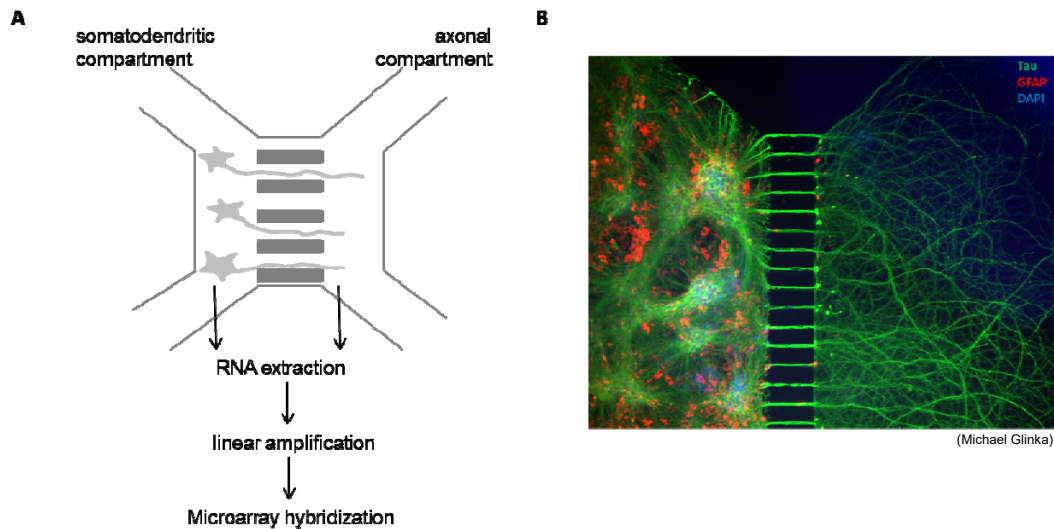
Figure 1: Compartmentalized motoneuron cultures for microarray analysis of somatodendritic and axonal RNA.

(A) Schematic representation of a microfluidic chamber. Primary mouse motoneurons (E12.5) are plated into the left mainchannel (somatodendritic compartment) and extend their axons through 150 µm long microchannels into the right mainchannel (axonal compartment). Directed growth of the axons is achieved via the establishment of a BDNF gradient. (B) Immunofluorescence staining of Tau (green), GFAP (glial fibrillary acidic protein; red) and DAPI (4',6-Diamidin-2-phenylindol; blue). A dense network of axonal processes can be observed in the axonal compartment of the microfluidic chamber. No somata are present in the axonal compartment.

As the separation of cell bodies and axons of primary mouse motoneurons was successful via the microfluidic chambers we subsequently isolated total RNA separately from both compartments. Because especially the RNA amount of the axonal compartment showed to be in the range of 10-50 pg and the microarray analysis requires ~15 µg we decided for linear amplification of the isolated RNA by using an mRNA specific primer. In total we applied two rounds of linear amplification ending up with an RNA amount of ~ 50-60 µg for the somatodendritic compartment and 20-30 µg for the axonal compartment. Thereafter, the RNA was hybridized on a 3'IVT Affymetrix Gene Chip® Mouse Genome 430 2.0 Array and obtained results were analyzed as follows: microarray signal intensities were normalized by quantile normalization (Bolstad et al., 2003) and logarithmized. Normalization and differential expression analysis was done separately for the somatodendritic and axonal compartment to avoid any bias.

3.1.1 Correlation analysis

To get a first impression of the composition of the somatodendritic and especially the axonal transcriptome we started with the analysis of the three replicates of the wildtypic cultures. For the somatodendritic compartment expression values after normalization were highly reproducible for each experiment among the three distinct replicates for each of the 45,101 probesets (R^2=0.99 for all comparisons) (Fig. 2A). On the contrary, the expression values for the three different axonal replicates of the wildtypic cultures were more irregular (R^2=0.74-0.82) and showed a higher variance (Fig. 2B). This observed variability is explained by the low amount of RNA which could be extracted from the axonal compartment. Furthermore, the degree of correlation for single probesets was dependent on their signal intensities. This means that probesets with low expression values correlated less among the replicates compared to probesets with high expression values.
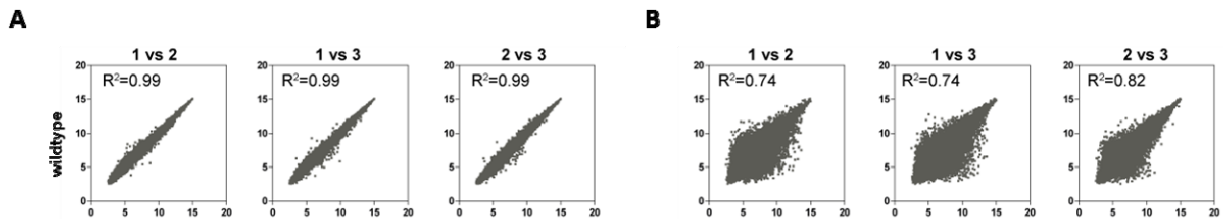
Figure 2: Correlation analysis of wildtype compartmentalized motoneurons. (A) Correlation analysis for the somatodendritic compartments of the microarray experiments of the three wildtypic replicates showing the reproducibility of microarray data. (B) Correlation analysis for the axonal compartments of the microarray experiments of all three wildtypic replicates showing the reproducibility of microarray data. R^2=Pearson correlation coefficient.

To see furthermore the correlation between the composition of motor axons and the somatodendritic compartment we compared the axonal microarray data with the data of their corresponding somatodendritic counterparts. This was done for each of the three independent wildtype motoneuron compartmentalized cultures (Fig. 3). Here, the correlation coefficient R^2 was in the range of 0.71-0.80, showing a robust correlation between somatodendritic and axonal microarray data, indicating a highly similar RNA composition in both compartments.
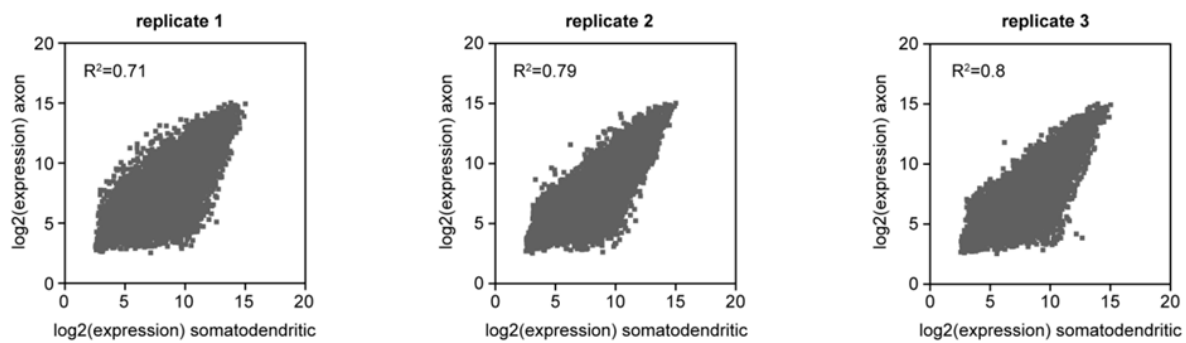
Figure 3: Correlation analysis of both compartments of wildtype compartmentalized motoneurons. Correlation of somatodendritic with axonal microarray expression values for all three replicates of the wildtype motoneuron compartmentalized cultures. R^2=Pearson correlation coefficient.

3.1.2 GO (gene ontology) term analysis

In a next step, we analyzed via GOterm analysis the axonal transcriptome of wild-type motoneurons by examining the functions which are associated with the top 5000 ranked probesets. In the same way we obtained GOterms enriched among the top 5000 somatodendritic probesets (Fig. 4). Likewise, we also examined the bottom 5000 ranked probesets for each compartment to control the specificity of our data sets. 3764 probesets (75.3%) were shared among the top 5000 probesets between the somatodendritic and axonal compartments. This overlap is also reflected by the uniformity of the GOterms enriched for each compartment. The most significant GOterms were related to translation, protein transport, energy production and RNA binding for both compartments. In contrast, GOterms associated with the 5000 bottom ranked transcripts were related to pheromone response or plasma membrane localization and showed less significance. Moreover, the level of significance for a number of GOterms enriched among the top 5000 ranked probesets was much higher for the axonal than for the somatodendritic compartment.
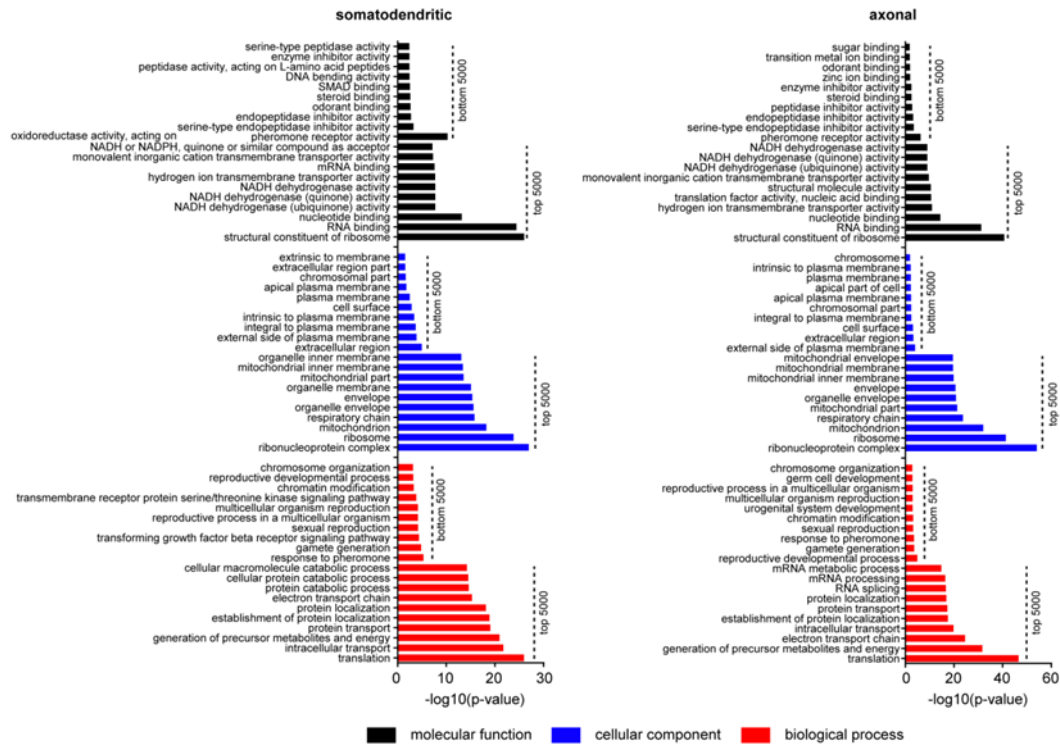
Figure 4: GOterm analysis for wildtype compartmentalized motoneurons.
GOterm analysis of the top 5000 expressed and bottom 5000 expressed transcripts in the somatodendritic and axonal compartment.

Because of this reason we selected all GOterms of the three ontologies common to both compartments to match their significance (Fig. 5). For each of the three ontologies "biological process", "cellular component" and "molecular function" GOterms related to protein synthesis (e.g. "translation", "ribosome" and "structural constituent of ribosome"), energy metabolism ("generation of precursor metabolites and energy", "electron transport chain" and "mitochondrion") or RNA binding ("ribonucleoprotein complex" and "RNA binding") were more significantly enriched in the axonal compartment compared to the somatodendritic compartment. Interestingly, the GOterm "synapse" was significantly enriched in the somatodendritic compartment, although this can be explained by the inclusion of postsynaptic components in this GOterm as well as the enrichment of further GOterms related to synaptic functions ("regulation of neurotransmitter levels" and "synaptic transmission) on the somatodendritic side.
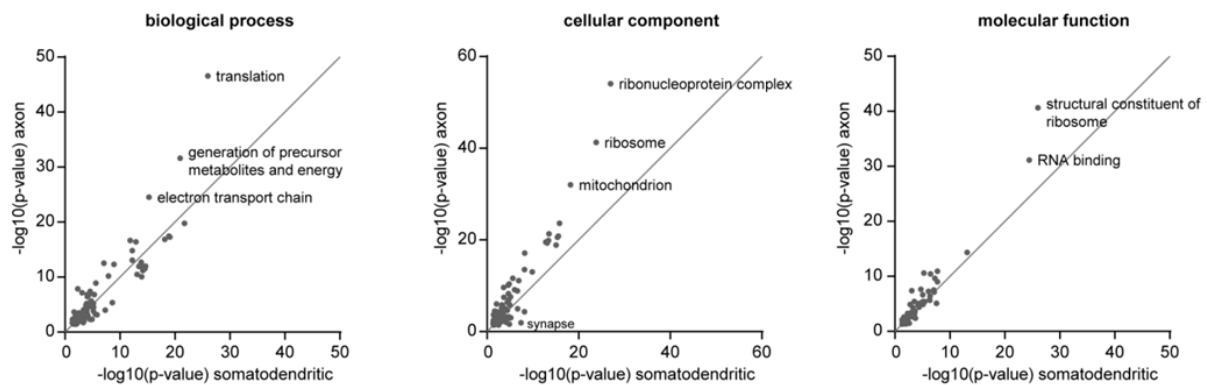
**Figure 5: Enrichment analysis for GOterms enriched in either compartment.**

The enrichment of GOterms common to the top 5000 expressed somatodendritic and axonal transcripts for the different ontologies.

3.2 Microarray results for hnRNP R knockdown

As we already obtained interesting results for the axonal transcriptome of wildtypic motoneurons grown in compartmentalized cultures, we asked whether these transcriptome changes upon knockdown of RNA binding proteins associated with functions in the axonal localization of mRNAs. First we started with a knockdown of the RNA binding protein hnRNP R and continued later on with a knockdown of Tdp-43 and Smn. Although Smn itself is no RNA binding protein we still thought it to be an interesting candidate considering its known function in RNP complexes and its protein interactions with hnRNP R and Tdp-43.

3.2.1 Verification of hnRNP R knockdown

Before hybridization of the amplified RNA on the microarray the knockdown efficiency of hnRNP R was verified via quantitative PCR (qPCR). Although the knockdown efficiency was slightly different for all three replicates, a knockdown efficacy of 50-60% could be achieved in all experiments (Fig. 6).
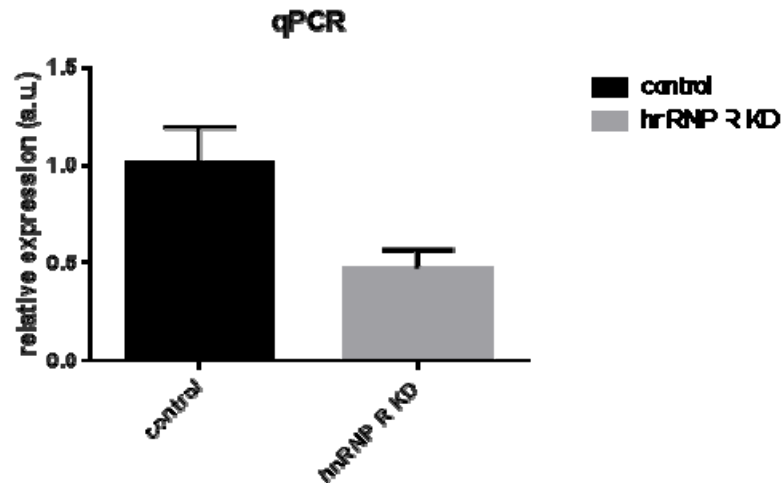
Figure 6: Determination of hnRNP R knockdown efficiency.

hnRNP R transcript expression levels on the somatodendritic side of compartmentalized hnRNP R knockdown motoneurons. Transcript levels are measured relative to controls and are presented as relative expression validated by quantitative PCR. Data are mean with standard deviation.

3.2.2 Correlation and differential expression analysis for hnRNP R knockdown

For analysis of the microarray data we first investigated the correlation of the somatodendritic and axonal transcriptome upon hnRNP R knockdown. Motoneuron cultures transfected with the empty lentiviral expression vector plus the wildtype motoneuron cultures described above were used as reference data sets. Correlation analysis of the individual replicate data sets of hnRNP R knockdown motoneurons and controls showed comparable results (Fig. 7). As already described above for the wildtype cultures, also the hnRNP R knockdown cultures showed a reproducible correlation for the somatodendritic compartment (R^2=0.99) (Fig. 7A). In contrast, the expression values for the three replicates of the axonal compartment were again more variable (R^2=0.48-0.61) (Fig. 7B).
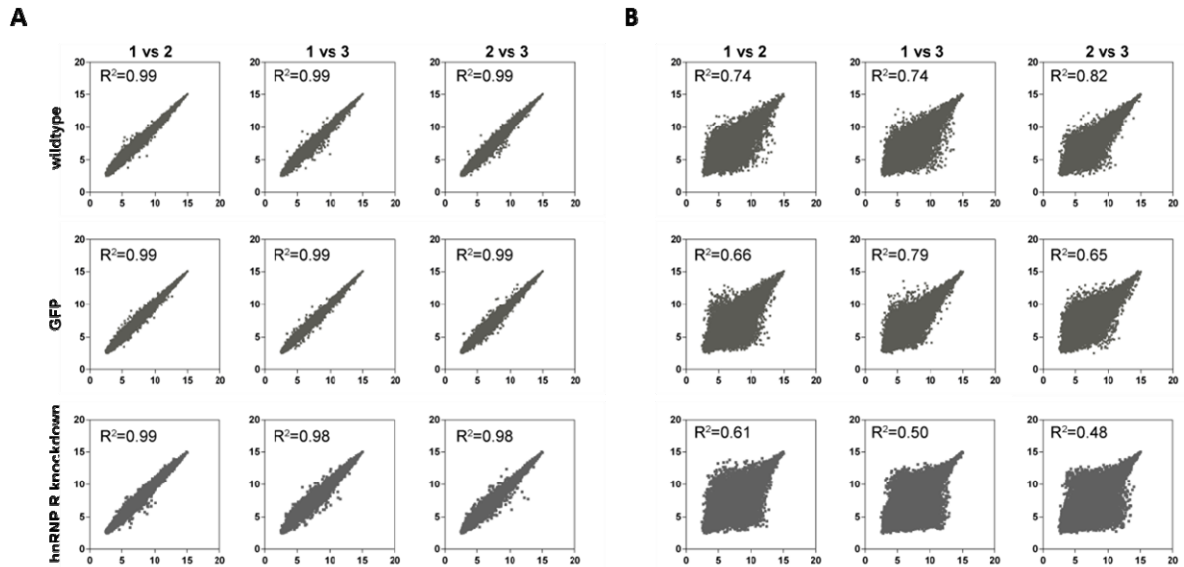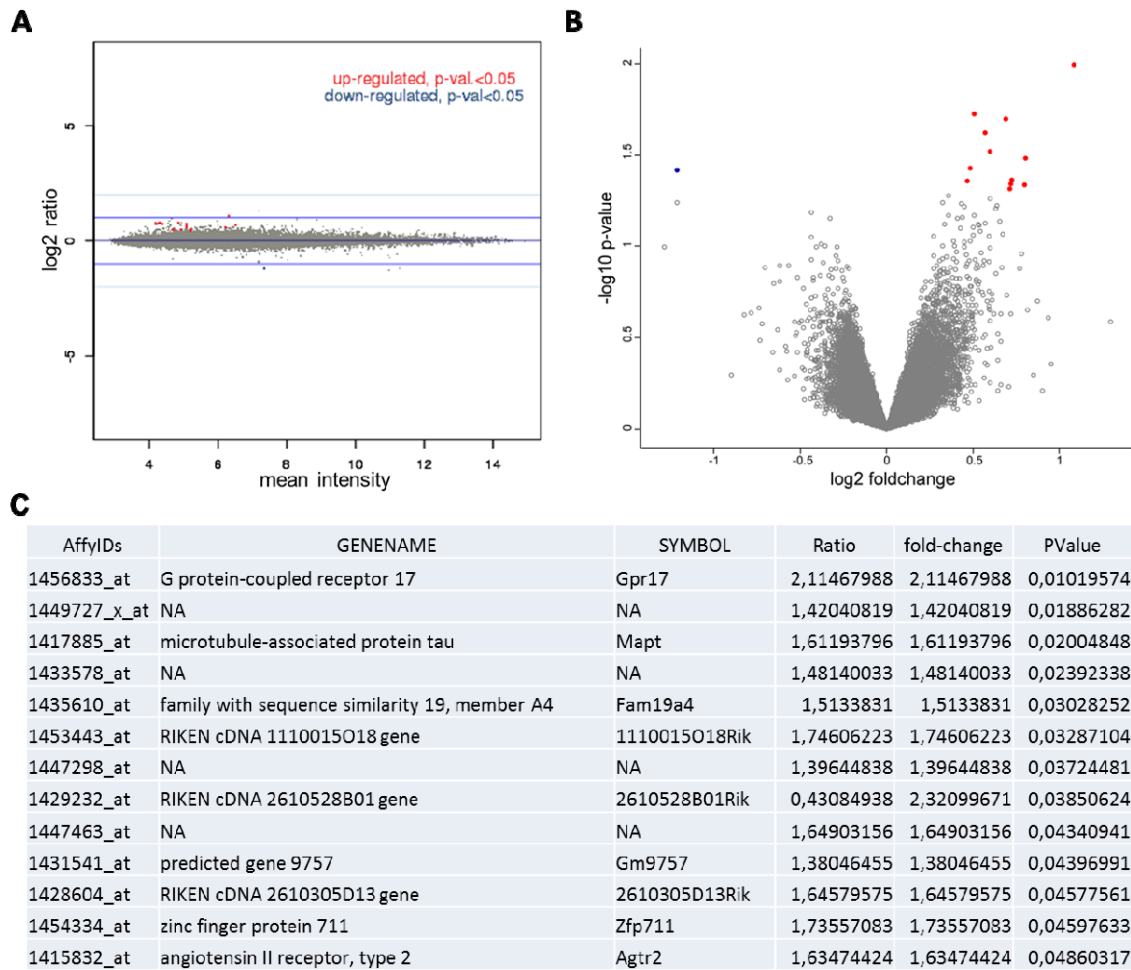
Figure 7: Correlation analysis of hnRNP R knockdown compartmentalized motoneurons.
(A) Correlation analysis for the somatodendritic compartments of the microarray experiments of the three hnRNP R knockdown replicates in comparison to the controls showing the reproducibility of microarray data. (B) Correlation analysis for the axonal compartments of the microarray experiments of the three hnRNP R knockdown replicates in comparison to the controls showing the reproducibility of microarray data. R^2=Pearson correlation coefficient.

Differential expression analysis of the microarray data for the somatodendritic compartment of hnRNP R knockdown motoneurons revealed just a few transcript changes (Fig. 8). Altogether 13 probesets were significantly deregulated ($P<0.05$), of which 12 were upregulated and 1 probeset showed downregulation. The latter corresponded to the *hnRNP R* transcript.
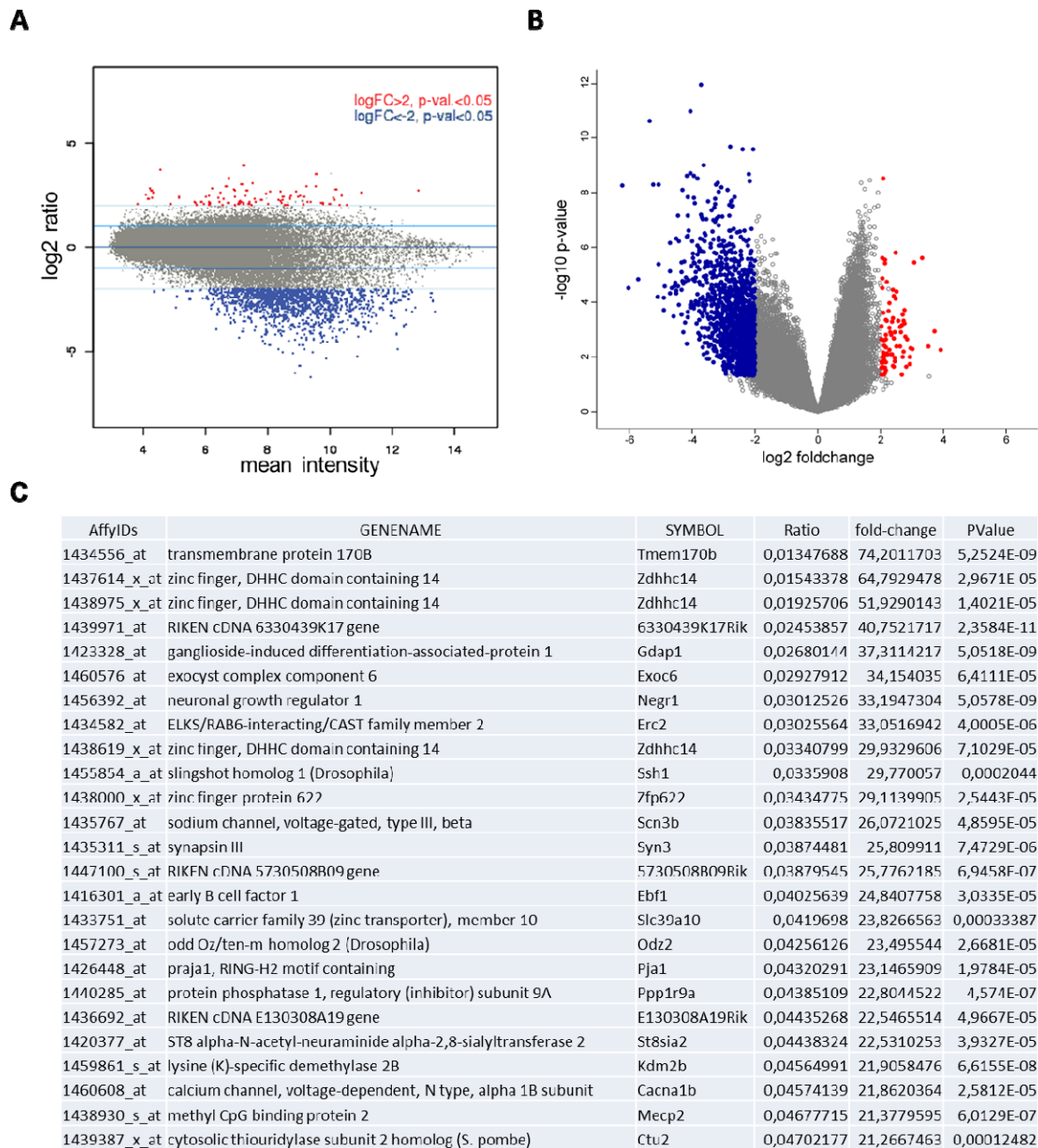
Figure 8: Differential gene expression analysis of the somatodendritic compartment of hnRNP R knockdown compartmentalized motoneurons.

(A) MA plot for the somatodendritic compartment of hnRNP R knockdown motoneurons. The relationship between the change in gene expression (log$_2$ ratio) upon hnRNP R knockdown relative to wildtype motoneurons and control vector and the average level of gene expression (mean intensity) for each microarray probeset is shown. Significantly ($P<0.05$) upregulated (red) and downregulated (blue) transcripts are indicated. (B) Volcano plot for the somatodendritic compartment of hnRNP R knockdown motoneurons. The significance of gene expression [log$_{10}(P)$] for each probeset relative to the magnitude of change (log$_2$ ratio) is indicated. Significantly ($P<0.05$) upregulated (red) and downregulated (blue) transcripts are indicated. (C) Probesets deregulated in the somatodendritic compartment of hnRNP R knockdown motoneurons. Probesets are ranked according to *p*-value.

In contrast, the same analysis of the axonal compartment showed substantial changes in transcript abundance (Fig. 9).

A

B

C

AffyIDs	GENENAME	SYMBOL	Ratio	fold-change	PValue
1434556_at	transmembrane protein 170B	Tmem170b	0,01347688	74,2011703	5,2524E-09
1437614_x_at	zinc finger, DHHC domain containing 14	Zdhhc14	0,01543378	64,7929478	2,9671E 05
1438975_x_at	zinc finger, DHHC domain containing 14	Zdhhc14	0,01925706	51,9290143	1,4021E-05
1439971_at	RIKEN cDNA 6330439K17 gene	6330439K17Rik	0,02453857	40,7521717	2,3584E-11
1423328_at	ganglioside-induced differentiation-associated-protein 1	Gdap1	0,02680144	37,3114217	5,0518E-09
1460576_at	exocyst complex component 6	Exoc6	0,02927912	34,154035	6,4111E-05
1456392_at	neuronal growth regulator 1	Negr1	0,03012526	33,1947304	5,0578E-09
1434582_at	ELKS/RAB6-interacting/CAST family member 2	Erc2	0,03025564	33,0516942	4,0005E-06
1438619_x_at	zinc finger, DHHC domain containing 14	Zdhhc14	0,03340799	29,9329606	7,1029E-05
1455854_a_at	slingshot homolog 1 (Drosophila)	Ssh1	0,0335908	29,770057	0,0002044
1438000_x_at	zinc finger protein 622	Zfp622	0,03434775	29,1139905	2,5443E-05
1435767_at	sodium channel, voltage-gated, type III, beta	Scn3b	0,03835517	26,0721025	4,8595E-05
1435311_s_at	synapsin III	Syn3	0,03874481	25,809911	7,4729E-06
1447100_s_at	RIKEN cDNA 5730508B09 gene	5730508B09Rik	0,03879545	25,7762185	6,9458E-07
1416301_a_at	early B cell factor 1	Ebf1	0,04025639	24,8407758	3,0335E-05
1433751_at	solute carrier family 39 (zinc transporter), member 10	Slc39a10	0,0419698	23,8266563	0,00033387
1457273_at	odd Oz/ten-m homolog 2 (Drosophila)	Odz2	0,04256126	23,495544	2,6681E-05
1426448_at	praja1, RING-H2 motif containing	Pja1	0,04320291	23,1465909	1,9784E-05
1440285_at	protein phosphatase 1, regulatory (inhibitor) subunit 9A	Ppp1r9a	0,04385109	22,8044522	4,574E-07
1436692_at	RIKEN cDNA E130308A19 gene	E130308A19Rik	0,04435268	22,5465514	4,9667E-05
1420377_at	ST8 alpha-N-acetyl-neuraminide alpha-2,8-sialyltransferase 2	St8sia2	0,04438324	22,5310253	3,9327E-05
1459861_s_at	lysine (K)-specific demethylase 2B	Kdm2b	0,04564991	21,9058476	6,6155E-08
1460608_at	calcium channel, voltage-dependent, N type, alpha 1B subunit	Cacna1b	0,04574139	21,8620364	2,5812E-05
1438930_s_at	methyl CpG binding protein 2	Mecp2	0,04677715	21,3779595	6,0129E-07
1439387_x_at	cytosolic thiouridylase subunit 2 homolog (S. pombe)	Ctu2	0,04702177	21,2667463	0,00012482

Figure 9: **Differential gene expression analysis of the axonal compartment of hnRNP R knockdown compartmentalized motoneurons.**

(A) MA plot for the axonal compartment of hnRNP R knockdown motoneurons. The relationship between the change in gene expression (log$_2$ ratio) upon hnRNP R knockdown relative to wildtype motoneurons and control vector and the average level of gene expression (mean intensity) for each microarray probeset is shown. Significantly ($P<0.05$) upregulated (red) and downregulated (blue) transcripts are indicated. (B) Volcano plot for the axonal compartment of hnRNP R knockdown motoneurons. The significance of gene expression [log$_{10}$(P)] for each probeset relative to the magnitude of change (log$_2$ ratio) is indicated. Significantly ($P<0.05$) upregulated (red) and

downregulated (blue) transcripts are indicated. (C) Probesets downregulated in the axonal compartment of hnRNP R knockdown motoneurons. Probesets are ranked according to fold-change. The 25 most downregulated probesets are shown.

3.2.3 GOterm analysis for hnRNP R knockdown

Subsequently, we also applied GOterm analysis to the hnRNP R knockdown data. As we hardly detected any changes (Fig. 8C) in the somatodendritic compartment after hnRNP R knockdown, we only applied the analysis to the deregulated probesets of the axonal compartment (Fig. 10). Because the total number of changed probesets was too high to obtain a significant GOterm result, we decided to narrow down the number of probesets used for GOterm analysis. Therefore we set the cutoff at p-value <0.05 and foldchange >4. This threshold was consecutively used for the GOterm analysis of changed probesets in the axonal compartment of all knockdown microarray experiments.

Interestingly, among the downregulated transcripts in the axonal compartment upon hnRNP R deficiency we found an enrichment for GOterms associated with synapse function (for transcripts like ankyrin 3 and neurexin 1) and neuron projection (for transcripts like MYC binding protein 2, N-type calcium channel 1B (Cav2.2) and neurofilament light chain). Even GOterms for RNA or nucleotide binding showed an enrichment. Interesting transcripts to mention here are mRNAs encoding different translation initiation factors or RNA-binding proteins. In contrast, axonally upregulated transcripts were shown to have functions in cell proliferation (cyclin D2 and endothelin 3).
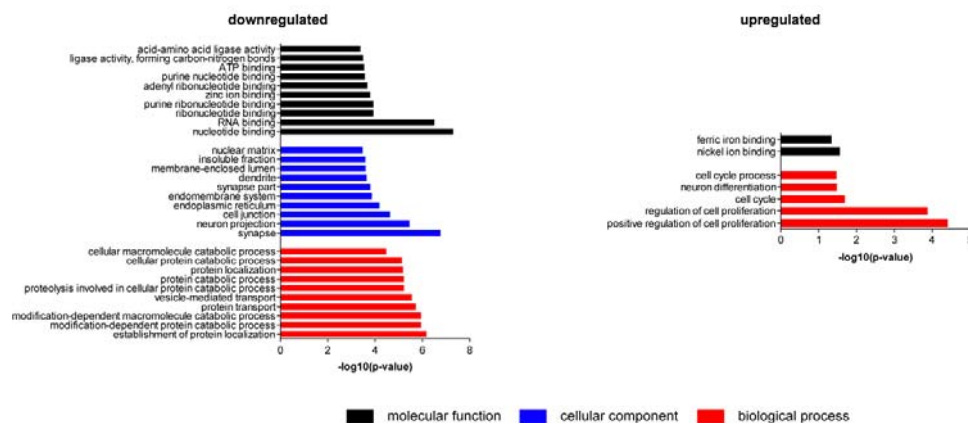
Figure 10: GOterm analysis for hnRNP R knockdown compartmentalized motoneurons.

GOterm analysis of transcripts deregulated in the axonal compartment of hnRNP R knockdown motoneurons. The top ten GO categories "molecular function", "cellular component" and "biological process" are shown for transcripts downregulated or upregulated upon hnRNP R depletion relative to wildtype motoneurons and vector control. Only significantly ($P<0.05$) deregulated transcripts were considered.

3.3 Microarray results for Tdp-43 knockdown

3.3.1 Verification of Tdp-43 knockdown

For the Tdp-43 knockdown experiments knockdown efficency was again first verified via qPCR before hybridization of RNA onto the microarray (Fig. 11). Knockdown efficiency was conclusive for all three replicates as a mean knockdown efficacy of 70% could be achieved.
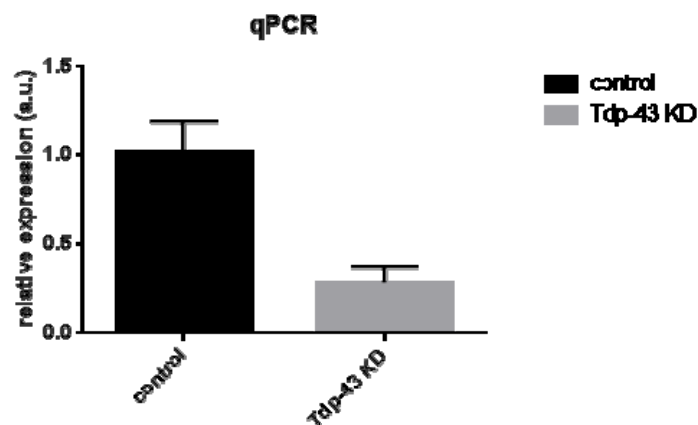
Figure 11: Determination of Tdp-43 knockdown efficiency.
Tdp-43 transcript expression levels on the somatodendritic side of compartmentalized Tdp-43 knockdown motoneurons. Transcript levels are measured relative to controls and are presented as relative expression validated by quantitative PCR. Data are mean with standard deviation.

3.3.2 Correlation and differential expression analysis for Tdp-43 knockdown

Subsequently, we again analyzed the correlation of both separate compartments among the three different replicates of the Tdp-43 knockdown cultures. Again the somatodendritic compartments showed a high correlation ($R^2=0.98$-0.99) (Fig. 12A)

compared to the three distinct axonal compartments being more variable (R^2=0.44-0.82) (Fig. 12B).
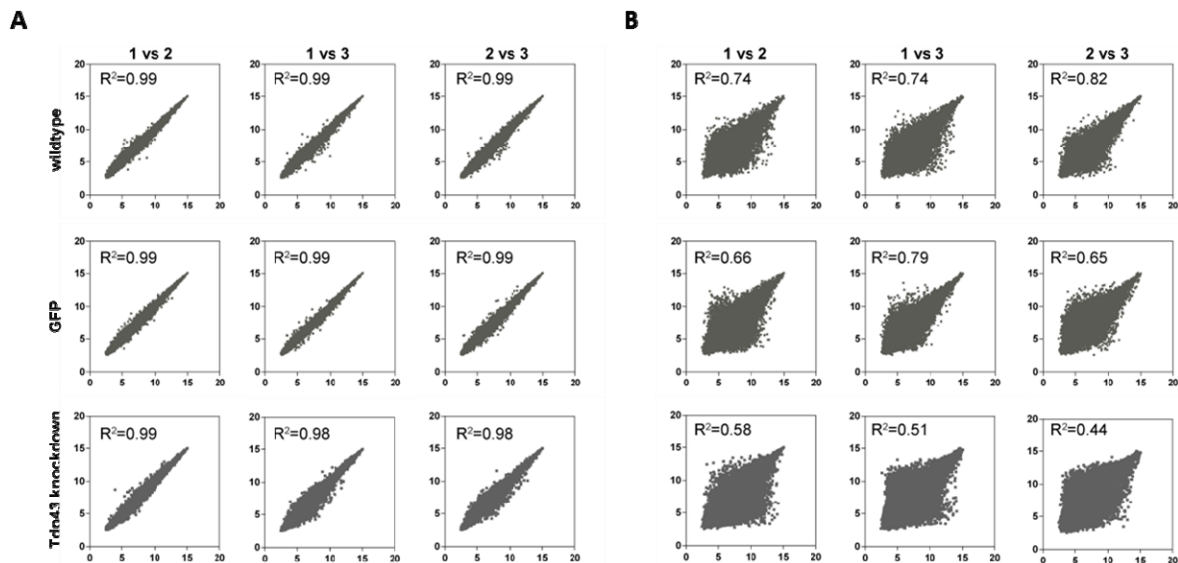
Figure 12: Correlation analysis of Tdp-43 knockdown compartmentalized motoneurons.
(A) Correlation analysis for the somatodendritic compartments of the microarray experiments of the three Tdp-43 knockdown replicates in comparison to the controls showing the reproducibility of microarray data. **(B)** Correlation analysis for the axonal compartments of the microarray experiments of the three Tdp-43 knockdown replicates in comparison to the controls showing the reproducibility of microarray data. R^2=Pearson correlation coefficient.

The MA plot for the somatodendritic compartment of the Tdp-43 knockdown looks quite similar to the MA plot of the somatodendritic compartment of the hnRNP R knockdown (Fig. 8) although there were some more changes detected (Fig. 13). In total, via differential expression analysis we detected 213 probesets (corresponding to 145 genes) (Fig. 13C) to be significantly deregulated in the somatodendritic compartment after Tdp-43 depletion. Of these, 134 probesets (86 genes) showed an upregulation compared to 79 probesets (59 genes) which appeared to be downregulated upon Tdp-43 deficiency. As probesets for Tdp-43 mRNA were also present on the microarray chip and also revealed a downregulation of Tdp-43 mRNA after differential expression analysis (Fig. 13B and C), this further confirmed the previously obtained qPCR results of the knockdown validation (Fig. 11).
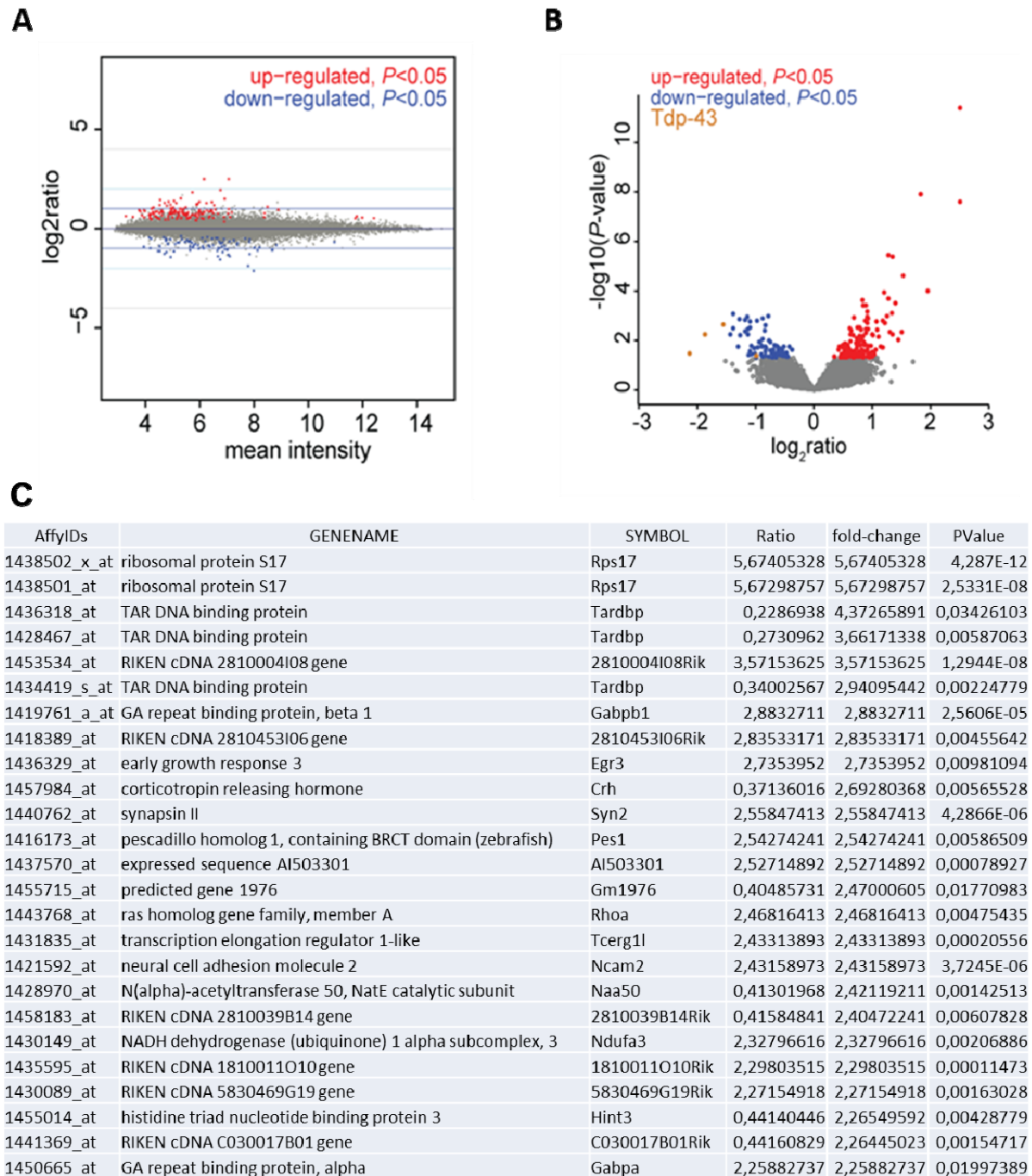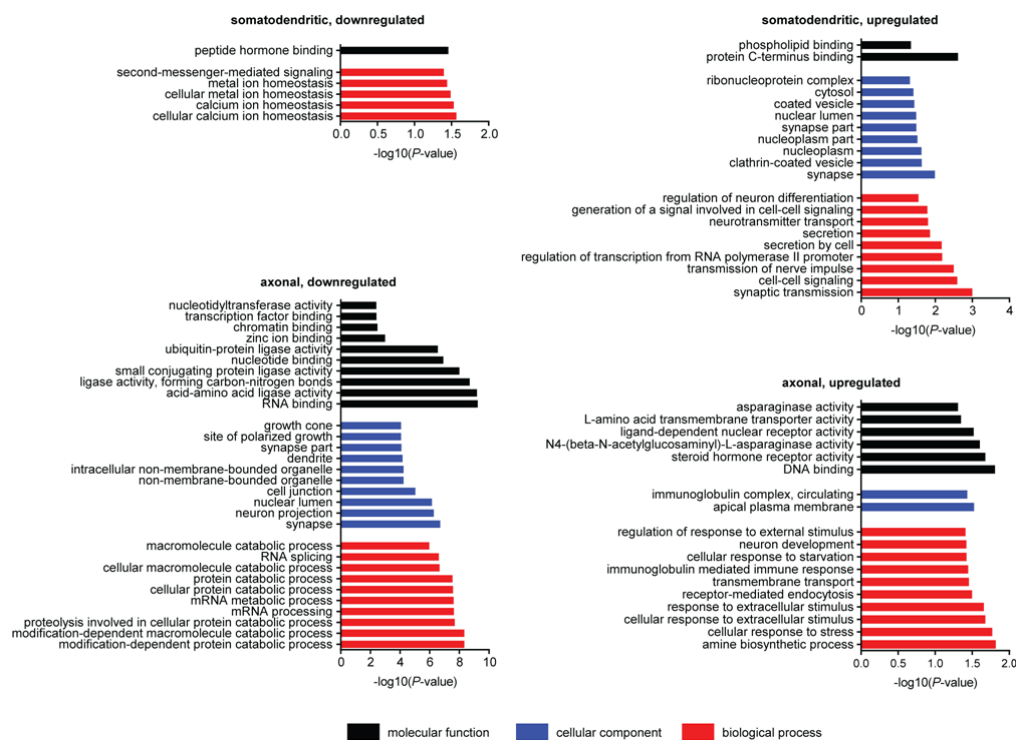
Figure 13: Differential gene expression analysis of the somatodendritic compartment of Tdp-43 knockdown compartmentalized motoneurons.

(A) MA plot for the somatodendritic compartment of Tdp-43 knockdown motoneurons. The relationship between the change in gene expression ($\log_2$ ratio) upon Tdp-43 knockdown relative to wildtype motoneurons and control vector and the average level of gene expression (mean intensity) for each microarray probeset is shown. Significantly ($P<0.05$) upregulated (red) and downregulated (blue) transcripts are indicated. (B) Volcano plot for the somatodendritic compartment of Tdp-43 knockdown motoneurons. The significance of gene expression [$\log_{10}(P)$] for each probeset relative to the

magnitude of change (log$_2$ ratio) is indicated. Significantly (*P*<0.05) upregulated (red) and downregulated (blue) transcripts are indicated. Tdp-43 transcripts are shown in brown. (C) Probesets deregulated in the somatodendritic compartment of Tdp-43 knockdown motoneurons. Probesets are ranked according to fold-change. The 25 most deregulated probesets are shown.

In contrast, the MA plot and the volcano plot for the axonal compartment of the Tdp-43 knockdown again show a higher number of changes, revealing mostly downregulated probesets (Fig. 14). In detail, differential expression analysis revealed 1886 probesets (1602 genes) to be deregulated in the axonal compartment after Tdp-43 suppression. 246 probesets (203 genes) displayed an upregulation in contrast to 1640 probesets (1399 genes) showing a downregulation (Fig. 14C). Also in the axonal compartment, probesets for Tdp-43 mRNA could be identified among the downregulated probesets.

A

log2ratio>2, *P*<0.05
log2ratio<-2, *P*<0.05

B

log2ratio>2, *P*<0.05
log2ratio<-2, *P*<0.05
Tdp-43

C

| AffyIDs	GENENAME	SYMBOL	Ratio	fold-change	PValue
1456293_s_at	cyclin H	Ccnh	0,00884369	113,074997	1,1363E-06
1428379_at	solute carrier family 17 (sodium dependent inorganic phosphate cotransporter), member 6	Slc17a6	0,01512833	66,1011553	2,7365E 07
1425837_a_at	CCR4 carbon catabolite repression 4-like (S. cerevisiae)	Ccrn4l	0,01539127	64,9718949	1,4872E-09
1424463_at	major facilitator superfamily domain containing 6	Mfsd6	0,01701993	58,7546329	3,2918E-06
1459860_x_at	tripartite motif-containing 2	Trim2	0,01736451	57,588721	3,482E-07
1416065_a_at	ankyrin repeat domain 10	Ankrd10	0,01747794	57,2149877	6,4518E-09
1448443_at	serine (or cysteine) peptidase inhibitor, clade I, member 1	Serpini1	0,02019652	49,5134766	1,2504E-08
1435805_at	lin-7 homolog A (C. elegans)	Lin7a	0,02587453	38,6480418	5,0363E-06
1460608_at	calcium channel, voltage-dependent, N type, alpha 1B subunit	Cacna1b	0,02719895	36,7661306	3,0091E-06
1437528_x_at	RIKEN cDNA A730017C20 gene	A730017C20Rik	0,02822035	35,4354263	2,9639E-07
1433552_a_at	polymerase (RNA) II (DNA directed) polypeptide B	Polr2b	0,02847474	35,1188435	0,00061688
1447825_x_at	protocadherin 8	Pcdh8	0,0289506	34,5416018	8,4144E-07
1452700_s_at	kelch repeat and BTB (POZ) domain containing 7	Kbtbd7	0,02938172	34,034/684	0,0001098
1433794_at	senataxin	Setx	0,02996302	33,3744697	1,385E-07
1439627_at	zinc finger protein of the cerebellum 1	Zic1	0,03013821	33,1804696	0,00180754
1455324_at	phosphatidylinositol-specific phospholipase C, X domain containing 2	Plcxd2	0,03092989	32,3311812	9,4317E-09
1454672_at	neurofilament, light polypeptide	Nefl	0,03178482	31,4615552	0,00063336
1426956_a_at	transformation related protein 53 binding protein 1	Trp53bp1	0,03284363	30,4473012	0,00026824
1435933_at	sodium channel, voltage-gated, type II, alpha 1	Scn2a1	0,03401232	29,4011132	1,3952E-06
1455444_at	gamma-aminobutyric acid (GABA) A receptor, subunit alpha 2	Gabra2	0,03405505	29,3642217	5,2317E-07
1416767_a_at	RIKEN cDNA 1110003F01 gene	1110003F01Rik	0,03420037	29,239449	9,8264F-05
1452771_s_at	acyl-CoA synthetase long-chain family member 3	Acsl3	0,03596462	27,8051034	5,8831E-10
1436602_x_at	calcium channel, voltage-dependent, N type, alpha 1B subunit	Cacna1b	0,03610602	27,6962112	1,0056E-05
1438006_a_at	deoxythymidylate kinase	Dtymk	0,03706325	26,9809012	1,9639E-06
1439971_at	RIKEN cDNA 6330439K17 gene	6330439K17Rik	0,03770382	26,5225082	2,6652E-10

Figure 14: Differential gene expression analysis of the axonal compartment of Tdp-43 knockdown compartmentalized motoneurons.

(A) MA plot for the axonal compartment of Tdp-43 knockdown motoneurons. The relationship between the change in gene expression (log_2 ratio) upon Tdp-43 knockdown relative to wildtype motoneurons and control vector and the average level of gene expression (mean intensity) for each microarray probeset is shown. Significantly ($P<0.05$) upregulated (red) and downregulated (blue) transcripts are indicated. (B) Volcano plot for the axonal compartment of Tdp-43 knockdown motoneurons. The significance of gene expression [$log_{10}(P)$] for each probeset relative to the magnitude of change (log_2 ratio) is indicated. Significantly ($P<0.05$) upregulated (red) and downregulated (blue) transcripts are indicated. (C) Probesets downregulated in the axonal compartment of Tdp-43 knockdown motoneurons. Probesets are ranked according to fold-change. The 25 most deregulated probesets are shown.

3.3.3 GOterm analysis for Tdp-43 knockdown

GOterm analysis for the probesets downregulated in the somatodendritic compartment upon Tdp-43 depletion revealed an enrichment for GOterms like peptide hormone binding and calcium ion homeostasis (Fig. 15). Upregulated probesets showed an enrichment for GOterms like synapse (synapsin II, synaptotagmin I and VII), synaptic transmission (ataxin 1, syntaxin 1B) and protein C-terminus binding (ataxin 1, zinc finger and BTB domain containing 16).

The few upregulated transcripts in the axonal compartment after Tdp-43 suppression referred to GOterms like DNA binding, and amine biosynthetic process. Interestingly, the GOterms for the downregulated transcripts in the axonal compartment showed the highest enrichment. Here, we found GOterms for RNA binding, synapse, neuron projection and GOterms describing catabolic processes to be highly enriched.

Figure 15: GOterm analysis for Tdp-43 knockdown compartmentalized motoneurons.
GOterm analysis of transcripts deregulated in the somatodendritic and axonal compartment of Tdp-43 knockdown motoneurons. The top ten GO categories "molecular function", "cellular component" and "biological process" are shown for transcripts downregulated or upregulated upon Tdp-43 depletion relative to wildtype motoneurons and vector control. Only significantly ($P<0.05$) deregulated transcripts were considered.

3.4 Microarray results for Smn knockdown

3.4.1 Verification of Smn knockdown

For Smn knockdown we verified in a first experiment the knockdown efficiency of the lentivirus via quantitative PCR (Fig. 16). In all three replicates a reduction of the Smn transcript level by >90% relative to controls could be observed.
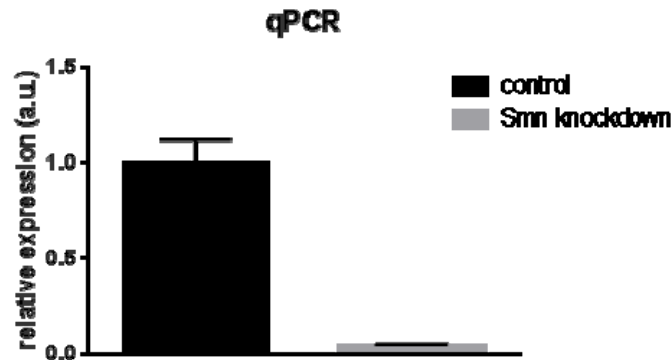
Figure 16: Determination of Smn knockdown efficiency.

Smn transcript expression levels on the somatodendritic side of compartmentalized Smn knockdown motoneurons. Transcript levels are measured relative to controls. Transcript levels are presented as relative expression validated by quantitative PCR. Data are mean with standard deviation.

3.4.2 Correlation and differential expression analysis for Smn knockdown

Again we first started with a correlation analysis of the separate compartments among all the three replicates. Even here, the somatodendritic compartments revealed a robust correlation (R^2=0.99) (Fig. 17A) compared to the axonal compartments (R^2=0.65-0.82) (Fig. 17B).
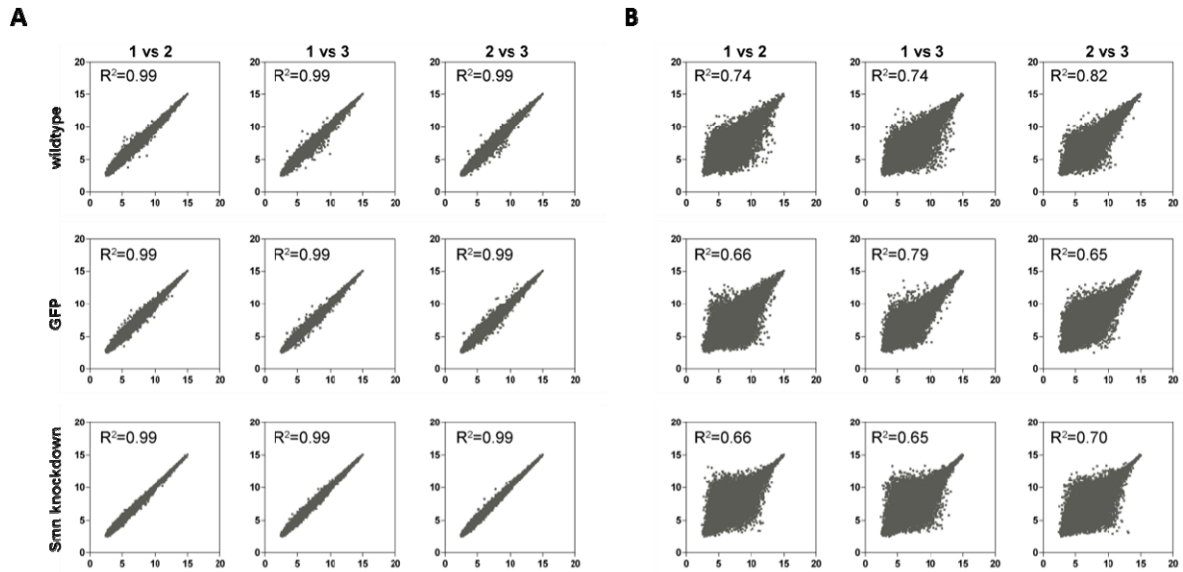
Figure 17: Correlation analysis of Smn knockdown compartmentalized motoneurons.
(A) Correlation analysis for the somatodendritic compartments of the microarray experiments of the three Smn knockdown replicates in comparison to the controls showing the reproducibility of microarray data. **(B)** Correlation analysis for the axonal compartments of the microarray experiments of the three Smn knockdown replicates in comparison to the controls showing the reproducibility of microarray data. R^2=Pearson correlation coefficient.

For differential expression analysis of the Smn knockdown microarray data MA plots were performed revealing substantial changes in transcript abundance in both the somatodendritic and the axonal compartment after Smn knockdown. Overall 2058 probesets were changed significantly ($P<0.05$) on the somatodendritic side (Fig. 18A), among which the top 50 most significantly deregulated probesets were all upregulated (Fig. 18B).
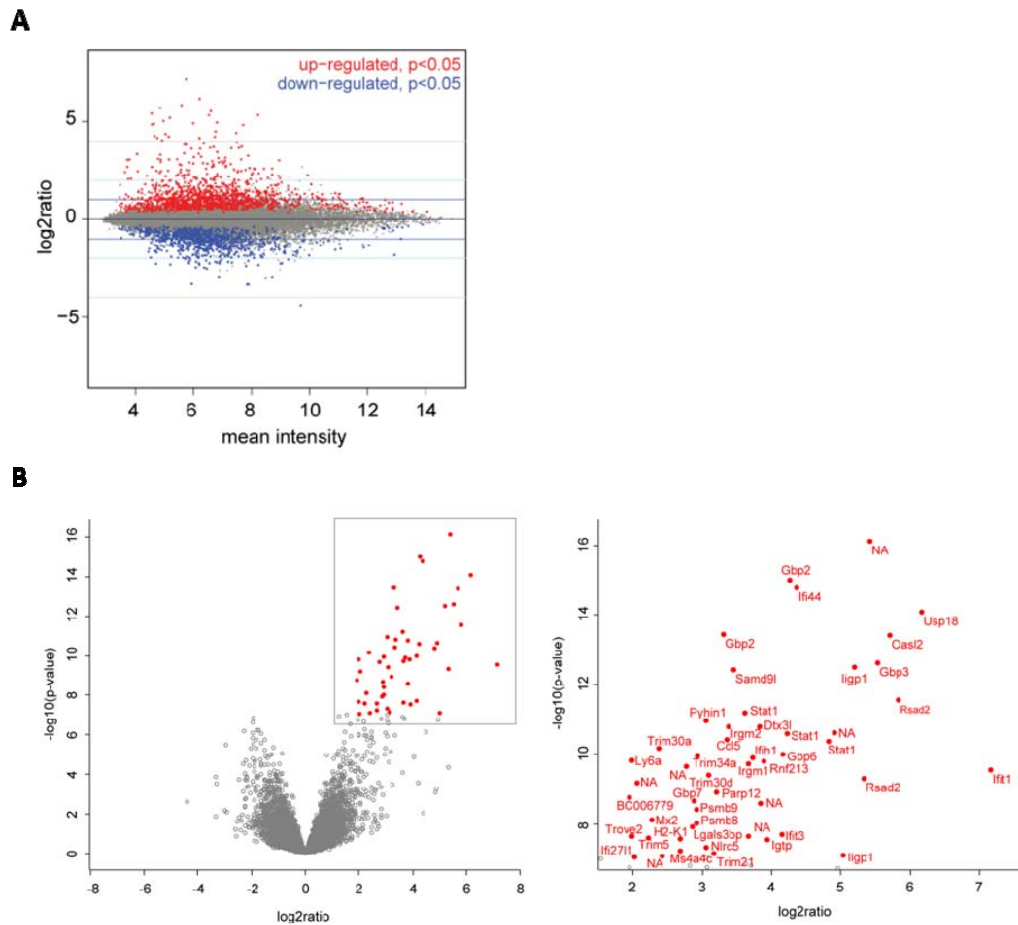
Figure 18: Differential gene expression analysis of the somatodendritic compartment of Smn knockdown compartmentalized motoneurons.

(A) MA plot for the somatodendritic compartment of Smn knockdown motoneurons. The relationship between the change in gene expression ($\log_2$ ratio) upon Smn knockdown relative to wildtype motoneurons and control vector and the average level of gene expression (mean intensity) for each microarray probeset is shown. Significantly ($P<0.05$) upregulated (red) and downregulated (blue) transcripts are indicated. (B) Volcano plot for the somatodendritic compartment of Smn knockdown motoneurons. The significance of gene expression [$\log_{10}(P)$] for each probeset relative to the magnitude of change ($\log_2$ ratio) is indicated. The top 50 most significantly deregulated transcripts are shown in red.

Especially transcripts with relation to the interferon pathway like signal *transducer and activator of transcription 1* (*Stat1*), *guanylate binding protein 3* (*Gbp3*) and *ubiquitin specific peptidase* (*Usp18*) showed a remarkable increase in transcript abundance.

In contrast to the somatodendritic compartment with transcriptional changes occurring in both directions, in the axonal compartment mostly downregulated

transcripts were detected (Fig. 19). In total, we detected changes for 1354 probesets. 1189 probesets were asigned as downregulated (Table 7) compared to only 165 probesets being upregulated (Table 8).
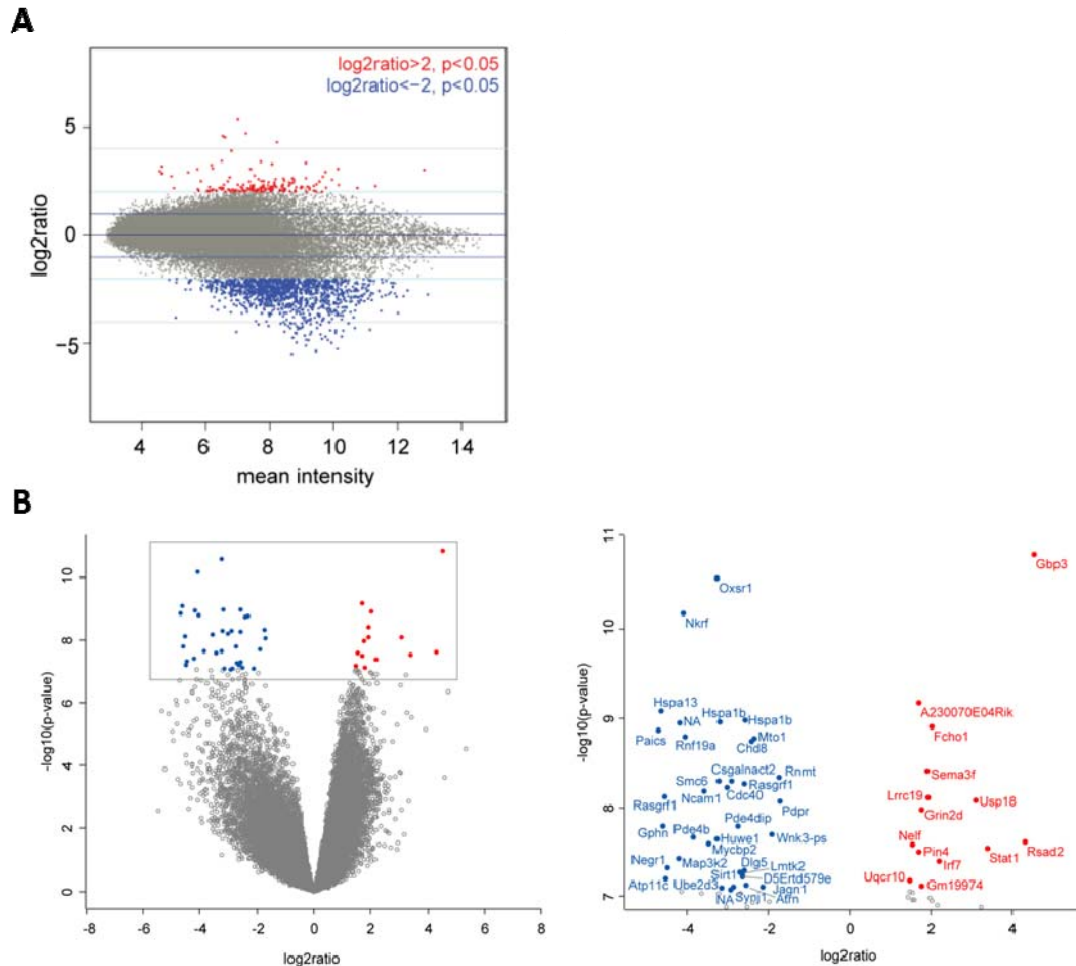
Figure 19: Differential gene expression analysis of the axonal compartment of Smn knockdown compartmentalized motoneurons.

(A) MA plot for the axonal compartment of Smn knockdown motoneurons. The relationship between the change in gene expression (log$_2$ ratio) upon Smn knockdown relative to wildtype motoneurons and control vector and the average level of gene expression (mean intensity) for each microarray probeset is shown. Significantly (P<0.05) upregulated (red) and downregulated (blue) transcripts are indicated. (B) Volcano plot for the axonal compartment of Smn knockdown motoneurons. The significance of gene expression [log$_{10}$(P)] for each probeset relative to the magnitude of change (log$_2$ ratio) is indicated. Upregulated transcripts are shown in red, downregulated transcripts are shown in blue.

Table 7: Probesets downregulated in the axonal compartment of Smn knockdown motoneurons.

Probesets are ranked according to Fold change. The 25 most downregulated probesets are shown.

AffyIDs	GENENAME	SYMBOL	Ratio	Fold change	p-value
1449732_at	zinc finger and SCAN domain containing 21	Zscan21	0,02265462	44,1411037	0,00272014
1434582_at	ELKS/RAB6-interacting/CAST family member 2	Erc2	0,02471102	40,4677787	1,7468E-06
1440201_at	solute carrier family 8 (sodium/calcium exchanger), member 1	Slc8a1	0,02623088	38,1230044	0,00013117
1435311_s_at	synapsin III	Syn3	0,02923022	34,2111665	2,2564E-06
1438531_at	RIKEN cDNA A730054J21 gene	A730054J21Rik	0,03180125	31,4453093	8,198E-06
1448339_at	transmembrane protein 30A	Tmem30a	0,03222293	31,0337991	1,5416E-05
1437528_x_at	RIKEN cDNA A730017C20 gene	A730017C20Rik	0,03485763	28,6881236	7,8045E-07
1437852_x_at	cleavage and polyadenylation specificity factor 3	Cpsf3	0,03505689	28,5250633	4,7004E-06
1452860_at	F-box and leucine-rich repeat protein 17	Fbxl17	0,03522612	28,3880251	1,1279E-06
1418501_a_at	oxidation resistance 1	Oxr1	0,03612416	27,6823032	0,00026893
1434895_s_at	protein phosphatase 1, regulatory (inhibitor) subunit 13B	Ppp1r13b	0,03763955	26,5677968	1,9224E-07
1417435_at	like-glycosyltransferase	Large	0,03883506	25,7499309	0,00037593
1423564_a_at	phosphoribosylaminoimidazole carboxylase, phosphoribosylaminoribosylaminoimidazole	Paics	0,03905865	25,6025224	1,3657E-09
1433772_at	heat shock protein 70 family, member 13	Hspa13	0,04040951	24,7466507	8,2724E-10
1438971_x_at	ubiquitin-conjugating enzyme E2H	Ube2h	0,04169801	23,9819593	8,9422E-06
1426462_at	gephyrin	Gphn	0,04176974	23,9407757	1,6121E-08
1435614_s_at	RAS protein-specific guanine nucleotide-releasing factor 1	Rasgrf1	0,04317362	23,1622946	7,5043E-09
1455083_at	ATPase, class VI, type 11C	Atp11c	0,04391885	22,7692661	6,2182E-08
1416698_a_at	CDC28 protein kinase 1b	Cks1b	0,04395529	22,7503915	4,5871E-05
1445642_at	LEM domain containing 1	Lemd1	0,0452765	22,0865146	8,3627E-05
1434403_at	sprouty-related, EVH1 domain containing 2	Spred2	0,04530789	22,071212	8,4714E-07
1456392_at	neuronal growth regulator 1	Negr1	0,04563879	21,9111847	4,7302E-08
1436237_at	tetratricopeptide repeat domain 9	Ttc9	0,04720861	21,1825756	0,0024188
1433476_at	expressed sequence C78339	C78339	0,04776776	20,9346219	1,0258E-05
1460315_s_at	TANK-binding kinase 1	Tbk1	0,04778398	20,9275147	7,3928E-06

Table 8: Probesets upregulated in the axonal compartment of Smn knockdown motoneurons.

Probesets are ranked according to Fold change. The 25 most upregulated probesets are shown.

AffyIDs	GENENAME	SYMBOL	Ratio	Fold change	p-value
1447743_x_at	exostoses (multiple) 2	Ext2	26,3894859	26,3894859	4,2194E-07
1445897_s_at	interferon-induced protein 35	Ifi35	24,3486722	24,3486722	0,0002427
1418392_a_at	guanylate binding protein 3	Gbp3	23,2253263	23,2253263	1,4407E-11
1436058_at	radical S-adenosyl methionine domain containing 2	Rsad2	19,8564939	19,8564939	2,421E-08
1418580_at	receptor transporter protein 4	Rtp4	14,9787416	14,9787416	6,926E-06
1426278_at	interferon, alpha-inducible protein 27 like 2A	Ifi27l2a	10,8065499	10,8065499	2,9018E-06
1450034_at	signal transducer and activator of transcription 1	Stat1	10,6047186	10,6047186	2,8355E-08
1441899_x_at	brevican	Bcan	10,1270222	10,1270222	0,00132974
1436775_a_at	ankyrin repeat domain 17	Ankrd17	9,77268081	9,77268081	2,0865E-06
1436717_x_at	hemoglobin Y, beta-like embryonic chain	Hbb-y	9,08065781	9,08065781	0,01574633
1418191_at	ubiquitin specific peptidase 18	Usp18	8,56911598	8,56911598	8,2943E-09
1459783_s_at	cappuccino	Cno	8,40786644	8,40786644	0,00251345
1415859_at	eukaryotic translation initiation factor 3, subunit C	Eif3c	8,36438563	8,36438563	2,7202E-07
1450783_at	interferon-induced protein with tetratricopeptide repeats 1	Ifit1	8,29647013	8,29647013	0,00016647
1450779_at	fatty acid binding protein 7, brain	Fabp7	8,15209251	8,15209251	0,00015687
1436823_x_at	hemoglobin Y, beta-like embryonic chain	Hbb-y	7,7961335	7,7961335	0,0277514
1419799_at	ribosomal protein L27A	Rpl27a	7,52900646	7,52900646	5,1225E-06
1440774_x_at	WEE1 homolog 2 (S. pombe)	Wee2	7,24287982	7,24287982	0,0002187
1421053_at	kinesin family member 1A	Kif1a	6,7645394	6,7645394	1,6471E-05
1439059_at	family with sequence similarity 199, X-linked	Fam199x	6,60685625	6,60685625	0,00115443
1448591_at	cathepsin S	Ctss	6,52236923	6,52236923	0,03921953
1417601_at	regulator of G-protein signaling 1	Rgs1	6,37118304	6,37118304	0,00023432
1453003_at	sortilin-related receptor, LDLR class A repeats-containing	Sorl1	6,15817796	6,15817796	0,01495679
1417026_at	prefoldin 1	Pfdn1	6,02677303	6,02677303	0,00041977
1430837_a_at	methyl-CpG binding domain protein 1	Mbd1	6,01932049	6,01932049	0,00060918

3.4.3 GOterm analysis for Smn knockdown

Among the 2058 deregulated transcripts in the somatodendritic compartment 856 probesets were downregulated after Smn depletion. For these transcripts, GOterm analysis presented an enrichment of transcripts associated with nuclear functions such as cell division (Fig. 20). Examples for such transcripts are different cyclins (cyclin A2, B2, E2) and septins (septin 2, 7 and 10).
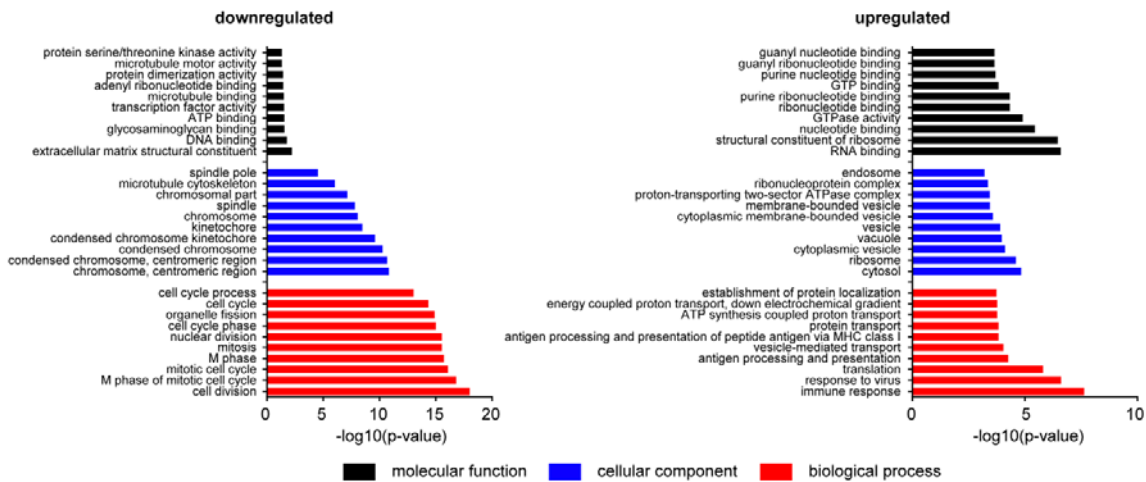
Figure 20: GOterm analysis of the somatodendritic compartment of Smn knockdown compartmentalized motoneurons.
GOterm analysis of transcripts deregulated in the somatodendritic compartment of Smn knockdown motoneurons. The top ten GO categories "molecular function", "cellular component" and "biological process" are shown for transcripts downregulated or upregulated upon Smn depletion relative to wildtype motoneurons and vector control. Only significantly ($P<0.05$) deregulated transcripts were considered.

In contrast, the 1202 upregulated probesets in the somatodendritic compartment after Smn depletion exhibitied an enrichment for transcripts involved in cytosolic functions such as translation, protein localization or RNA binding (Fig. 20). Furthermore, transcripts related to RNA splicing were detected as upregulated (Fig. 21). These transcripts included *spliceosomal components like splicing factor 1* (*Sf1*), *splicing factor 3b, subunit 3* (*Sf3b3*) and *U2 small nuclear RNA auxiliary factor 1* (*U2af1)* as well as splicing regulators such as *splicing factor, serine/arginine-rich 1* (*Sfrs1*), *transformer 2 beta homolog* (*Tra2b*) and *CUGBP, elav-like family member 2* (*Celf2*). Moreover, we found transcripts encoding components of the major histocompatibility

complex I (MHC class I) as well as the *β₂-microglobulin* transcript to be increased in the somatodendritic compartment after Smn knockdown (Fig. 21). As especially these transcripts were absent in the compartments of control motoneurons which were transfected with an empty lentiviral construct this rules out the possibility that the upregulation of MHC class I components is a consequence of the viral delivery of the knockdown construct. Instead it seems to be a direct consequence of Smn depletion.

"RNA splicing" (upregulated)

AffymetrixIDs	Gene name	Symbol	Fold change	p-value
1450743_s_at	synaptotagmin binding, cytoplasmic RNA interacting protein	Syncrip	2.54	1.00E-04
1417135_at	serine/arginine-rich protein specific kinase 2	Srpk2	3.45	5.88E-04
1422769_at	synaptotagmin binding, cytoplasmic RNA interacting protein	Syncrip	2.68	2.32E-03
1431044_at	THO complex 1	Thoc1	2.09	5.10E-03
1418573_a_at	hnRNP-associated with lethal yellow	Raly	1.74	6.22E-03
1418245_a_at	RNA binding protein, fox-1 homolog (C. elegans) 2	Rbfox2	2.13	9.03E-03
1430982_at	serine/arginine-rich splicing factor 1	Srsf1	1.76	9.70E-03
1460633_at	PRP19/PSO4 pre-mRNA processing factor 19 homolog (S. cerevisiae)	Prpf19	2.01	1.14E-02
1422509_at	U2 small nuclear ribonucleoprotein auxiliary factor (U2AF) 1	U2af1	1.91	1.25E-02
1423971_at	THO complex 3	Thoc3	2.32	1.78E-02
1439777_at	CUGBP, Elav-like family member 2	Celf2	1.89	1.87E-02
1437322_at	RNA binding motif protein 4	Rbm4	2.04	1.92E-02
1454798_at	RNA binding motif protein 15B	Rbm15b	1.63	2.21E-02
1429748_at	RIKEN cDNA B930003M22 gene	B930003M22Rik	1.52	2.23E-02
1417136_s_at	serine/arginine-rich protein specific kinase 2	Srpk2	2.74	2.29E-02
1441466_at	transformer 2 beta homolog (Drosophila)	Tra2b	1.50	2.44E-02
1423895_a_at	CUGBP, Elav-like family member 2	Celf2	1.90	2.70E-02
1423750_a_at	splicing factor 1	Sf1	1.62	3.32E-02
1420934_a_at	serine/arginine repetitive matrix 1	Srrm1	1.43	3.80E-02
1430075_at	splicing factor 3b, subunit 3	Sf3b3	1.69	4.06E-02
1416736_at	cancer susceptibility candidate 3	Casc3	1.58	4.29E-02
1428171_at	PRP39 pre-mRNA processing factor 39 homolog (yeast)	Prpf39	1.30	4.91E-02

"antigen processing and presentation of peptide antigen via MHC class I" (upregulated)

AffymetrixIDs	Gene name	Symbol	Fold change	p-value
1427746_x_at	histocompatibility 2, K1, K region	H2-K1	6.40	2.59E-08
1421812_at	TAP binding protein	Tapbp	4.84	1.03E-06
1450534_x_at	histocompatibility 2, K1, K region	H2-K1	2.38	6.94E-06
1418536_at	histocompatibility 2, Q region locus 7	H2-Q7	4.28	7.23E-05
1417876_at	Fc receptor, IgG, high affinity I	Fcgr1	5.59	4.62E-04
1451784_x_at	histocompatibility 2, D region locus 1	H2-D1	6.15	5.39E-04
1451593_at	histocompatibility 2, K1, K region	H2-K1	4.09	8.73E-04
1451931_x_at	histocompatibility 2, D region locus L	H2-L	5.99	1.04E-03
1452544_x_at	histocompatibility 2, D region locus 1	H2-D1	4.30	1.13E-03
1425336_x_at	histocompatibility 2, K1, K region	H2-K1	4.68	1.77E-02
1452428_a_at	beta-2 microglobulin	B2m	6.01	1.93E-02
1436625_at	Fc receptor, IgG, high affinity I	Fcgr1	1.39	3.42E-02

Figure 21: Analysis of transcripts deregulated in the somatodendritic compartment of Smn knockdown compartmentalized motoneurons.
Transcripts in the GO category "RNA splicing" and "antigen processing and presentation of peptide antigen via MHC class I". The transcripts shown are upregulated in the somatodendritic compartment of Smn knockdown motoneurons.

Closer examination of the set of downregulated transcripts in the axonal compartment after Smn depletion revealed an overrepresentation of mRNAs associated with synaptic localization (Fig. 22). This included transcripts such as *piccolo* (*Pclo*), *synapsin II* (*Syn2*), *cytoplasmic FMR1 interacting protein 1* (*Cyfip1*) and *2* (*Cyfip2*), as well as *neurofilament, medium polypeptide* (*Nefm*). In contrast, transcripts upregulated in axons of Smn knockdown motoneurons functionally match those upregulated in the somatodendritic compartment. These transcripts are either associated with translation such as the ribosomal proteins L13, S13 and S9 or the translation initiation factor Eif3c or are implicated in MHC class I antigen presentation.
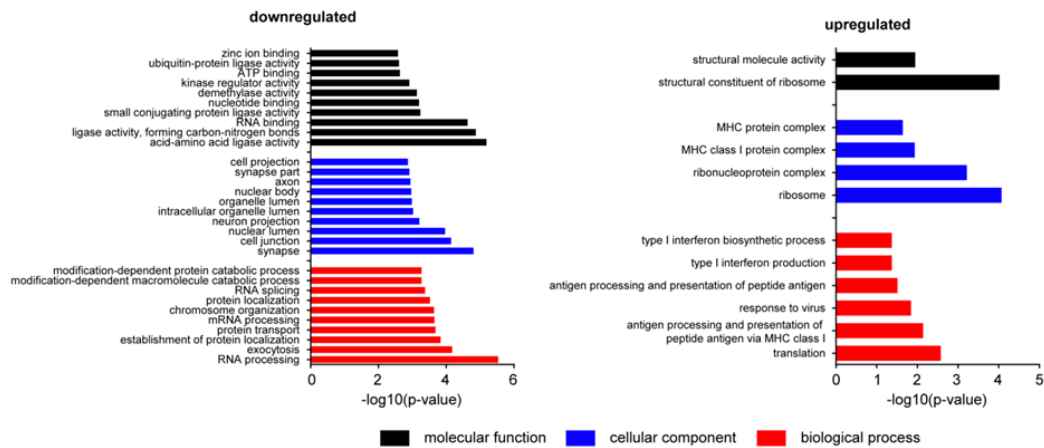
Figure 22: GOterm analysis of the axonal compartment of Smn knockdown compartmentalized motoneurons.
GOterm analysis of transcripts singnificantly ($P<0.05$ and $|log_2ratio| >2$) downregulated or upregulated in the axonal compartment of Smn knockdown motoneurons.

As the correlation analysis of the individual microarray replicate data sets from the axonal compartment already showed higher variations for low and medium expressed transcripts, we decided to focus our analysis on probesets with a mean expression value of >10 in the control data sets (wildtype and vector control). Thereby, we were able to detect 195 highly expressed probesets changed after Smn depletion with a P-value <0.5 and foldchange >4 in the axonal compartment (Fig. 23).
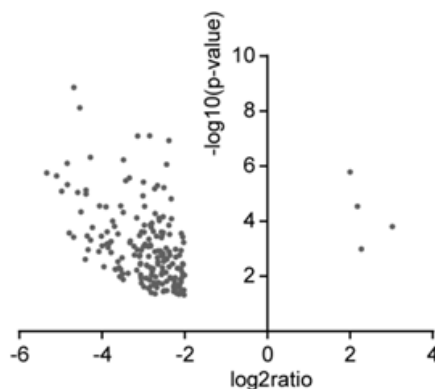
Figure 23: Analysis of transcripts deregulated in the axonal compartment of Smn knockdown motoneurons.
Volcano plot showing 195 microarray probesets with an average expression >10 in wildtype motoneuron axons and vector control axons. The 195 probesets are significantly ($P<0.05$ and $|log_2ratio| >2$) downregulated in axons of Smn knockdown motoneurons.

A comparison with the somatodendritic data sets showed only eight of these 195 probesets to be significantly changed also in the somatodendritic compartment upon Smn knockdown. These transcripts included *solute carrier family 25, member 39* (*Slc25a39*), *zinc finger protein 706* (*Zfp706*), *methyltransferase like 9* (*Mettl9*), *ankyrin 3* (*Ank3*), *ELKS/RAB6-interacting/CAST family member 2* (*Erc2*), *RNA binding protein, Fox-1 homolog* (*Rbfox1*), *2610005L07Rik* (Fig. 24).

AffymetrixIDs	Symbol	Ratio soma	Ratio axon
1439410_x_at	Slc25a39	0.41	0.19
1456177_x_at	Zfp706	0.28	0.15
1456176_x_at	Slc25a39	0.35	0.20
1417710_at	Mettl9	0.34	0.15
1451628_a_at	Ank3	0.27	0.23
1434582_at	Erc2	0.28	0.02
1455358_at	Rbfox1	0.44	0.16
1452997_at	2610005L07Rik	0.47	0.17
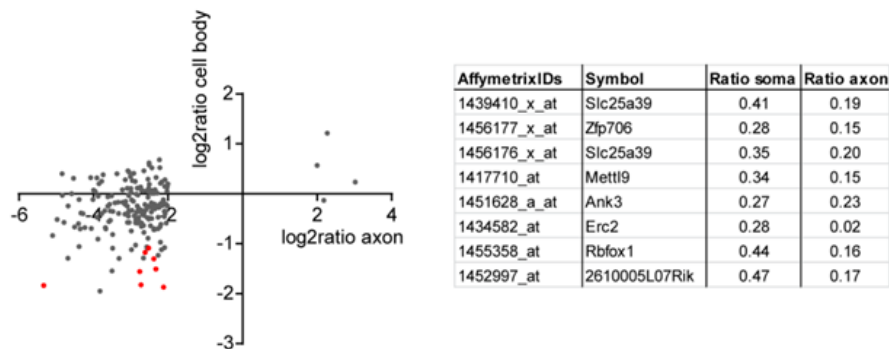
Figure 24: Analysis of transcripts deregulated in the somatodendritic and axonal compartment of Smn knockdown motoneurons.

Volcano plot showing the transcript level changes of the 195 transcripts presented in Fig. 23 in the axonal and somatodendritic compartment of Smn knockdown motoneurons. Data points marked in red indicate a *P*-value <0.05 in the somatodendritic compartment. *Slc25a39=solute carrier family 25, member 39*, *Zfp706=zinc finger protein 706*, *Mettl9=methyltransferase like 9*, *Erc2=ELKS/RAB6-interacting /CAST family member 2*, *Rbfox1=RNA binding protein, FOX-1 homolog*

Thus, changes in the axonal transcriptome of Smn deficient motoneurons are not necessarily dependent on transcript level alterations in the somatodendritic compartment. Further GOterm analysis with the 195 altered axonal mRNAs revealed transcripts related to GOterms for neuron projections, axons and growth cones to be significantly downregulated (Fig. 25).
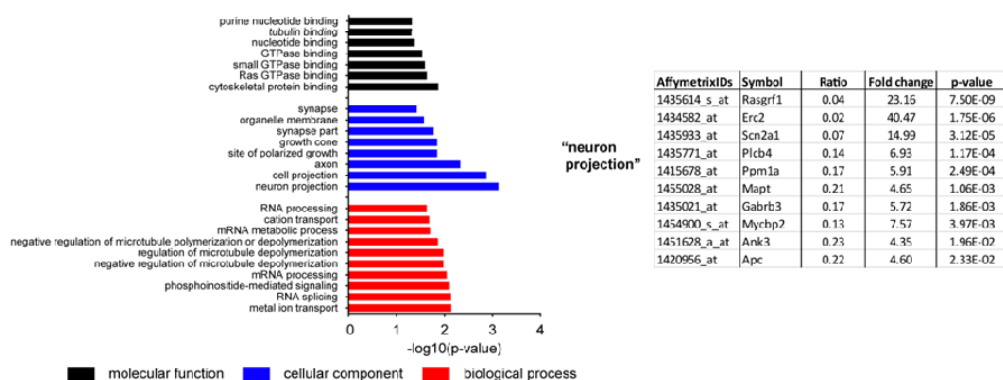
Figure 25: GOterm analysis of significantly downregulated transcripts in the axonal compartment of Smn knockdown motoneurons.

GOterm analysis of the 195 transcripts described in Fig. 23. The table presents probesets changed in the axonal compartment of Smn knockdown motoneurons and contained in the GOterm "neuron projection". *Rasgrf1=Ras protein-specific guanine nucleotide-releasing factor 1, Erc2=ELKS/RAB6-interacting /CAST family member 2, Scn2a1= sodium channel, voltage gated, type II alpha subunit, Plcb4=phospholipase c, beta 4, Ppm1a=protein phosphatase, Mg2+/Mn2+ dependent 1a, Mapt=microtubule-associated protein tau, Gabrb3=gamma-aminobutyric acid a receptor, beta 3, Mycbp2=MYC binding protein 2, Ank3=Ankyrin 3, Apc=adenomatous polyposis coli*

3.4.4 Validation of microarray data of Smn knockdown

To validate the data of the microarray analysis, quantitative realtime PCR (qPCR) was performed on RNA amplified for one round from somatodendritic as well as axonal compartments of Smn knockdown and wildtype motoneurons. Hereby, the changes detected in transcript levels by microarray in the somatodendritic compartment of Smn depleted motoneurons were in line with the relative transcript levels detected by qPCR (Fig. 26A). In contrast, the transcript levels of the axonal compartment measured by qPCR showed again a higher degree of variability (Fig. 26B). Nevertheless, reductions in transcript levels for *adenomatous polyposis coli* (*Apc*), *doublecortin* (*Dcx*), *methyltransferase like 9* (*Mettl9*), *ankyrin 3* (*Ank3*), *gephyrin* (*Gphn*), *cleavage and polyadenylation specific factor 3* (*Cpsf3*) and *synapsin 3* (*Syn3*) could be detected by qPCR in Smn deficient motor axons.
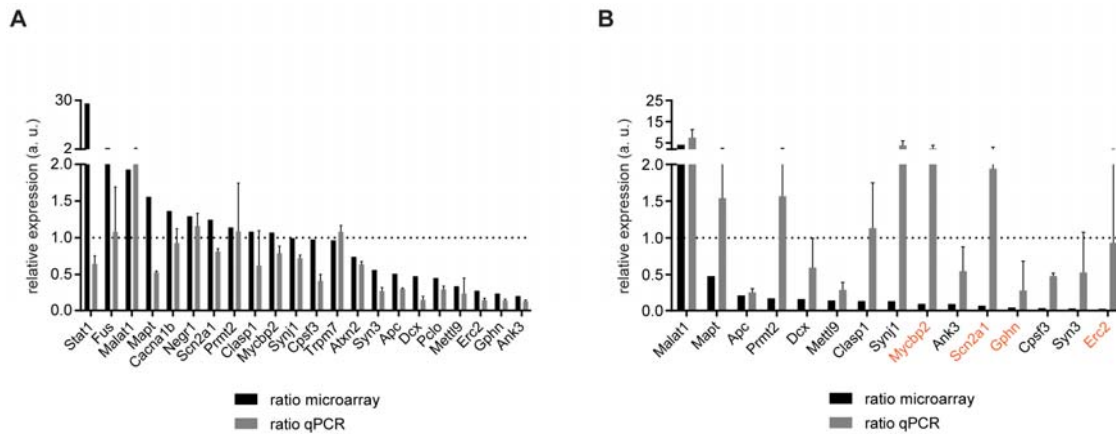
Figure 26: Validation of transcript level changes after microarray profiling of Smn knockdown motoneurons.

(A) Transcript levels of different candidates deregulated in the somatodendritic compartment of Smn knockdown motoneurons were measured by quantitative PCR. The relative expression as reported by microarray (black) or quantitative PCR (grey) relative to controls is shown. Data are mean with standard deviation. (B) Transcript levels of different candidates deregulated in the axonal compartment of Smn knockdown motoneurons were measured by quantitative PCR. The relative expression as reported by microarray (black) or quantitative PCR (grey) relative to controls is shown. Transcripts highlighted in orange have average crossing points >30 in the wildtype samples. Data are mean with standard deviation. *Stat1=signal transducer and activator of transcription 1*, *Fus=fused in sarcoma*, *Malat1=metastasis associated lung adenocarcinoma transcript 1*, *Mapt=microtubule-associated protein tau*, *Cacna1b=calcium channel, voltage dependent, N type, alpha 1b subunit*, *Negr1=neuronal growth regulator 1*, *Scn2a1=sodium channel, voltage gated, type II alpha subunit*, *Prmt2=protein arginine methyltransferase 2*, *Clasp1=cytoplasmic linker associated protein 1*, *Mycbp2=MYC binding protein 2*, *Synj1=synaptojanin 1*, *Cpsf3=cleavage and polyadenylation specific factor 3*, *Trpm7=transient receptor potential cation channel, subfamily M, member 7*, *Atxn2=ataxin 2*, *Syn3=synapsin 3*, *Apc=adenomatous polyposis coli*, *Dcx=doublecortin*, *Pclo=piccolo*, *Mettl9=methyltransferase like 9*, *Erc2=ELKS/RAB6-interacting /CAST family member 2*, *Gphn=gephyrin, Ank3=Ankyrin 3*

3.5 Whole transcriptome amplification followed by high-throughput sequencing

In order to investigate transcript changes in the somatodendritic and axonal compartment of motoneurons in an unbiased manner, we decided to make use of an RNA-Sequencing method. Current methods for transcriptome amplification usually use poly(dT)-based reverse transcription. This step is followed by either template switching and exponential amplification or *in vitro* transcription for linear amplification as we already did it in combination with the microarrays. But since we wanted to obtain a complete picture of the local transcriptome diversity, including also ribosomal and non-polyadenylated non-coding RNAs, we thought a potential approach for whole transcriptome amplification would be double-random priming. Therefore, we established a new protocol by first systematically optimizing the method and applying it to a serial dilution of total spinal cord RNA ranging from 5 ng down to 10 pg. Later on we used this method in combination with our compartmentalized motoneuron cultures. The basis for the method is an oligonucleotide containing a random 3' end, which is used for reverse transcription as well as second strand synthesis. The third step of the protocol is a PCR amplification followed by ligation of Illumina sequencing primers.

3.5.1 Optimization of whole transcriptome amplification efficency

As already said at the beginning, our main interest is the transcriptome of motoneuron axons. But, since the amount of RNA that can be extracted is estimated to be in the lower picogram range, amplification of reverse-transcribed cDNA is necessary to generate a sufficient cDNA amount for high-throughput sequencing. Moreover, because we are interested in the total RNA content of motor axons, we did not decide for a RNA-Sequencing protocol based on ribosomal removal or poly(dT)-based reverse transcription. Instead, we focused on an oligonucleotide used previously for whole genome amplification [multiple annealing and looping-based amplification cycles (MALBAC)] which contains a 3' random octamer and a 5' adapter sequence (Zong et al., 2012) (Fig. 27). By usage of this oligonucleotide for reverse transcription as well as for second strand synthesis we were able to generate cDNA

fragments containing the adapter sequence in a reverse complement manner at both ends. These fragments were afterwards amplified by PCR using adapter oligonucleotides. Thus we generated sufficient amounts of cDNA to generate high throughput sequencing libraries. The advantage of this method is the covering of each transcript by multiple cDNAs of varying length thereby preventing any amplification bias.
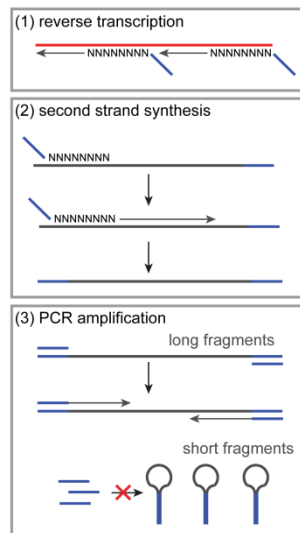
Figure 27: Schematic outline of whole transcriptome amplification strategy.
Schematic outline of the double-random priming strategy to amplify cDNA. RNA (red) is reverse transcribed using random octamers coupled to an oligonucleotide adapter (blue). For second strand synthesis the same primer is used generating amplicons with complementary ends. PCR amplification is done with a primer recognizing the adapter ends thereby preventing the amplification of short fragments due to the formation of panhandle-like structures by these short fragments. Only amplicons with a sufficient size are amplified.

In a first step we optimized the protocol using 40 pg of total spinal cord mouse RNA and monitored amplification efficiency of the PCR reactions. The following three different parameters were tested:

1) two different polymerases for second strand synthesis (Accuprime *Taq* DNA polymerase and strand displacement polymerase *Bst*, Large fragment)
2) four different primer concentrations for second strand synthesis (0.2 µM, 1.725 µM, 5 µM, 10 µM final concentration)
3) three different adapter primer concentrations for PCR amplification (0.2 µM, 3.15 µM, 10 µM final concentration)

To get an estimation of amplification efficiency of the PCR reactions we furthermore removed aliquots every two cycles starting at cycle 10. Obtained yield was subsequently measured by quantitative PCR (qPCR) for the abundant housekeeping mRNA *glyceraldehyde-3-phosphate dehydrogenase* (*Gapdh*) (Fig. 28A) as well as the less abundant mRNA *ubiquilin 2* (*Ubqln2*) (Fig. 28B). Our result was that all three parameters seemed to be critical for amplification efficiency. First, although both polymerases performed similarly for second strand synthesis of *Gapdh*, Accuprime *Taq* performed better for *Ubqln2* than *Bst*. Because of this reason we decided to use Accuprime *Taq* for second strand synthesis later on. Second, whilst a primer concentration of 0.2 µM for second strand synthesis was sufficient for *Gapdh* amplification, amplification efficiency for *Ubqln2* required a primer concentration of at least 1.725 µM. As a further increase in primer concentration did not show any improvement in amplification efficiency so far, we decided for 1.725 µM primer concentration for second strand synthesis. Third, a primer concentration of 3.15 µM showed to be optimal for PCR amplification. Taken together, the results show that the amplification of *Gapdh* is quite robust under a variety of conditions. In contrast, amplification of the less abundant *Ubqln2* seems to require optimized reaction conditions.
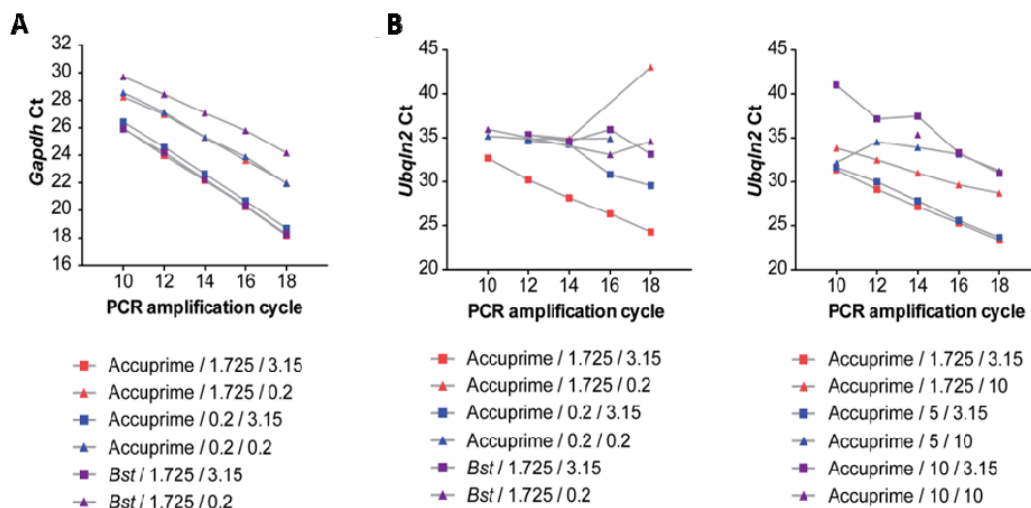
Figure 28: Optimization of whole transcriptome amplification efficiency.
(A) Whole transcriptome amplification efficiency for different polymerases and primer concentrations. *Gapdh* mRNA levels were measured by quantitative PCR before and after PCR amplification. The legend describes the different parameters tested as following: polymerase used during second strand synthesis / final primer concentration in µM for second strand synthesis / final primer concentration in

µM for PCR amplification. Ct, crossing point. (B) Whole transcriptome amplification efficiency for different polymerases and primer concentrations. *Ubqln2* mRNA levels were measured by quantitative PCR. The legend describes the different parameters tested as in (A). *Gapdh=glyceraldehyde-3-phosphate dehydrogenase, Ubqln2=ubiquilin 2*

3.5.2 Whole transcriptome sequencing of serially diluted RNA

After initial optimization of the protocol for whole transcriptome amplification we investigated its dynamic range and used mouse spinal cord total RNA in serial dilutions. First, we determined the optimal number of PCR cycles to amplify the products of the second strand synthesis obtained from 5 ng total RNA. Therefore, we removed PCR aliquots from cycle 12 to 20 and resolved the products on a polyacrylamide gel (Fig. 29) After 12 cycles the PCR amplicons were sized in the range of 150-600 bp. If we used more than 12 cycles for PCR amplification, larger-sized fragments appeared indicating overamplification. Because of this reason we concluded that for 5 ng total RNA 12 cycles are suitable to obtain sufficient amounts of PCR products without overamplification.
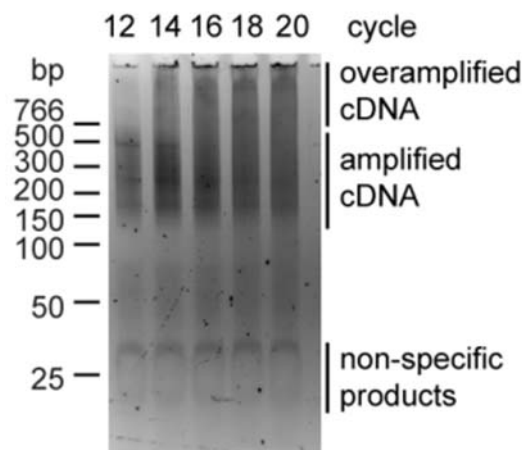
Figure 29: Whole transcriptome amplification of spinal cord total RNA.
Whole transcriptome amplification of 5 ng mouse spinal cord total RNA. PCR aliquots were removed at the indicated cycles and separated by polyacrylamide gel electrophoresis.

As we also noticed the presence of non-specific products with a size of approximately 25 bp we decided for subsequent experiments to purify amplicons that are further

processed into high-throughput libraries with AMPure beads to remove such non-specific products.

In a next step we applied the optimized whole transcriptome amplification protocol to a serial dilution of 5 ng, 500 pg, 50 pg and 10 pg total embryonic mouse spinal cord RNA, each dilution arranged in triplicates. Obtained cDNA fragments after second strand synthesis were amplified for 12 (5 ng), 15 (500 pg), 18 (50 pg) or 20 (10 pg) cycles revealing final amplicons with a size of approximately 150-600 bp (Fig. 30A). Amplification efficiency of *Gapdh* was similarly reproducible in all samples (Fig. 30B). The PCR products were subsequently used for the generation of Illumina sequencing libraries without further size selection or adapter removal (Fig. 30C).
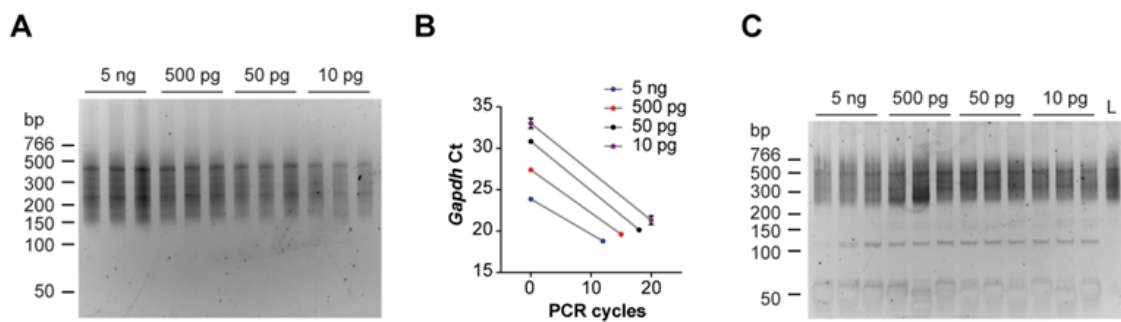
Figure 30: Whole transcriptome amplification of serial diluted spinal cord total RNA.
(A) Whole transcriptome amplification products of three technical replicates each with a total RNA input amount of 5 ng, 500 pg, 50 pg or 10 pg, respectively. (B) *Gapdh* mRNA levels detected by quantitative PCR before and after amplification. PCR products shown in (A) were amplified as follows: 5 ng 12 cycles, 500 pg 15 cycles, 50 g 18 cycles, 10 pg 20 cycles. Data are mean with standard deviation. Ct, crossing point. (C) Final libraries with attached Illumina primers. L: pooled libraries. *Gapdh=glyceraldehyde-3-phosphate dehydrogenase*

In our protocol we used four adapter primers of varying length for PCR that differed in sequence in order to cover a broad spectrum of hybridization probability. Thereby we achieved the necessary 5' end heterogeneity for cluster calling. Furthermore a custom bioinformatics pipeline was established for data analysis screening reads for presence of the adapter sequence and utilizing the random octamer region for 'molecule counting' of PCR duplicates. The adapter sequence was contained in >90% of the reads and the majority of sequencing reads was unique for all different RNA input amounts (Fig. 31). PCR duplicates were subsequently removed and reads

were mapped to the mouse genome. Thus, normalized read numbers per transcript expressed as FPKM values could be calculated.
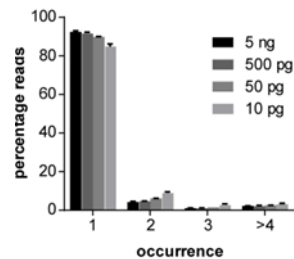
Figure 31: Quantification of PCR duplicates.

Random octamer sequences were used as unique molecular identifiers. Data are mean percentages with standard deviation.

By comparison of transcript levels we detected a high degree of correlation for genes with FPKM≥0.001 between individual technical replicates (Fig. 32). The Pearson correlation coefficient was 1.0 for all technical replicates, even for the ones derived from 10 pg total RNA. Nevertheless, we observed an increase in variability of FPKM values for lower expressed transcripts especially between 50 pg and 10 pg input RNA.
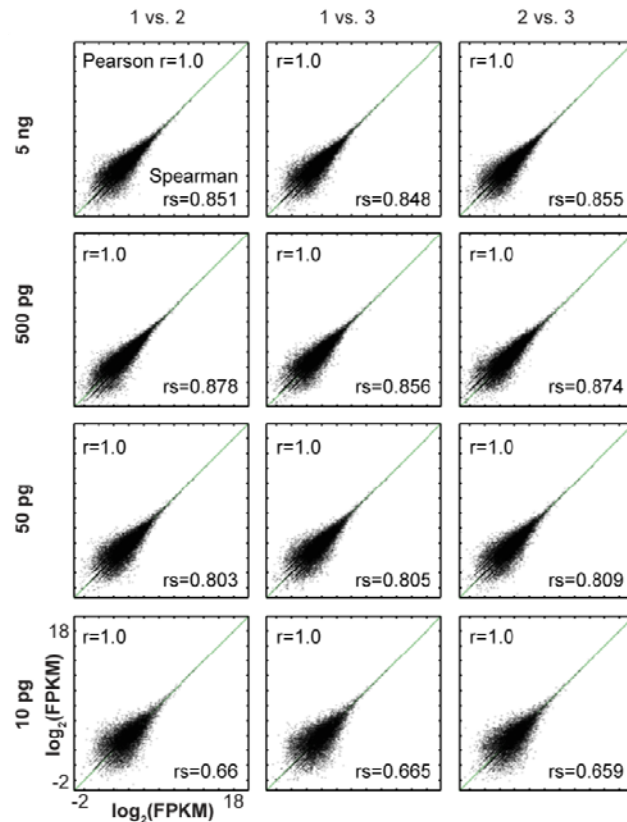
Figure 32: Correlation analysis of serial diluted spinal cord total RNA.
Correlation analysis of technical replicates of RNA-Seq libraries. FPKM values of genes with FPKM≥0.001 are shown in the scatter plots. For each comparison r Pearson correlation coefficient and rs Spearman coefficient are shown.

As it could be possible that the Pearson coefficient might overestimate the correlations because of highly expressed transcripts we also calculated the Spearman coefficient which considers gene ranks. Again this was done for all comparisons. For the 5 ng, 500 pg and 50 pg replicate comparisons the Spearman coefficient was >0.8. For the 10 pg replicates it was <0.7 (Fig. 32). Due to these results we estimate that 50 pg is the threshold of input RNA until which the protocol still reproducibly yields quantitative information.

But, besides that, transcripts encoding the housekeeping genes *Gapdh* and *Ppia* showed similar levels for all RNA inputs (Fig. 33A). The number of genes that were expressed in all three technical replicates was approximately 10,000 for 5 ng, 500 pg and 50 pg of input RNA and approximately 7,600 for 10 pg RNA (Fig. 33B). This corresponds to >80% as well as roughly 72% of expressed genes (Fig. 33C).
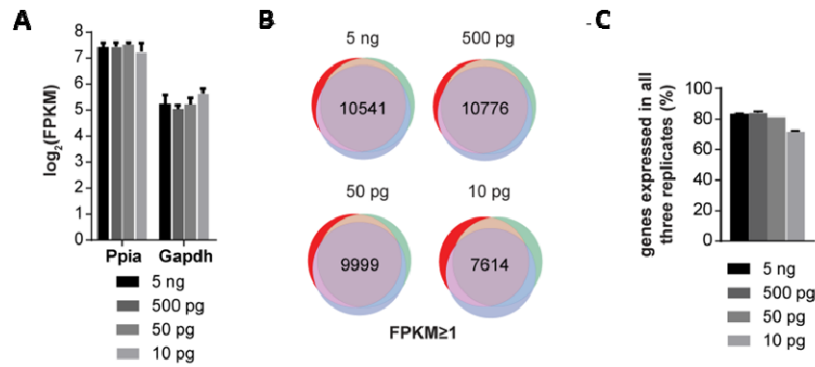
Figure 33: Analysis of serial diluted spinal cord total RNA after whole transcriptome amplification.

(A) Comparison of the transcript abundance for the housekeeping genes Ppia and Gapdh. Shown are logarithmized mean FPKM values with standard deviation. (B) Number of genes detectable (FPKM≥1) in all three technical replicates for each RNA input amount. (C) Quantification of the number of genes commonly detected in all three technical replicates. Data are mean with standard deviation. *Ppia=peptidylprolyl isomerase A (cyclophilin A), Gapdh=glyceraldehyde-3-phosphate dehydrogenase*

Finally, we determined the top 20 most abundant transcripts by FPKM value in all different input RNA samples revealing similar RNAs for all the samples (Fig. 34). The most abundant transcript was ribosomal RNA (Gm26924) in all the samples. As the most abundant protein-coding RNA we detected the transcript *Actb* encoding β-actin. Furthermore, non-coding RNAs like 7SK (*Rn7sk*), 7SL (*Metazoa-SRP*) and *ribonuclease P RNA component H1* (*Rpph1*) were also detected. For all samples, including the 10 pg total RNA replicates, the abundance of these top 20 transcripts was similar.
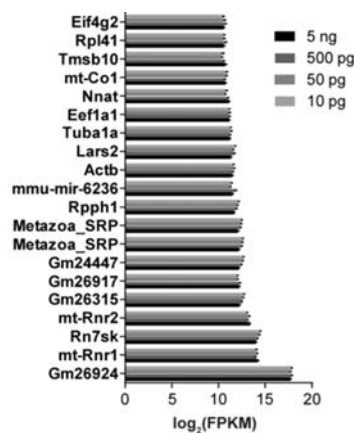
Figure 34: Analysis of the top 20 most abundant transcripts of serial diluted spinal cord total RNA.

Top 20 most abundant transcripts detected in the 5 ng total input RNA samples compared with the FPKM values of the 500 pg, 50 pg and 10 pg total input RNA samples. Shown are logarithmized mean FPKM values with standard deviation. *Eif4g2=eukaryotic translation initiation factor 4 gamma 2, Rpl41=ribosomal protein L41, Tmsb10=thymosin beta 10, mt-Co1=mitochondrially encoded cytochrome c oxidase I, Nnat=neuronatin, Eef1a1=eukaryotic translation elongation factor 1 alpha 1, Tuba1a=tubulin, alpha 1a, Lars2=leucyl-tRNA synthetase 2, mitochondrial, Actb=actin, beta, Rpph1=ribonuclease P RNA component H1, Rn7sk=RNA, 7SK small nuclear*

This is in line with the correlation analysis suggesting that the whole transcriptome amplification protocol preserves the expression levels of individual transcripts even at low input amounts of RNA. To further investigate if even the transcript levels among different RNA inputs are concordant on a global scale, we calculated correlation coefficients for all replicate comparisons. For all comparisons the Pearson correlation coefficient was ~1.0. In contrast, the Spearman correlation coefficient was >0.8 for the comparisons of the 5 ng, 500 pg and 50 pg samples (Fig. 35).
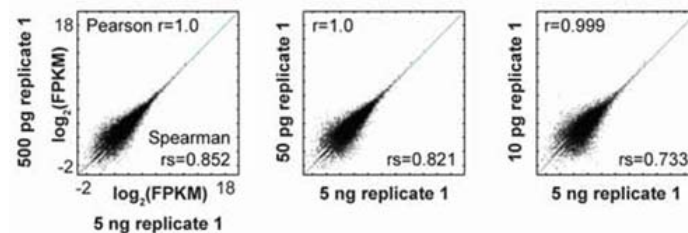
Figure 35: Correlation analysis of serial diluted spinal cord total RNA.

Scatter plots comparing FPKM values for all transcripts with FPKM ≥ 0.001. Pearson r and Spearman rs correlation coefficients of the absolute FPKM values are shown for each comparison.

3.5.3 Characteristics of transcript capture by whole transcriptome profiling

One difference of our protocol to the already established RNA-Sequencing protocols is the fact that we do not fragment the input RNA prior to library preparation. Therefore we wanted to find out if it is still possible with our protocol to capture different regions across a transcript. Hence, we visualized the read distribution for the long-noncoding RNA *metastasis associated lung adenocarcinoma transcript 1* (*Malat1*) (Fig. 36A). This transcript is highly abundant and no alternatively spliced transcripts exist. For all replicates we obtained a non-uniform read densitiy profile

leading to the suggestion that different subdomains of an individual transcript are differentially available for profiling. But, when we averaged the reads across the transcripts we observed a uniform distribution along the transcript lengths. Only the far 5' and 3' ends showed a relative underrepresentation (Fig. 36B).
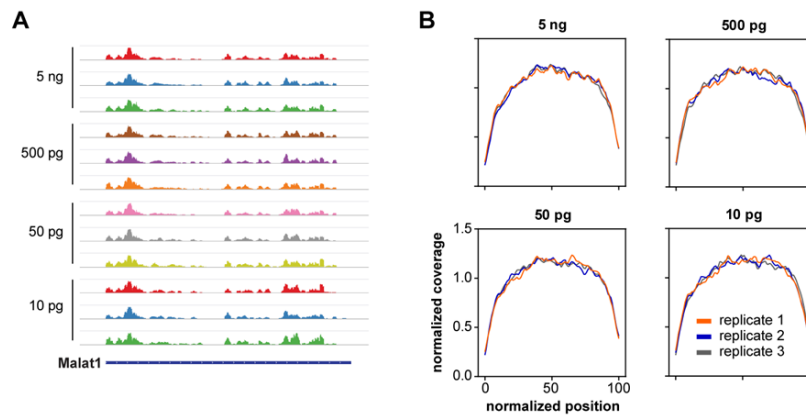
Figure 36: Analysis of serial diluted spinal cord total RNA after whole transcriptome amplification.
(A) Sashimi plots showing the read densities along the *Malat1* transcript. (B) Coverage plots depicting read coverage along the normalized length of genes.

Further analysis revealed that for all input amounts ~80% of aligned bases were derived from coding regions and UTR (Fig. 37) whereas only ~13.5% of aligned bases originated from intronic regions. This indicates that mostly spliced mRNAs rather than pre-mRNAs were present. Besides that, a small fraction of transcripts was also derived from intergenic RNAs becoming obvious from the ~6% of aligned bases within intergenic regions.
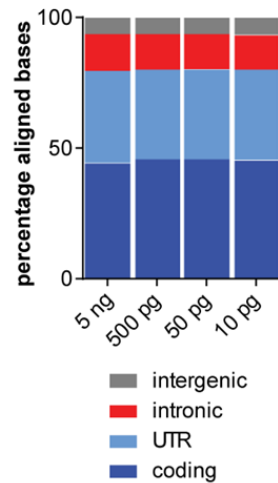
Figure 37: Whole transcriptome amplification of serial diluted spinal cord total RNA.
Percentage of aligned bases within intergenic, intronic, UTR and coding regions. Data are mean percentages of the combined total.

Additionally, we also examined the potential of the whole transcriptome amplification protocol to detect transcripts belonging to different gene classes. Therefore, we examined the percentage of the total FPKM for each sample derived from individual gene classes (Fig. 38). Interestingly, about 42-44% of the total FPKM was derived from protein-coding genes. Only 36-39% contributed to rRNAs. This is substantially below the expected percentage of about 80-90% in cells. As the detected rRNA fraction is the same for all different input amounts of RNA an amplification bias according to additional PCR cycles can be excluded.
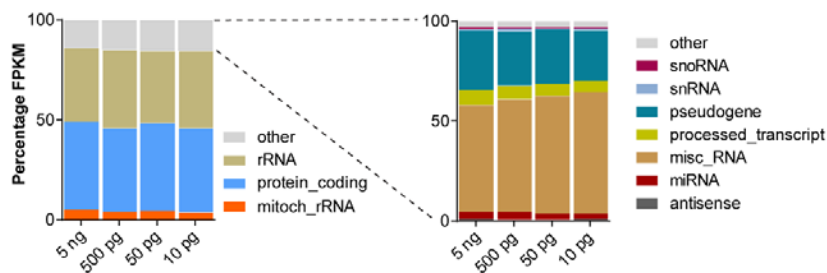
Figure 38: Analysis of different gene classes detected by whole transcriptome amplification.
Quantification of gene classes covered by whole transcriptome amplification. Only transcripts with FPKM≥1 were considered. Data are mean percentages.

To analyze this still in more detail we also calculated the proportion of aligned read bases falling within annotated rRNA genes. But even here, only ~60% of all aligned read bases showed to match within rRNA genes (Fig. 39).
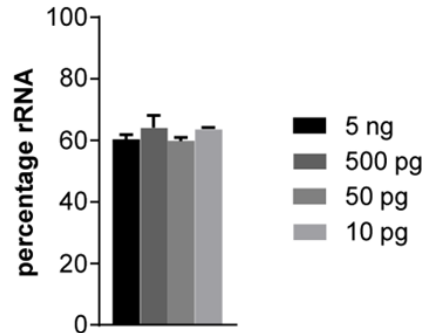
Figure 39: Analysis of rRNA genes after whole transcriptome amplification.
Quantification of ribosomal RNAs. Data are mean percentage of aligned bases within rRNA genes with standard deviation.

3.5.4 Whole transcriptome profiling of compartmentalized motoneurons

To investigate the axonal transcriptome of primary motoneurons we cultured wildtype embryonic mouse motoneurons in microfluidic chambers as described before (Saal et al., 2014) and applied our established protocol to the extracted total RNA from both compartments of five independent compartmentalized cultures (Fig. 40).
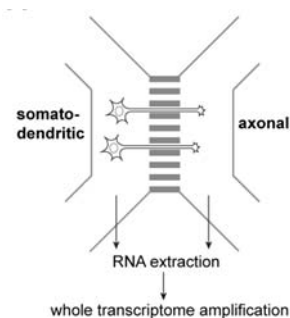
Figure 40: Whole transcriptome profiling of compartmentalized motoneurons.
Schematic of a microfluidic chamber for compartmentalized motoneurons. The microfluidic chamber allows separate RNA extraction from both compartments.

As we observed after reverse transcription an average crossing point for *Gapdh* of 18.38 for the somatodendritic samples and of 28.35 for the axonal samples we decided to amplify somatodendritic cDNAs for 6 cycles and axonal cDNAs for 18 cycles. Correlation analysis revealed us two axonal samples showing poor correlation with the remaining three axonal samples with respect to gene-by-gene FPKM values. These two samples we also identified previously as those samples containing the lowest amount of RNA corresponding to an average *Gapdh* crossing point of 31.33. Comparison of this crossing point to the spinal cord samples indicated an equivalent of a total RNA amount of ~20 pg, which is below the threshold at which we find our method to be quantitative. Thus we only considered those three datasets for further analysis that showed the highest degree of correlation among each other.

In both compartments, the number of expressed transcripts was similar. On the somatodendritic side we detected 10,433 transcripts compared to the axonal compartment with 11,127 transcripts (Fig. 41A). Even the transcript coverage was comparable for both compartments shown on a global scale (Fig. 41B) as well as for individual transcripts like *Malat1* (Fig. 41C).
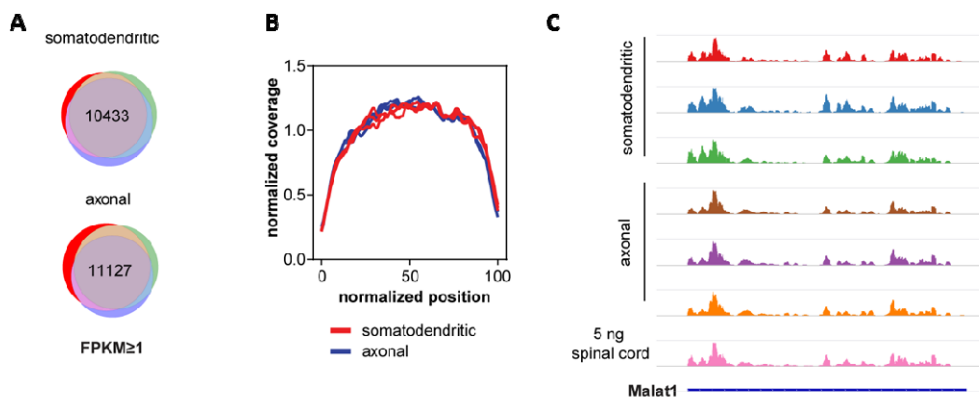
Figure 41: Analysis of compartmentalized motoneurons after whole transcriptome amplification.

 (A) Number of expressed genes (FPKM≥1) in all three replicate datasets of both compartments. (B) Coverage plot of whole transcriptome profiling data of both compartments. (C) Sashimi plots showing the read densities for the *Malat1* transcript in both compartments compared to the dataset of 5 ng spinal cord total RNA.

In order to get a first impression of the RNA composition of the somatodendritic and axonal compartments we determined the different transcript classes that could be

detected in each compartment (Fig. 42). We observed that both compartments showed a quite similar RNA composition as it was already revealed by our microarray experiments containing transcripts of multiple classes. Around 50% of FPKM values were derived from transcripts annotated as protein coding in both compartments. Another 30% to 40% of FPKM values were annotated as ribosomal RNA or other RNAs. Interestingly, ~10% of FPKM values in the somatodendritic compartment but twice as many, namely ~20% of FPKM values in the axonal compartment belonged to mitochondrial RNAs. This suggests an enrichment of mitochondria in the axonal cytoplasm relative to the somatodendritic cytoplasm.
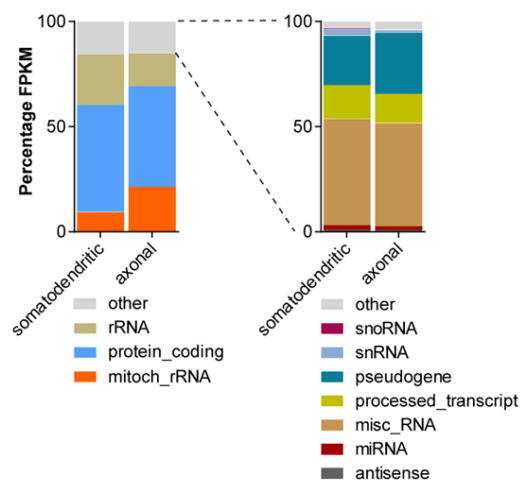
Figure 42: Analysis of different gene classes detected by whole transcriptome amplification of compartmentalized motoneurons.

Stacked bars showing the RNA composition of the somatodendritic and axonal compartment. Only expressed transcripts (FPKM≥1) were considered. Data are mean percentages.

As our whole transcriptome amplification method is able to capture the whole transcriptome we also identified long non-coding RNAs and evaluated their relative abundance. Hereby, we detected an axonal enrichment for *7SL*, *rhabdomyosarcoma 2 associated transcript* (*Rmst*) and also slightly for *Malat1*. *7SK*, *maternally expressed 3* (*Meg3*), *X inactive specific transcript* (*Xist*) and *myocardial infarction associated transcript* (*Miat*) showed either an equal distribution or an enrichment in the somatodendritic compartment. Validation of the presence or enrichment of some selected transcripts via qPCR verified these observations (Fig. 43A). In a final analysis we mapped the reads to the gene segments and found that both introns and

RNAs derived from intergenic regions were more prevalent in the axonal compartment compared to the somatodendritic compartment (introns: 30.2% compared to 22.0%; intergenic: 14.9% compared to 7.8%) (Fig. 43B). These results indicate the existence of non-coding RNAs of different length and origin in axons of motoneurons.
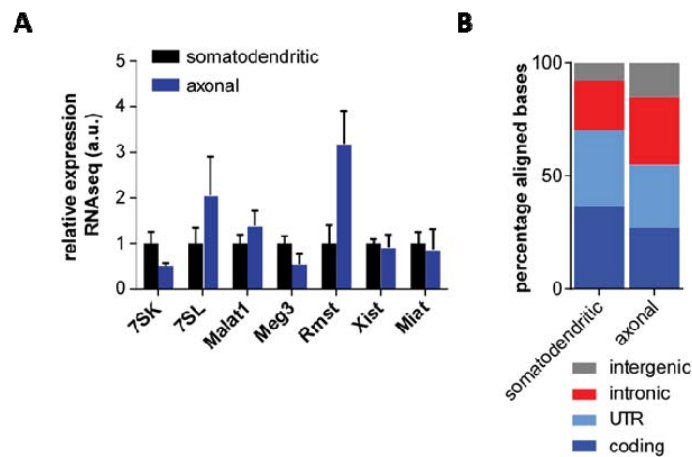
Figure 43: Ananlysis of non-coding RNAs after whole transcriptome amplification of compartmentalized motoneurons.
(A) Enrichment of individual non-coding RNAs in both compartments. Data are mean with standard deviation relative to the mean of the somatodendritic datasets. (B) Percentage of aligned bases within intergenic, intronic, UTR and coding regions. Data are mean percentages of the combined total. *7SK=RNA, 7SK small nuclear, 7SL=RNA, 7SL cytoplasmic 1, Malat1=metastasis associated lung adenocarcinoma transcript 1, Meg3=maternally expressed 3, Rmst=rhabdomyosarcoma 2 associated transcript, Xist=X inactive specific transcript, Miat=myocardial infarction associated transcript*

Subsequently, we concentrated on the analysis of protein-coding transcripts in the somatodendritic and axonal compartment. Therefore, we selected synaptic marker proteins in our RNA-Seq data and validated the relative enrichment of their transcripts by qPCR (Fig. 44). In concordance with already existing knowledge we found postsynaptic markers like *glutamate receptor, ionotropic, N-methyl-D-aspartate 3a* (*Grin3a*), *glutamate receptor, ionotropic, AMPA 1* (*Gria1*) and *glutamate receptor, ionotropic, AMPA 2* (*Gria2*) to be enriched on the somatodendritic side. The transcript encoding *piccolo* (*Pclo*), a protein involved in the organization of the presynaptic apparatus, also showed an enrichment in the somatodendritic compartment.
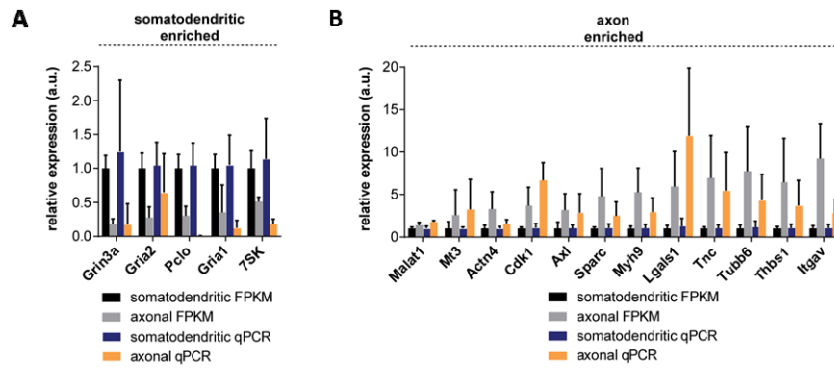
Figure 44: Validation of individual transcripts after whole transcriptome amplification of compartmentalized motoneurons.

(A) Validation of individual transcripts in the somatodendritic compartment of compartmentalized motoneurns. Data are mean with standard deviation relative to the mean of the somatodendritic dataset. (B) Validation of individual transcripts in the axonal compartment of compartmentalized motoneurons. Data are mean with standard deviation relative to the mean of the somatodendritic datasets. *Grin3a=glutamate receptor, ionotropic, N-methyl-D-aspartate 3a*, *Gria2=glutamate receptor, ionotropic, AMPA 2*, *Pclo=piccolo*, *Gria1=glutamate receptor, ionotropic, AMPA 1*, *7SK=RNA, 7SK small nuclear*, *Malat1=metastasis associated lung adenocarcinoma transcript 1*, *Mt3=metallothionein 3*, *Actn4=actinin 4*, *Cdk1=cyclin-dependent kinase 1*, *Axl=AXL receptor tyrosine kinase*, *Sparc=secreted protein, acidic, cysteine-rich*, *Myh9=myosin, heavy chain 9, non-muscle*, *Lgals1=lectin, galactoside-binding, soluble, 1*, *Tnc=tenascin*, *Tubb6=tubulin, beta 6*, *Thbs1=thrombospondin 1*, *Itgav=integrin, alpha V*

Next, we performed differential gene expression analysis to find transcripts enriched in either compartment in an unbiased manner. For this, we compared the dataset of the somatodendritic compartment with the axonal dataset (Fig. 45). Overall, we found 681 transcripts to be significantly ($P<0.05$) enriched in the somatodendritic compartment and 633 transcripts significantly ($P<0.05$) enriched in the axonal compartment. Some of the candidates enriched in the axonal compartment were also validated by qPCR (Fig. 44B). Although axonal mRNAs showed a high variability in their transcript levels, the direction of enrichment was in agreement with the predictions by differential expression analysis.
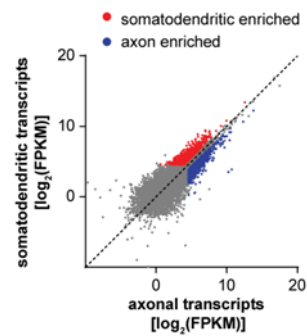
Figure 45: Differential expression analysis of compartmentalized motoneurons.
Differential expression analysis of whole transcriptome data from compartmentalized motoneurons. Colour-coded transcripts are significantly (*P*<0.05) enriched.

To rule out the possibility that the differential expression of transcripts in either compartment is a consequence of differences in the cycle number used for PCR amplification we performed another differential expression analysis. Hereby, we compared the already obtained RNA-Seq data for 5 ng with those for 10 pg mouse spinal cord RNA and measured the fold change for transcripts enriched in the somatodendritic and axonal compartment. We found no correlation between the fold change of enrichment in compartmentalized motoneurons and the fold change due to differences in amplification for these specific transcripts.

Subsequent GOterm analysis for the transcripts significantly enriched in the somatodendritic and axonal compartment gained an overview over the specific functions of these transcripts. In the somatodendritic compartment, we found an enrichment for transcripts associated with synaptic GOterms ("synapse", "synaptic transmission", "synapse part", "synaptic vesicle") (Fig. 46). In contrast, following GOterm analysis for transcripts enriched in the axonal compartment we found transcripts associated with RNA processing ("ribonucleoprotein complex", "RNA binding") or protein synthesis ("translation", "ribosome") to be enriched (Fig. 46). Interestingly, transcripts involved in cell cycle regulation were also enriched in the axonal compartment.
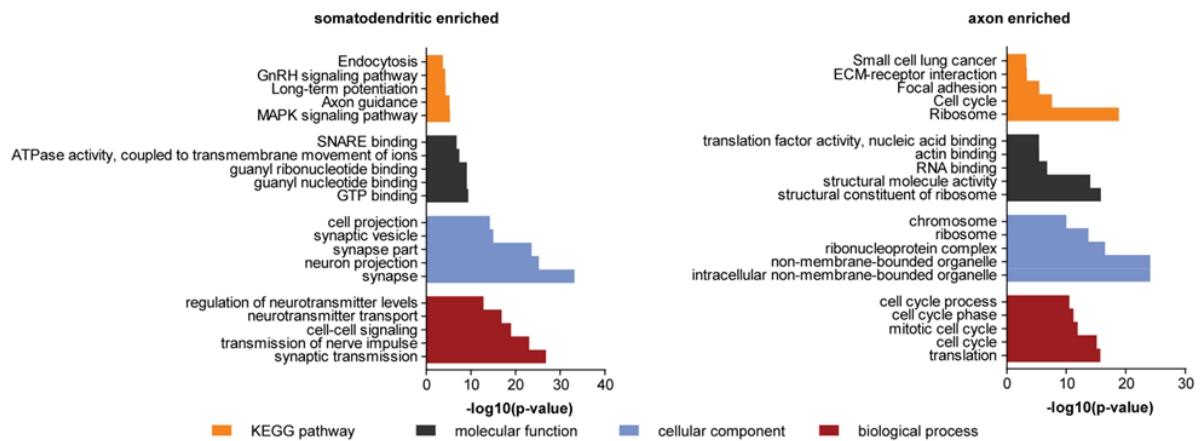
Figure 46: GOterm analysis of compartmentalized motoneurons.

GOterm analysis of significantly (*P*<0.05) enriched transcripts in the somatodendritic or axonal compartment. The top five GOterms for each category as well as for the KEGG pathway analysis are presented in the bar diagrams.

3.5.5 Comparison of whole transcriptome profiling results with microarray expression data for compartmentalized motoneurons

To evaluate the accuracy of transcript detection by whole transcriptome profiling of compartmentalized motoneurons we thought about comparing our lists of transcripts with the already existing datasets of compartmentalized wildtype motoneurons generated by microarray expression analysis. Therefore, we first generated a list of 17,587 transcripts covered by both microarray analysis and whole transcriptome profiling. To any given transcript we assigned either the microarray probeset showing the lowest expression value or the probeset showing the highest expression value. For both compartments, the correlation between the RNA-Seq FPKM and microarray intensitiy values was low at ~0.2 when the microarray probesets with the lowest expression value were assigned (Fig. 47). But the correlation coefficient increased to >0.5 when the microarray probesets with the highest expression level were assigned to each transcript. These results suggest that probesets with the highest expression value are more representative of RNA levels. Hence, these probesets were used for further analysis.
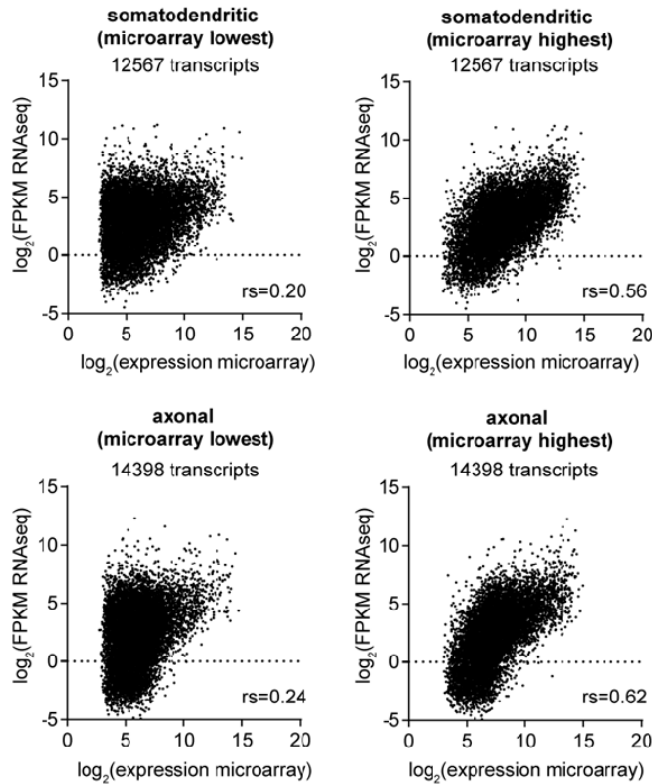
Figure 47: Comparison of compartmentalized motoneuron RNA-Seq data with microarray profiling data.

Scatter plots show mean logarithmized microarray expression values and mean logarithmized FPKM values for transcripts detected by both methods. Spearman correlation coefficients are shown for each comparison. For analysis, only transcripts with an average FPKM>0.04125 were considered.

Furthermore, we selected from the list of 17,587 transcripts only transcripts found to be expressed by both methods RNA-Seq and microarray. By microarray we found 8,245 transcripts to be expressed in the somatodendritic compartment compared to 8,989 transcripts considered to be expressed by whole transcriptome RNA-Seq (Fig. 48). 6,867 transcripts were common to both datasets. This corresponds to 83.3% of the transcripts detected by microarray and to 76.4% of transcripts detected by RNA-Seq. This difference possibly reflects the inclusion of noncoding RNAs in the RNA Seq approach which were not covered on the microarrays. For the axonal compartment, 5,707 transcripts were considered as expressed by microarray analysis and 9,427 transcripts were considered as expressed by RNA-Seq. 4,998 transcripts were common to both datasets corresponding to 87.6% of transcripts identified by microarray and to 53.0% of transcripts identified by RNA-Seq in axons.

This suggests that whole transcriptome profiling identifies a larger number of transcripts in axons of motoneurons than microarray profiling.
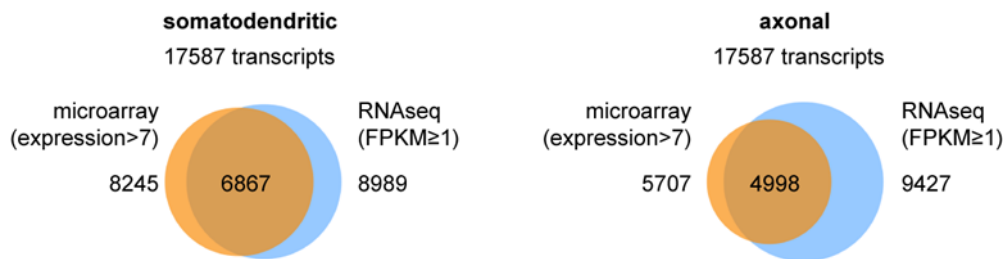
Figure 48: Comparison of transcripts detectable in both compartments by both methods.
Comparison of transcripts detectable in each compartment by whole transcriptome RNA-Seq and microarray profiling.

3.6 RNA-Seq results for hnRNP R knockdown

The idea to apply our whole transcriptome amplification method also to compartmentalized hnRNP R knockdown cultures resulted from the already obtained microarray data but also from different previous experiments. There, iCLIP was used to identify the RNA interactome of hnRNP R in motoneurons and ~3,500 direct RNA targets could be obtained. These results led to the question how a loss of hnRNP R affects especially the axonal transcriptome of motoneurons. Furthermore, as we already detected transcript changes in both compartments of knockdown motoneurons by microarray analysis and could show that the RNA-Seq method is able to detect more transcripts especially in the axonal compartment we thought of improving our already obtained results. Therefore, we again cultured hnRNP R knockdown and control primary motoneurons in microfluidic chambers and separately extracted total RNA from the somatodendritic and axonal compartment followed by whole transcriptome amplification as described above. Knockdown efficiency was measured by qPCR as well as by RNA-Seq showing a reduction of hnRNP R transcripts by ≥50% relative to controls (Fig. 49).
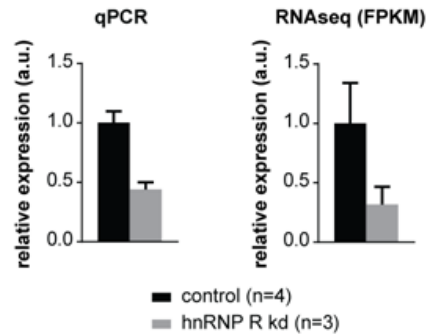
Figure 49: Validation of hnRNP R knockdown.

hnRNP R transcript expression levels on the somatodendritic side of compartmentalized hnRNP R knockdown (kd) motoneurons. Transcript levels are measured relative to controls. Levels are presented as relative expression validated by quantitative PCR or whole transcriptome RNA-seq. Data are mean with standard deviation.

To select for deregulated transcripts in both compartments after hnRNP R depletion, we performed differential gene expression analysis (Fig. 50A) and detected 159 transcripts to be significantly ($P<0.05$) upregulated and 181 transcripts showing a significant ($P<0.05$) downregulation in the somatodendritic compartment (Fig. 50B). On the axonal side, transcript levels of 110 transcripts were increased and levels of 52 transcripts were reduced after hnRNP R knockdown. 12 transcripts showed an upregulation in both compartments. This corresponds to 7.5% of the somatodendritic and to 10.9%, respectively, of the axonal deregulated transcripts. Among the downregulated transcripts, we found 7 transcripts to be downregulated in both compartments, corresponding to 3.9% of the somatodendritic and 13.5% of the axonal transcripts. Only 1 transcript was found in each case to be regulated in opposite directions.
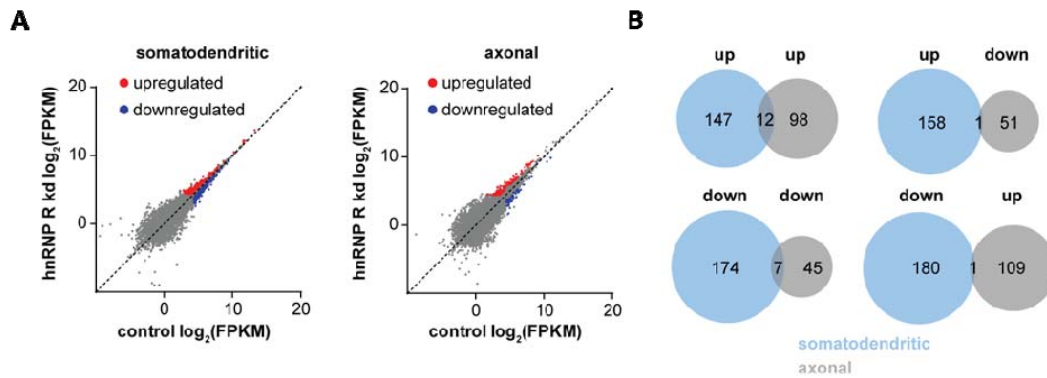
Figure 50: hnRNP R knockdown changes the somatodendritic and axonal transcriptome of motoneurons.
(A) Differential expression analysis of compartmentalized hnRNP R knockdown motoneurons relative to controls. Logarithmized FPKM values as reported by cuffdiff are depicted. (B) Overlap of deregulated transcripts in the somatodendritic and axonal compartment of compartmentalized hnRNP R knockdown motoneurons. Only significantly (*P*<0.05) deregulated transcripts were considered.

The observation that different transcripts are deregulated in both compartments is also reflected by GOterm analysis (Fig. 51). While transcripts downregulated in the somatodendritic compartment are mostly enriched for GOterms like "synaptic transmission", "neurotransmitter transport" or "generation of precursor metabolites and energy", transcripts reduced in the axonal compartment are more related to secretion ("secretion by cell", "secretion"). In contrast, transcripts associated with translation were upregulated in both compartments.
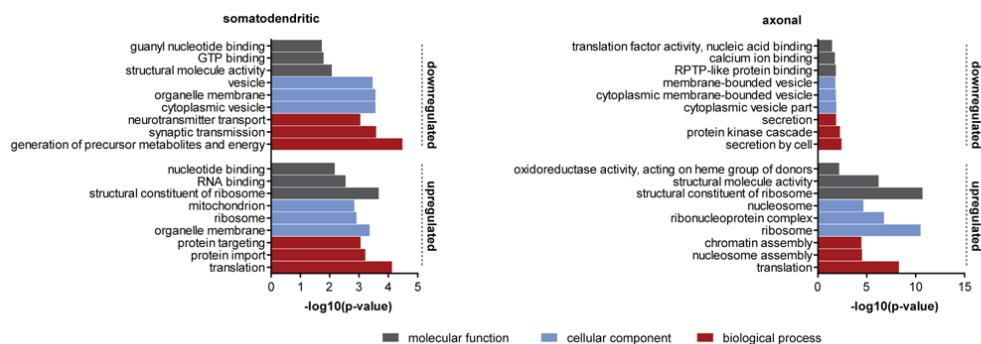
Figure 51: GOterm analysis for hnRNP R knockdown compartmentalized motoneurons.
GOterm analysis for deregulated transcripts in the somatodendritic and axonal compartment of compartmentalized hnRNP R knockdown motoneurons. Only significantly (*P*<0.05) deregulated transcripts were considered.

Some of the axonal transcript changes we also validated by qPCR (Fig. 52). As expected, the results showed a quite high variability of the measurements due to the low input amounts of RNA. Nevertheless, the direction of change predicted by the data of the differential gene expression analysis was in concordance.
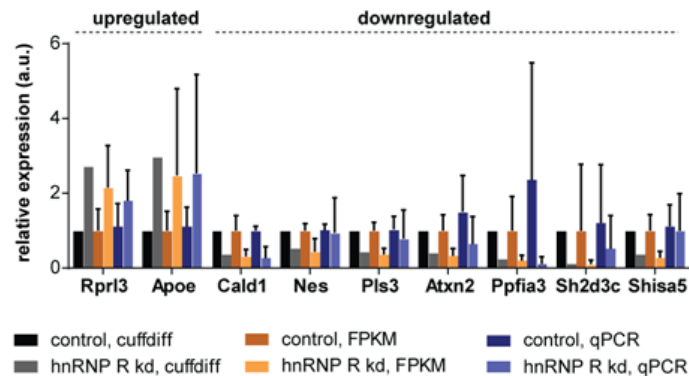
Figure 52: Validation of individual transcripts in the axonal compartment of hnRNP R knockdown motoneurons.

Validation of deregulated transcripts in the axonal compartment of hnRNP R knockdown motoneurons by quantitative PCR. The relative expression as reported by cuffdiff (black/grey), cufflinks (brown/orange) and quantitative PCR (dark blue/light blue) is shown. Data are mean with standard deviation. *Rprl3=ribonuclease P RNA-like 3*, *Apoe=apolipoprotein 3*, *Cald1=caldesmon 1*, *Nes=nestin*, *Pls3=plastin 3*, *Atxn2=ataxin 2*, *Ppfia3=protein tyrosine phosphatase, F polypeptide, interactin protein alpha 3*, *Sh2d3c=SH2 domain containing 3c*, *Shisa5=shisa family member 5*

Next, we thought about comparing our RNA-Seq data with the previously obtained iCLIP data. Therefore, we asked the question if the transcripts deregulated after hnRNP R knockdown in both compartments also contain iCLIP hits and used for this analysis the number of iCLIP hits per gene of the grouped motoneuron data we obtained previously. We first selected for transcripts present in both datasets leading to 85 upregulated, 41 downregulated and 18516 unchanged transcripts for the axonal compartment and to 129 upregulated, 161 downregulated and 18352 unchanged transcripts for the somatodendritic compartment and subsequently assessed the percentage of transcripts with iCLIP hits (Fig. 53A). We found that 98% of the downregulated transcripts after hnRNP R depletion in the axonal compartment contained iCLIP hits as well as 79% of the upregulated and 62% of the unchanged

transcripts. For the somatodendritic compartment we obtained 95% of the upregulated transcripts containing iCLIP hits compared to 98% of the downregulated and 62% of the unchanged transcripts. Furthermore, we also analyzed the total number of iCLIP hits per transcript just considering transcripts with at least 1 iCLIP hit (Fig. 53B). Here we found that the downregulated transcripts in the axonal compartment contained significantly more iCLIP hits than the upregulated or unchanged transcripts. In the somatodendritic compartment both, upregulated and downregulated transcripts contained statistically significant more iCLIP hits than unchanged ones.
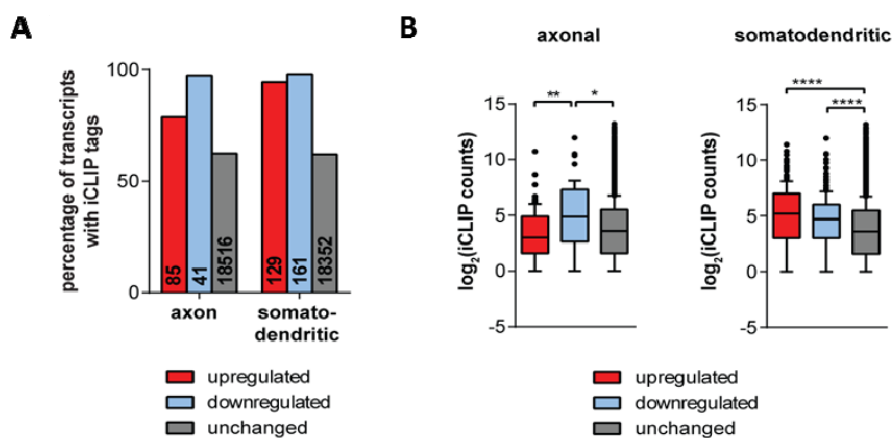
Figure 53: Comparison of RNA-Seq data of compartmentalized hnRNP R knockdown motoneurons with iCLIP data.

(A) hnRNP R binding to transcripts deregulated in motoneurons upon hnRNP R knockdown. The percentage of transcripts with at least one iCLIP tag is shown. Grouped hnRNP R iCLIP motoneuron data were used for analysis and unchanged transcripts were defined as $P \geq 0.05$. Numbers on the bars represent the total number of transcripts considered. (B) Tukey box plots. The number of iCLIP tags per transcript are presented. Only transcripts with at least one iCLIP tag as identified in (A) were considered. (*: $P \leq 0.05$, **: $P \leq 0.01$, ****: $P \leq 0.0001$; Kruskal-Wallis ANOVA with Dunn's multiple comparison test).

3.7 RNA-Seq results for 7SK knockdown

As we obtained with the previous iCLIP experiments also the result that the non-coding RNA 7SK is the main binding partner of hnRNP R and complexes of 7SK and hnRNP R could also be found in the cytosolic fraction of motoneurons, we asked the question, if the knockdown of the non-coding RNA 7SK changes the axonal

transcriptome. A disturbed axonal outgrowth phenotype in cultured 7SK knockdown motoneurons has also been observed before. Therefore we cultured 7SK knockdown motoneurons in microfluidic chambers and performed the whole amplification protocol described above. Knockdown efficiency was measured via qPCR as well as by analysis of RNA-Seq data, showing in both cases a reduction of transcript levels ~50% (Fig. 54).
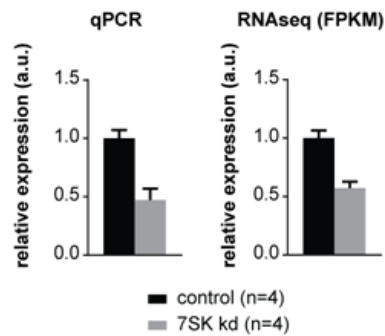
Figure 54: Validation of 7SK knockdown.

7SK transcript expression levels on the somatodendritic side of compartmentalized 7SK knockdown (kd) motoneurons. Transcript levels are measured relative to controls. Levels are presented as relative expression validated by quantitative PCR or whole transcriptome RNAseq. Data are mean with standard deviation.

Subsequent differential gene expression analysis revealed deregulated transcripts in both compartments upon 7SK depletion (Fig. 55A). In the somatodendritic compartment we found 162 transcripts upregulated compared to 137 significantly ($P<0.05$) downregulated transcripts. On the axonal side, 137 transcripts appeared to be up- and 46 transcripts to be downregulated after 7SK knockdown compared to controls. Among the upregulated transcripts we found 30 transcripts upregulated in both compartments, corresponding to 18.5% of somatodendritically upregulated transcripts and 28% of transcripts upregulated in the axonal compartment. In contrast the downregulated transcripts just shared 2 transcripts in both compartments (Fig. 55B). Transcripts regulated in opposite directions also just showed an overlap of 5 or 2 transcripts, respectively.
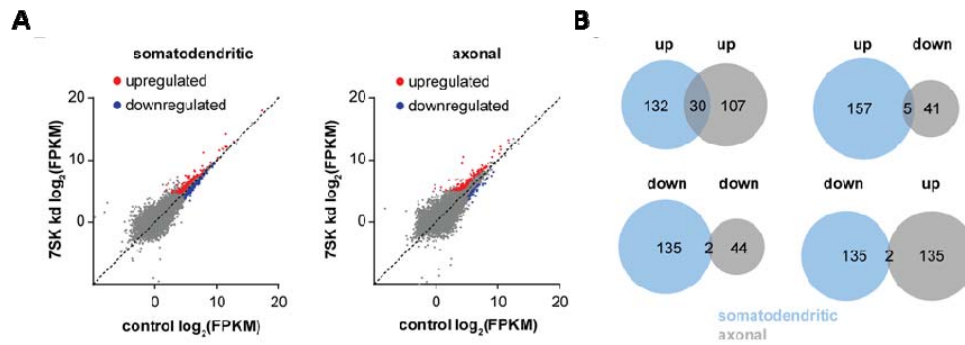
Figure 55: 7SK knockdown changes the somatodendritic and axonal transcriptome of motoneurons.

(A) Differential expression analysis of compartmentalized 7SK knockdown motoneurons relative to controls. Logarithmized FPKM values as reported by cuffdiff are depicted. (B) Overlap of deregulated transcripts in the somatodendritic and axonal compartment of compartmentalized 7SK knockdown motoneurons. Only significantly ($P<0.05$) deregulated transcripts were considered.

Interestingly, the 30 transcripts upregulated in both compartments revealed in GOterm analysis an enrichment for GOterms related to translation pointing to a possible role of 7SK as a translational regulator. (Fig. 56).
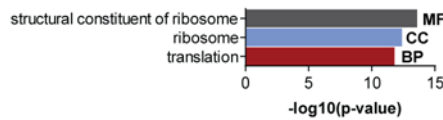
Figure 56: GOterm analysis of upregulated transcripts in both compartments of 7SK knockdown motoneurons

GOterm analysis of 30 upregulated transcripts upon 7SK knockdown in motoneurons. Transcripts are upregulated in both compartments.

GOterm analysis on all up- or downregulated transcripts in each compartment furthermore resulted in an enrichment of GOterms related to translation for the upregulated datasets (Fig. 57A and B). Downregulated transcripts in the axonal compartment showed an overrepresentation for RNAs with cytoskeletal functions like *Nestin* (*Nes*) and actin binding such as *Caldesmon1* (*Cald1*) and *Tropomyosin1* (*Tpm1*). In contrast, transcripts associated with axons or neuronal differentiation were enriched in the somatodendritic compartment. Some up- or downregulated transcripts of the axonal compartment were subsequently validated by qPCR (Fig. 57 C).
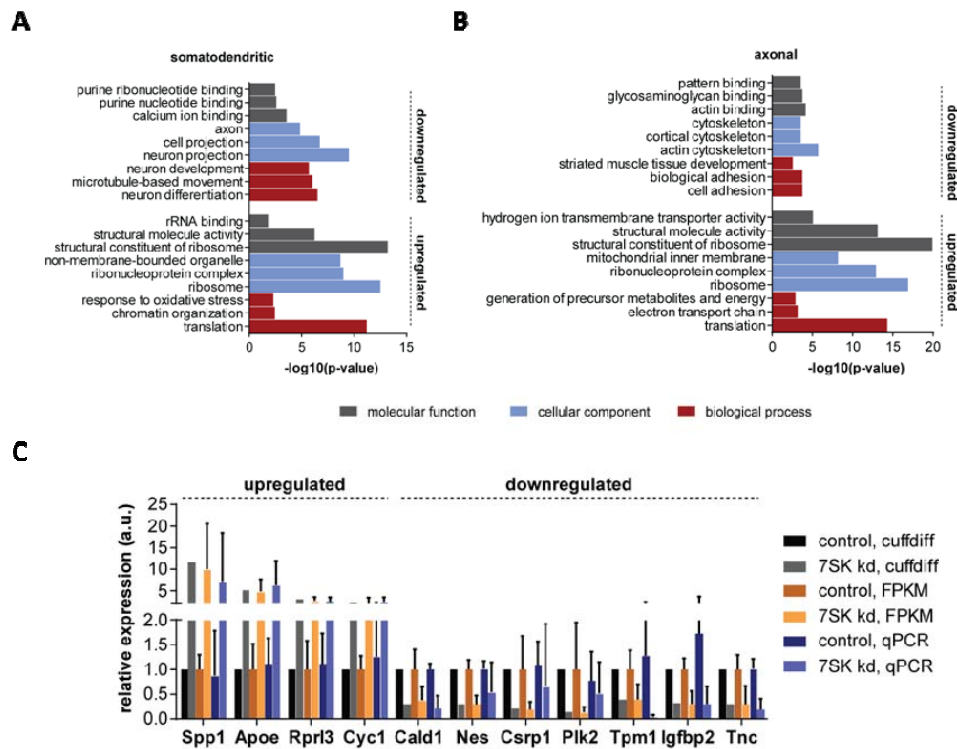
Figure 57: GOterm analysis for 7SK knockdown compartmentalized motoneurons.

(A) GOterm analysis of deregulated transcripts in the somatodendritic compartment of 7SK knockdown motoneurons. Only significantly (*P*<0.05) deregulated transcripts were considered. (B) GOterm analysis of deregulated transcripts in the axonal compartment of 7SK knockdown motoneurons. Only significantly (*P*<0.05) deregulated transcripts were considered. (C) Validation of deregulated transcripts in the axonal compartment of 7SK knockdown motoneurons by quantitative PCR. The relative expression as reported by cuffdiff (black/grey), cufflinks (brown/orange) and quantitative PCR (dark blue/light blue) is shown. Data are mean with standard deviation. *Spp1=secreted phosphoprotein 1*, *Apoe=apolipoprotein E*, *Rprl3=ribonuclease P RNA-like 3*, *Cyc1=cytochrome c-1*, *Cald1=caldesmon 1*, *Nes=nestin*, *Csrp1=cysteine and glycine-rich protein 1*, *Plk2=polo-like kinase 2*, *Tpm1=tropomyosin 1*, *Igfbp2=insulin-like growth factor binding protein 2*, *Tnc=tenascin*

Since the axon outgrowth phenotype of hnRNP R knockdown and 7SK knockdown motoneurons was similarly displaying shortened axons in culture and 7SK appeared to be the main binding partner of hnRNP R in the iCLIP experiments we investigated how the RNA-Seq datasets of hnRNP R knockdown and 7SK knockdown correlate with each other (Fig. 58). First, we plotted the foldchange for all transcripts but we were not able to detect any correlation between both datasets. However, when the

foldchange of only significantly altered transcripts in both knockdown conditions was plotted, an increase in correlation could be observed. This effect was most pronounced in the axonal compartment, revealing 37 transcripts (29 upregulated, 7 downregulated, 1 altered in opposite directions) significantly changed upon knockdown of hnRNP R and 7SK, respectively (Fig. 58B).
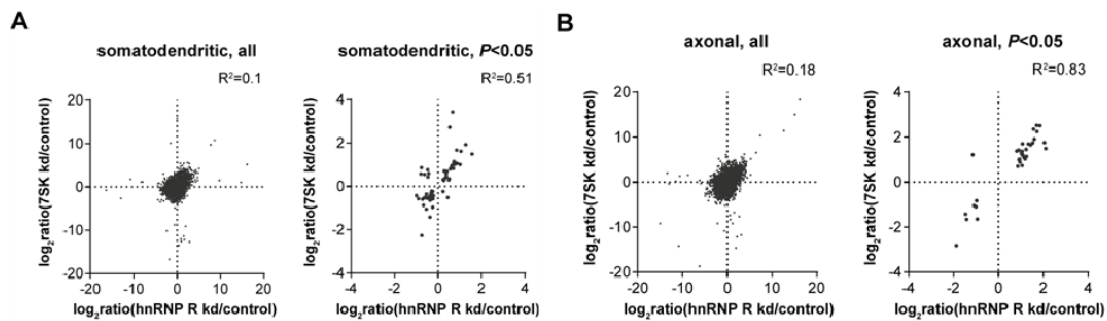
Figure 58: Comparison of RNA-Seq data of hnRNP R ans 7SK knockdown compartmentalized motoneurons.

(A) A common subset of transcripts is deregulated in the somatodendritic compartment upon hnRNP R as well as 7SK knockdown in motoneurons. Transcript foldchange in 7SK knockdown motoneurons relative to controls versus transcript foldchange in hnRNP R knockdown motoneurons relative to controls is shown. (B) A common subset of transcripts is deregulated in the axonal compartment upon hnRNP R as well as 7SK knockdown in motoneurons. Transcript foldchange in 7SK knockdown motoneurons relative to controls versus transcript foldchange in hnRNP R knockdown motoneurons relative to controls is shown.

3.8 RNA-Seq results for Tdp-43 knockdown

As RNA-Seq is able to give an unbiased view on the transcriptome compared to microarray analysis we decided to apply our whole transcriptome amplification method also on Tdp-43 knockdown motoneurons.

Knockdown efficiency of Tdp-43 was measured by qPCR and RNA-Seq and showed in both approaches a similar reduction of *Tdp-43* mRNA levels of ~80% relative to controls (Fig. 59).
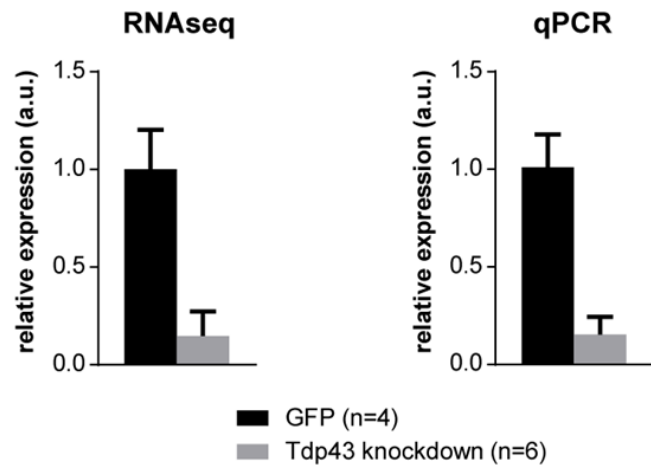
Figure 59: Validation of Tdp-43 knockdown.

Tdp-43 transcript expression levels on the somatodendritic side of compartmentalized Tdp-43 knockdown (kd) motoneurons. Transcript levels are measured relative to controls. Levels are presented as relative expression validated by quantitative PCR or whole transcriptome RNA-seq. Data are mean with standard deviation.

To get a first impression on the deregulated transcripts upon Tdp-43 depletion in motoneurons we performed differential expression analysis revealing 371 upregulated and 287 downregulated transcripts in the somatodendritic compartment (Fig. 60). In contrast, analysis of the axonal compartment showed 118 transcripts upregulated and 136 transcripts downregulated in Tdp-43 knockdown motoneurons.
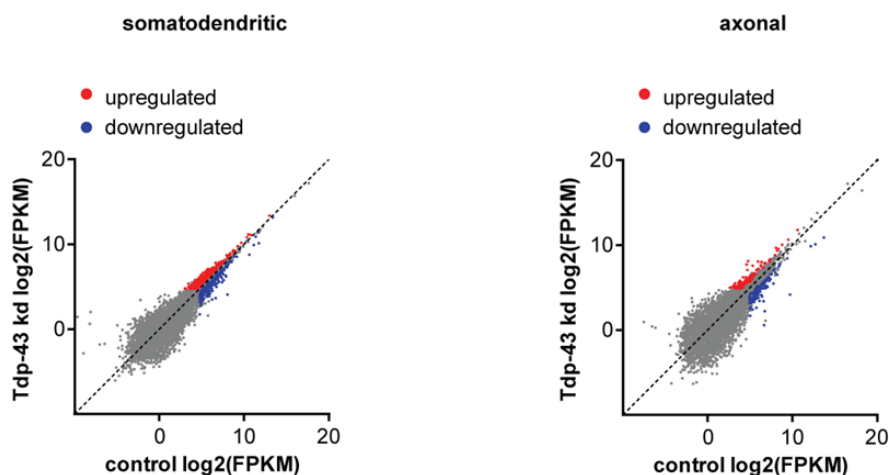

Figure 60: Tdp-43 knockdown changes the somatodendritic and axonal transcriptome of motoneurons.

Differential expression analysis of compartmentalized Tdp-43 knockdown motoneurons relative to controls. Scatter plots show logarithmized FPKM values as reported by cuffdiff.

GOterm analysis on all significantly (*P*<0.05) deregulated transcripts in the somatodendritic and axonal compartment upon Tdp-43 depletion revealed an enrichment for the GOterms "synapse" and "neuron projection" among the upregulated transcripts in the somatodendritic compartment (Fig. 61). Downregulated transcripts in the somatodendritic compartment were associated with energy production and mitochondria as well as some KEGG pathways for neurodegenerative diseases. In contrast, transcripts related to the KEGG pathway "Ribosome" or the GO terms "regulation of cell morphogenesis" and "cation homeostasis" were upregulated in the axonal compartment of Tdp-43 knockdown motoneurons compared to the downregulated transcripts in the axonal compartment, showing an enrichment for GOterms associated with translation.
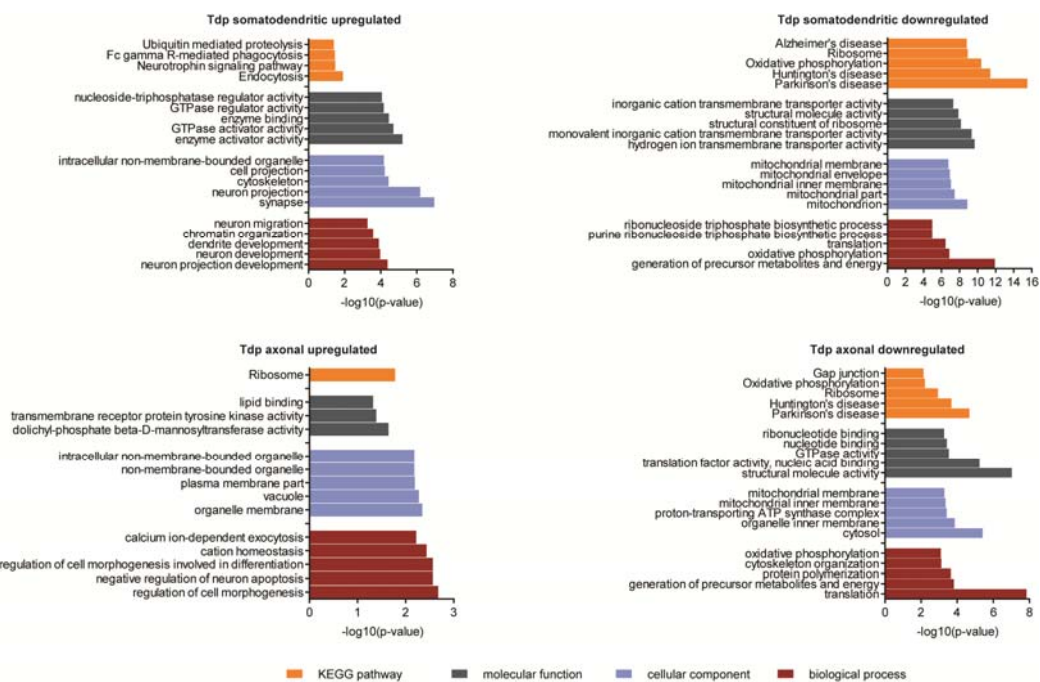

Figure 61: GOterm analysis for Tdp-43 knockdown compartmentalized motoneurons.
GOterm analysis of deregulated transcripts in the somatodendritic and axonal compartment of Tdp-43 knockdown motoneurons. Only significantly (*P*<0.05) deregulated transcripts were considered.

Some of the candidates deregulated in the axonal compartment of Tdp-43 knockdown motoneurons were also validated by qPCR, being in the most cases in line with the predictions by RNA-Seq (Fig. 62).
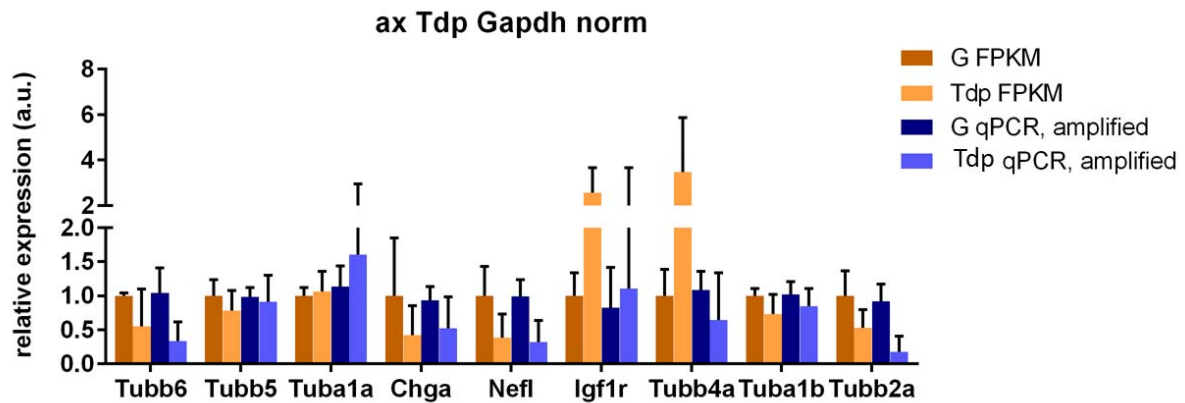
Figure 62: Validation of individual transcripts in the axonal compartment of Tdp-43 knockdown motoneurons.

Validation of deregulated transcripts in the axonal compartment of Tdp-43 knockdown motoneurons by quantitative PCR. The relative expression as reported by cufflinks (brown/orange) and quantitative PCR (dark blue/light blue) is shown. Data are mean with standard deviation. *Tubb6=tubulin*, *beta 6*, *Tubb5=tubulin, beta 5, Tuba1a=tubulin, alpha 1a, Chga=chromogranin a, Nefl=neurofilament*, *light polypeptide*, *Igf1r=insulin-like growth factor 1 receptor*, *Tubb4a=tubulin, beta 4a, Tuba1b=tubulin, alpha 1b, Tubb2a=tubulin, beta 2a*

3.9 RNA-Seq results for Smn knockdown

For Smn knockdown motoneurons, efficiency of knockdown was also first confirmed by qPCR as well as RNA-Seq (Fig. 63). Although qPCR showed a knockdown efficiency >90%, a knockdown efficiency ≥60% could also be confirmed by RNA-Seq.
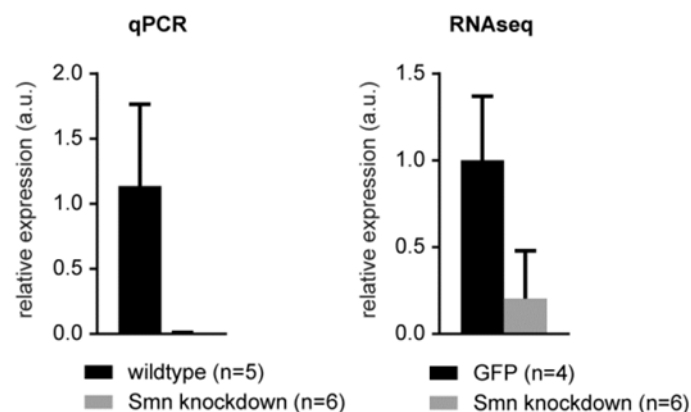
Figure 63: Validation of Smn knockdown.

Smn transcript expression levels on the somatodendritic side of compartmentalized Smn knockdown motoneurons. Transcript levels are measured relative to controls. Levels are presented as relative

expression validated by quantitative PCR or whole transcriptome RNA Seq. Data are mean with standard deviation.

Next, we again performed differential expression analysis revealing deregulated transcripts in both compartments of Smn knockdown motoneurons (Fig. 64). In total, 420 transcripts were up- and 184 transcripts were downregulated in the somatodendritic compartment upon Smn depletion. In the axonal compartment, 249 transcripts appeared to be upregulated compared to 272 downregulated transcripts.
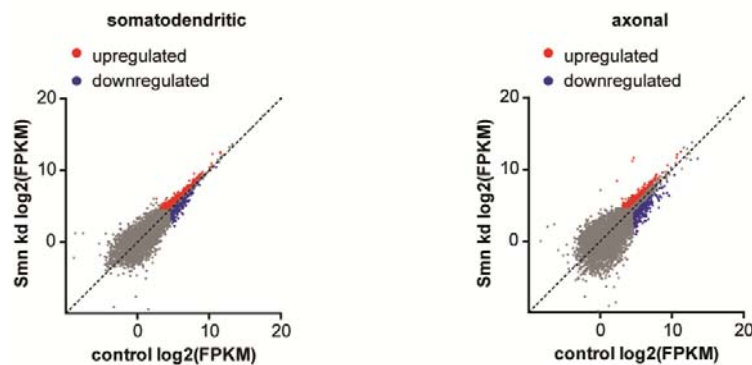
Figure 64: Smn knockdown changes the somatodendritic and axonal transcriptome of motoneurons.
Differential expression analysis of compartmentalized Smn knockdown motoneurons relative to controls. Scatter plots show logarithmized FPKM values as reported by cuffdiff.

Further GOterm analysis resulted in an enrichment of transcripts associated with energy production and oxidative phosphorylation among the significantly ($P<0.05$) upregulated transcripts in the somatodendritic compartment (Fig. 65). Downregulated transcripts were associated with GOterms like "synapse", "cytoskeleton" and "ribonucleotide binding". On the axonal side we also observed an enrichment for transcripts associated with "synapse" and "synaptic transmission" although these transcripts appeared to be upregulated. Furthermore, the GOterm oxidative phosphorylation was again upregulated in the axonal compartment of Smn knockdown motoneurons. Interestingly, transcripts downregulated in the axonal compartment upon Smn depletion showed an enrichment for GOterms related to actin binding and actin cytoskeleton as well as translation.
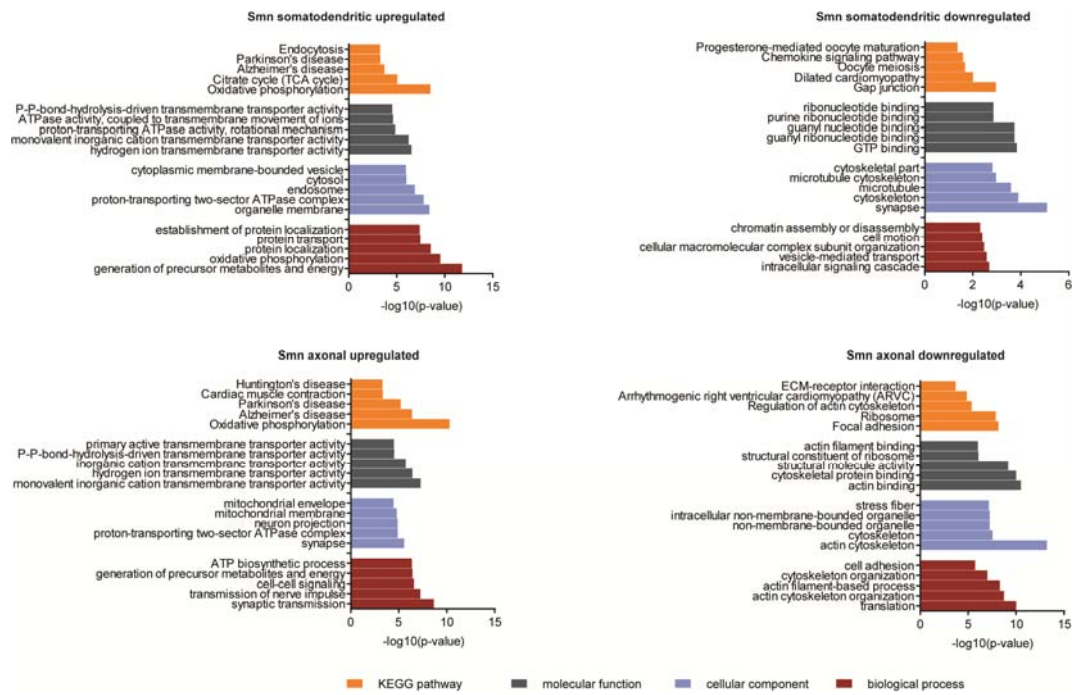
Figure 65: GOterm analysis for Smn knockdown compartmentalized motoneurons.

GOterm analysis of deregulated transcripts in the somatodendritic and axonal compartment of Smn knockdown motoneurons. Only significantly (*P*<0.05) deregulated transcripts were considered.

Some of the downregulated transcripts in the axonal compartment upon Smn deficiency were also validated by qPCR revealing corresponding results (Fig. 66).
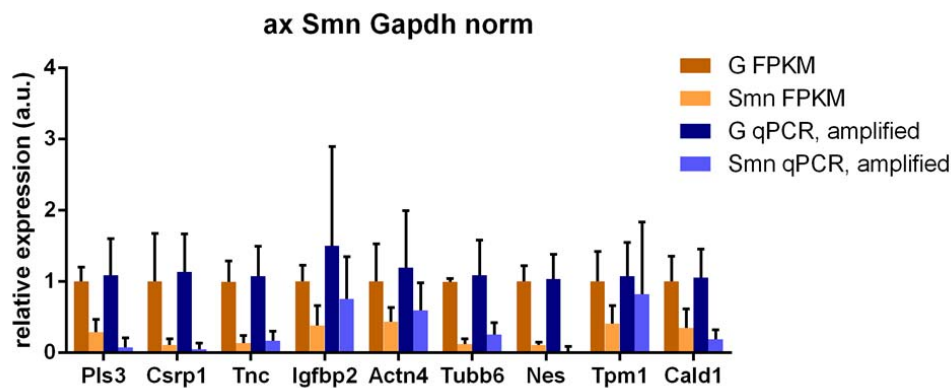
Figure 66: Validation of individual transcripts in the axonal compartment of Smn knockdown motoneurons.

Validation of deregulated transcripts in the axonal compartment of Smn knockdown motoneurons by quantitative PCR. The relative expression as reported by cufflinks (brown/orange) and quantitative PCR (dark blue/light blue) is shown. Data are mean with standard deviation. *Pls3=plastin3*,

Csrp1=cysteine and glycine-rich protein 1, *Tnc=tenascin*, *Igfbp2=insulin-like growth factor binding protein 2*, *Actn4=actinin4*, *Tubb6=tubulin, beta 6*, *Nes=nestin*, *Tpm=tropomyosin*, *Cald1=caldesmon1*

4 Discussion

4.1 Microarray profiling

In this study I have optimized and compared two different approaches especially used to investigate the axonal transcriptome of primary mouse motoneurons. The basis for both approaches are compartmentalized cultures combined either with microarray profiling or with whole transcriptome amplification followed by high-throughput sequencing. As such experiments have not been performed before with primary motoneurons our first interest was the axonal mRNA profile of wildtype motoneurons revealed after microarray analysis. First analysis of our data indicated that, in motoneurons, the composition of mRNAs in axons and the somatodendritic compartment is highly similar. This result was also reflected by the uniformity of the GOterms enriched for each compartment. Common significant GOterms for both compartments were related to translation, protein transport and RNA binding. Interestingly, these GOterms were more significantly enriched in the axonal compartment compared to the somatodendritic compartment. This result was also shown before in two different studies. The first one investigated axonal mRNAs in embryonic DRG neurons (Gumy et al., 2011), the second one also used microfluidic chambers for examination of naïve mature and regenerating cortical and hippocampal neurons (Taylor et al., 2009). Although the type of neurons used in both studies differs, the authors independently report an axonal enrichment in transcripts related to protein synthesis and energy production. This enrichment could reflect an increased energy demand especially for growing axons – embryonic or regenerating - facilitating localized protein production.

As one prominent feature of SMA and ALS is the degeneration of motor axons we asked the question if possibly changes in especially the axonal transcriptome of motoneurons could underlie the observed phenotype. Therefore, we performed knockdown for the two RNA binding proteins hnRNP R and Tdp-43 and the SMA causing protein Smn in motoneuron cultures and investigated changes by microarray profiling. With hnRNP R knockdown cultures we observed only few changes in mRNA levels in the somatodendritic compartment but substantial changes in transcript abundance for the axonal compartment exhibiting mostly downregulated

transcripts. GOterm analysis of these transcripts revealed an enrichment for GOterms associated with synapse, neuron projection and nucleotide binding among the downregulated transcripts. As it is known that hnRNP R knockdown motoneurons display shorter axons (Glinka et al., 2010) a downregulation of transcripts associated with neurite outgrowth appears quite interesting and could explain the previous findings.

In contrast, microarray profiling of Tdp-43 knockdown cultures resulted in substantial transcript level changes in both compartments. Interestingly, GOterms for downregulated transcripts in the axonal compartment showed again a very high enrichment for synapse, neuron projection and RNA binding. As both hnRNP R knockdown and Tdp-43 knockdown motoneurons present shorter axons in culture the common phenotype is even reflected in at least some common GOterms associated with downregulated transcripts under both conditions.

Upon Smn knockdown and subsequent microarray profiling, we also observed a large number of downregulated transcripts in the axonal compartment of motoneurons. These transcripts showed diverse functionality although we found an enrichment for biological processes related to RNA processing among the downregulated transcripts. Even transcripts encoding proteins located in neuron projections and growth cones appeared to be downregulated. For many of the validated downregulated transcripts functions in axon outgrowth and synapse formation have been described. For example, Apc is known to regulate the organization of the cytoskeleton as well as axon arborization (Chen et al., 2011). In contrast, Dcx plays an important role in neural migration and outgrowth and in the regulation of the actin cytoskeleton (Deuel et al., 2006, Fu et al., 2013). Syn3 and Cpsf3 have functions in neurotransmitter release and synapse and axon development (Feng et al., 2002, Van Epps et al., 2010) and Ank3 has been associated with the transport of voltage-gated Na^+-channels into axons (Barry et al., 2014). As these transcripts are downregulated upon Smn knockdown in axons of motoneurons this could explain the prominent phenotype in Smn-deficient motoneurons consisting of an impairment in action potential transmission and defects in presynaptic excitability (Jablonka et al., 2007, Kong et al., 2009, Ruiz et al., 2010). Furthermore, it is possible that the variations in transcript abundance contribute to the

functional deficits in the neurotransmitter release at neuromuscular endplates (Kong et al., 2009, Ruiz et al., 2010).

Another interesting finding of our microarray profiling studies was the observation of upregulated MHC class I transcripts simultaneously in both compartments upon depletion of Smn. An increase of MHC I expression in motoneurons has already been described in the case of axotomy, ventral-horn root avulsion, viral infection or after exposure to inflammatory cytokines (Boulanger and Shatz 2004). Even in motoneurons of C57Bl/6-SOD1[G93A] mice, a model of ALS, an upregulation of MHC class I genes at disease onset could be shown (Nardo et al., 2013). These findings could point to a potential neuroprotective function of upregulated MHC class I genes under consideration of other results showing the importance of increased MHC class I levels for regeneration of axons and for the stability of neuromuscular junctions after axonal damage (Oliveira et al., 2004, Thams et al., 2009). Furthermore, MHC class I genes have been suggested to be associated with synapse formation and synapse plasticity in the visual system and the hippocampus (Corriveau et al., 1998, Huh et al., 2000, Boulanger and Shatz 2004, Shatz 2009). An important role in the regulation of MHC class I expression seems to play neural activity. Previous results show that electrically active neurons are devoid of MHC class I expression. In contrast, MHC class I expression, including *β2-microglobulin*, can be induced by inhibiting spontaneous electrical currents with interferon-γ or tetrodotoxin (TTX) (Neumann et al., 1995). In contrast, in vivo experiments revealed a drastic downregulation of MHC class I expression upon TTX treatment (Corriveau et al., 1998). As even cultured motoneurons from Smn-deficient mice have been reported to displace reduced spontaneous activity in axons and growth cones at 4 DIV (Jablonka et al., 2007) the observed upregulation of MHC class I gene levels could be the consequence of the reduced neuronal activity. Furthermore, an increase in MHC class I transcripts could lead to subsequent reactions of nonneuronal cells involved in synaptic and axonal breakdown.

One difference of our results to previous studies (Baumer et al., 2009, Murray et al., 2010, Zhang et al., 2013) is the observation of a relatively large number of deregulated transcripts in the somatodendritic compartment. Although our finding is not surprising taking into account the essential role of Smn in several aspects of RNA processing, previous microarray and RNA-Seq studies only detected small

transcriptome changes in presymptomatic spinal cords or motoneurons of SMA mouse models. Explanations for these opposed findings could be differences in the remaining Smn transcript levels, differences in the progression of molecular defects or the fact that motoneurons only represent less than five percent of all cells in the spinal cord and these studies did not select for motoneurons. Furthermore, the previous described finding of an enrichment of minor-intron containing transcripts upon Smn loss could not be confirmed with our datasets. It has been shown that the levels of individual snRNPs are affected upon Smn deficiency in a tissue-specific manner. Particularly a decrease of minor spliceosomal snRNPs was observed, including U4atac, U11 and U12 (Gabanella et al., 2007, Zhang et al., 2008, Lotti et al., 2012, Praveen et al., 2012). In line with this is the detection of missplicing of minor intron containing transcripts in Smn deficient mouse cells and *Drosophila smn* mutant larvae, respectively. The consequence is the reduction of the transcript levels of these minor intron containing transcripts (Lotti et al., 2012). One example for a minor intron containing transcript is *Stasimon*. In Drosophila *smn* mutants a downregulation of Stasimon has been suggested to underlie dysfunctions in the motor circuit. But recent findings indicate that the observed splicing defects in *Drosophila smn* mutants could also result from a developmental arrest of these larvae rather than being a consequence of diminished smn levels (Praveen et al., 2012, Garcia et al., 2013). Even in presymptomatic SMA mice no defects in minor intron splicing could be observed (Zhang et al., 2013). Thus, further experiments are necessary to resolve if the alterations in the splicing of minor intron containing transcripts in Smn deficient cells and tissue are the result of reduced Smn levels or rather of the developmental timepoint.

Having a closer look onto the transcripts deregulated in the somatodendritic compartment upon Smn knockdown we found a high number of upregulated transcripts associated with different functions in RNA splicing. This finding is quite interesting taking into account the known function of Smn in the biogenesis of spliceosomal snRNPs. One example is the mRNA encoding Casc3 (also known as Btz or MLN51). Casc3 is part of the exon junction complex (EJC) (Le Hir et al., 2000, Le Hir et al., 2000) and was recently also found to enhance translation efficiency (Chazal et al., 2013). Further mRNAs upregulated after Smn depletion are the transcripts encoding Sf1 and U2af1. Both are components of the spliceosomal E

complex binding introns early during the splice cycle and marking branch point and 3' splice site (Wahl et al., 2009). Another interesting transcript is Srsf1 (also known as ASF/SF2), an SR protein stimulating U1 snRNP binding to the 5' splice site (Kohtz et al., 1994). Furthermore, we were able to detect an increased expression of Srpk2. This mRNA encodes a serine/arginine protein kinase phosphorylating the RS domains of SR proteins (Wang et al., 1998). Srsf1 was initially identified as a substrate for Srpk2 (Wang et al., 1998, Koizumi et al., 1999). Later publications instead suggested PRP28, a component of the U4/U6-U5 tri-snRNP, as the main target of Srpk2 (Mathew et al., 2008). Contrary to the ubiquitiously expressed Srpk1, Srpk2 displays a particularly high expression in the nervous system indicating a possible neuron-specific function (Wang et al., 1998). In line with this is the observation of Srpk2 upregulation in brains of a mouse model for Alzheimer's disease and the finding of a reduced axon length of primary neurons accompanied by reduced microtubule polymerization due to the phosphorylation of Tau upon overexpression of Srpk2 (Hong et al., 2012). In summary, our data show an upregulation of a number of different splicing factors in the somatodendritic compartment of motoneurons after Smn depletion. Still not solved is the question whether these alterations lead to altered splicing activities, to motoneuron dysfunction or whether they reflect a compensation mechanism to restore alterations in the snRNP repertoire.

In conclusion, the microarray profiling data of compartmentalized motoneurons upon Smn knockdown indicate an important role of Smn in the establishment of the axonal transcriptome. We show that depletion of Smn results in profound and distinct effects on transcripts in both the somatodendritic and the axonal compartment. The observed deregulated transcripts are associated with immune functions, splicing, synaptic vesicle release and maintenance of the cytoskeleton and therefore represent important parameters for appropriate motoneuron function.

4.2 Whole transcriptome amplification and high-throughput sequencing

Even though several studies gave insights into the subcellular transcriptome of neuron extensions so far revealing a complex composition (Deglincerti and Jaffrey

2012), an unbiased approach to obtain the whole transcriptome including coding and non-coding RNAs has not been done so far. Therefore, we optimized a protocol for whole transcriptome profiling based on a double-random priming strategy. Techniques for whole transcriptome amplification based on double-random priming have been described before (Froussard 1992, Pan et al., 2013). Although these methods have been successfully used for amplification of low RNA input amounts we applied some modifications. These improvements included the choice of polymerase during second strand synthesis as well as primer concentration during second strand synthesis and PCR. We could show that abundant transcripts like *Gapdh* are easily amplified under a wide range of reaction conditions. In contrast, less abundant RNAs seem to need adapted and optimal conditions. Furthermore, we could show that one round of second strand synthesis is sufficient for transcriptome capture, at least when *Taq* polymerase is used. In addition, it is possible to use PCR amplicons directly for Illumina library preparation without enzymatic interference. One problem we faced at the beginning was the missing 5' end heterogeneity. As the first few bases are normally used for cluster calling, Illumina MiSeq sequencing requires them to be heterogeneous (Fadrosh et al., 2014). Normally, for low diversity samples this 5' end heterogeneity is achieved by using higher amounts of the spike-in control phage library PhiX. We decided to overcome this problem by using four different adapter primers of various lengths at the same time during PCR. Therefore, we could obtain diverse 5' ends and could reduce the addition of spike-in control phage library PhiX to only 1%.

Another modification of our protocol, in contrast to existing methods is the scanning of all reads for presence of the adapter sequence. This makes sure that only reads derived from the amplification process are selected for. Besides that, we are able to eliminate PCR duplicates by using the random octamer sequence for molecule counting.

The adapted protocol I present here was tested on serially diluted mouse spinal cord total RNA. Interestingly, it was possible to scale the whole transcriptome profiling method down even to the lower picogram range of input RNA. At the moment, we estimate the lower limit of input RNA at around 50 pg. For this amount we obtained convincing quantitative results, but even for 10 pg total RNA a substantial number of transcripts was reliably detected. As even the relative transcript levels were

preserved for different numbers of amplification cycles this indicates that it is also possible to compare expression values across different RNA input amounts with our protocol.

To make now also use of this optimized method, we applied it to primary motoneurons. Therefore, we cultured the motoneurons in microfluidic chambers and extracted total RNA from the axonal as well as the somatodendritic compartment for comparison. The amount of RNA extracted from the axonal compartment is in the picogram range and therefore fits our protocol. Interestingly, our results show a highly similar RNA composition of motor axons compared to the somatodendritic compartment. The same result we already obtained from our microarray profiling experiments. Nevertheless, a large number of transcripts with distinct functions seem to be specifically enriched in either compartment. On the somatodendritic side, an enrichment of transcripts associated with synaptic functions became obvious most likely resulting from dendrites. In contrast, transcripts with described functions in protein synthesis, RNA processing and actin binding were enriched in the axonal compartment. As it is known that actin binding proteins and specifically the organization of the actin cytoskeleton play an important role in the establishment of growth cones (Pak et al., 2008) our results are in concordance with the current literature. Furthermore, defects of axonal translocation of the *β-actin* mRNA have been described in various models of motoneuron diseases (Rossoll et al., 2003). Another quite surprising finding was the observed existence of cell cycle associated mRNAs in the axonal compartment although this is in line with previous data showing the same result in embryonic dorsal root ganglia (Gumy et al., 2011). So far, these transcripts are primarily associated with nuclear functions although there is growing evidence that some of these transcripts could play important roles in axonal growth and pruning, neuronal migration, dendrite morphogenesis and spine formation as well as synaptic plasticity (Frank and Tsai 2009).

One crucial aspect of our whole transcriptome amplification protocol is that even non-coding RNAs including ribosomal RNAs are captured. In most existing protocols rRNAs are removed prior to library generation, but we think it could be advantegous to profile the whole transcriptome, especially for studies investigating the subcellular distribution of RNAs. Hence, one interesting finding was the detection of less rRNAs in the axonal compartment of motoneurons than expected when compared to the

somatodendritic compartment. Contrary, motor axons were enriched for transcripts coding for ribosomal proteins. One possible explanation for this observation could be that an alteration of the ribosomal RNA-to-protein stoichiometry might affect the number of functional ribosomes. Consequently, modification or regulation of local translation in motor axons could be achieved (Twiss and Fainzilber 2009). Furthermore, it should be noted, that ribosomal proteins have also been associated with extraribosomal functions. One example is the ribosomal protein Rpsa. It is described to have functions in ribosomal biogenesis and was found to bind cytoskeletal components like actin and tubulin as part of the 40S ribosomal subunit (Venticinque et al., 2011). In this function it also locally targets ribosomes to the cytoskeleton regulating thereby cell migration through protein synthesis. Furthermore, functions of Rpsa as laminin receptor and in the control of cell adhesion have been described (DiGiacomo and Meruelo 2015). Even a specific function of Rpsa in development should be taken into account regarding the observation that Rpsa mRNA levels increase during embryogenesis and decline in adulthood (Laurie et al., 1991). Still, the presence of transcripts encoding ribosomal proteins and translation factors in axons suggests a regulation of local translation, particularly in this subcellular compartment, but so far there are no clear proofs for this assumption. As the exact function of these transcripts in the axonal compartment is also highly discussed at the moment and many questions regarding this issue are still open, future studies are necessary to investigate in detail which transcripts are present and to what extent they are translated.

Additionaly, also other non-coding RNAs are captured by our whole transcriptome amplification protocol, providing an interesting opportunity to this field. In the last years it became evident that non-coding RNAs seem to have specific functions in the nervous system. First, they are especially enriched in the central nervous system (St Laurent et al., 2009) and are important for neurodevelopment. Second, even in neurodegenerative diseases they seem to have different functions although this needs to be examined in more detail as so far the most well understood ncRNA system are miRNAs and their post-transcriptional regulation of gene expression (Tal and Tanguay 2012).Therefore, it would be interesting to investigate the localization or enrichment of these non-coding RNAs in distinct subcellular compartments of neurons as well as their possible functions there. One example is the non-coding

RNA 7SK. In our datasets we found it to be highly abundant in the somatodendritic compartment compared to the axonal compartment. This is in line with its previous described nuclear function in transcriptional regulation (Zhou et al., 2012). In contrast, 7SL was enriched in the axonal compartment. 7SL is part of the signal recognition particle and therefore involved in the cotranslational transfer of proteins into the endoplasmic reticulum. Its enrichment in axons further points to the presence of a protein secretory machinery in axons (Merianda and Twiss 2013).

Another surprising finding was the observation of lincRNAs in the axonal compartment. So far, lincRNAs have been predominantly described with functions in the regulation of gene expression (Ulitsky and Bartel 2013). The axonal presence of these RNAs still suggests additional functions in the cytoplasm like translocation from the somatodendritic compartment into axons. It is known that RNA-binding proteins interact with lincRNAs mediating axonal transport. For example, *RMST* interacts with hnRNPA2/B1 (Ng et al., 2013). One possibility is that such RNA-protein complexes are sorted subcellularly mediating the axonal or dendritic trafficking of other RNAs as part of larger transport particles. Hence, our protocol could be helpful for the investigation of short and long non-coding RNAs and their influence on the axonal transcriptome upon loss of these RNAs.

In line with these data is furthermore the observation of intron-containing transcripts in the axonal compartment. So far, splicing is mostly only assumed to take place in the nucleus although the possibility for splicing in the cytoplasm has been discussed (Buckley et al., 2014). Another explanation for the presence of introns in axons is that introns themselves could give rise to functional RNAs independently of their associated RNAs and are therefore not only by-products of the splicing process (St Laurent et al., 2012). For both possibilities further investigation is needed to resolve the function of intron-containing transcripts in axons.

In this thesis I only present the application of our optimized whole transcriptome amplification protocol on compartmentalized motoneurons, but it may be also suitable for other detailed investigations. For example, also transcriptomes from other subcellular compartments like dendrites or growth cones could be profiled by our method. Additionally the protocol could also be applied to laser captured microdissection of the synaptic neuropil from hippocampal slices or other brain regions to investigate transcript alterations in association with synaptic plasticity.

Finally, even for single cell studies our protocol provides an opportunity to monitor both coding and non-coding transcripts.

To investigate also in more detail the influence of hnRNP R on the somatodendritic and axonal transcriptome of motoneurons, we performed both microarray profiling and whole transcriptome amplification followed by RNA-Sequencing of RNA isolated from both compartments of motoneurons grown in microfluidic chambers. Both different approaches gave similar results. In the somatodendritic compartment of hnRNP R knockdown motoneurons transcripts associated with RNA-binding were upregulated. In contrast, transcripts with functions in synaptic transmission were downregulated suggesting a different regulation of its RNA targets by hnRNP R. In line with this finding we also observed that both up- and downregulated transcripts harbor significantly more hnRNP R iCLIP tags than unregulated transcripts.

Also interesting was the finding that almost no overlap could be found between the deregulated transcripts in the somatodendritic compartment and the ones in the axonal compartment. This indicates that the transcript changes in the axonal compartment of compartmentalized knockdown motoneurons are not simply occurring due to alterations in their abundance in the cell body but are rather reflecting an active mechanism with respect to their transport or stability in axons. This observation is underlined by the association of only downregulated transcripts with significantly more iCLIP tags compared to unregulated transcripts. Nevertheless, in both compartments we found upregulated transcripts associated with translation.

As described in the result section above, we also performed iCLIP of hnRNP R in motoneurons. One prominent finding in these experiments was the short noncoding RNA 7SK as the main target of hnRNP R. Therefore we decided to investigate this candidate further. 7SK is a 331nt abundant nuclear RNA which regulates transcription through sequestering the positive transcription elongation factor b (P-TEFb) by forming the 7SK/P-TEFb complex (Nguyen et al., 2001, Yang et al., 2001). The fraction of 7SK RNA which is not bound to P-TEFb associates with other proteins. These proteins include hnRNP A1, A2/B1, R and Q, forming distinct 7SK/hnRNP complexes with 7SK (Barrandon et al., 2007, Hogg and Collins 2007, Van Herreweghe et al., 2007). The balance between both complexes, 7SK/P-TEFb

and 7SK/hnRNP, is regulated through transcriptional activity. This means that hnRNP proteins indirectly adjust the levels of active P-TEFb through competitive binding of 7SK RNA (Barrandon et al., 2007, Van Herreweghe et al., 2007, Barrandon et al., 2008). Recently, it has also been suggested that SR splicing factors bind to nascent RNA as part of the 7SK complex. This leads to P-TEFb release promoting transcriptional pause release (Ji et al., 2013). Furthermore, by genome-wide analysis of the transcriptional consequences upon 7SK knockdown novel functions for 7SK in the control of transcriptional termination and in the prevention of upstream antisense termination have been revealed (Castelo-Branco et al., 2013).

So far, only the regulation of P-TEFb activity through 7SK has been described in detail but not the potential roles of the 7SK/hnRNP subcomplexes. In our RNA-Seq experiments of wildtype compartmentalized motoneurons the non-coding 7SK RNA was detectable in axons. In addition, knockdown of 7SK RNA leads to shorter motor axons without affecting the survival. We therefore sought to investigate transcriptome changes in compartmentalized 7SK knockdown motoneuron cultures. Furthermore, we wanted to compare potential transcriptome changes with those obtained after hnRNP R knockdown. Our results showed that a subset of axonal transcripts is regulated in a similar manner by 7SK and hnRNP R.

Interestingly, among the upregulated transcripts in the axonal compartment of both knockdowns, many are either encoding ribosomal proteins and are therefore associated with translation or are involved in functions related to neurodegeneration, in particular in ALS (*ApoE*, *Fthl*, *Ftl1*). In contrast, downregulated transcripts mostly encode proteins involved in axon outgrowth or cytoskeleton assembly suggesting a possible reason for the disturbed axon outgrowth phenotype of 7SK or hnRNP R depleted motoneurons. Moreover, the upregulation of transcripts encoding ribosomal proteins suggests an enhanced capacity for protein synthesis. It has been suggested that growing axons exhibit an increased translational potential which decreases during maturation of the neurons (Jung et al., 2012) although experiments especially with motoneurons are lacking so far. In our culture systems motoneurons are maintained for 7 DIV. At this timepoint axonal outgrowth is largely completed. Therefore, it might be possible that an enhanced protein synthesis ability indicates either some celltype-specific quality or propably a delayed maturation. This also would be in line with the reduced axon outgrowth of our knockdown cultures.

Alternatively it is possible that the upregulation of the ribosomal proteins is a compensatory mechanism counteracting the loss of certain mRNAs and their associated proteins in motor axons. However, upregulation of specific ribosomal proteins can also have the opposite effect leading to a disruption of ribosomes due to an altered stoichiometry (Kim et al., 2014). Therefore, future experiments are needed to clarify the specific role of ribosomal proteins in the axons of motoneurons and to measure the rate of protein synthesis.

In summary, our results suggest that 7SK RNA participates in the role of hnRNP R in axon outgrowth of motoneurons. So far, we cannot rule out the possibility that the axonal 7SK knockdown phenotype is based on a transcriptional component. However, our results also suggest a mechanistic model according to which cytosolic 7SK/hnRNP complexes control axon elongation in motoneurons.

Analysis of the obtained results from Tdp-43 knockdown cultures also revealed highly interesting results. Especially the validation of distinct transcripts deregulated in the axonal compartment of motoneurons upon Tdp-43 knockdown showed interesting candidates. First of all, the previous reported downregulation of Nefl mRNA after Tdp-43 depletion (Strong et al., 2007) could be confirmed by us both with RNA-Seq and qPCR. Furthermore, closer examination of the list of downregulated transcripts in the axons of Tdp-43 knockdown motoneurons revealed several tubulin transcripts. Tubulins are built from αβ-heterodimers forming protofilaments (Wade 2009). Both α- and β-tubulins are highly conserved. Analysis of our RNA-Seq data upon Tdp-43 knockdown revealed deregulation of transcripts of both isoforms. Although most of these transcripts (Tubb6, Tubb5, Tuba1b and Tubb2a) were predicted to be downregulated in the axons of knockdown motoneurons, two of them (Tuba1a and Tubb4a) showed an upregulation in their transcript levels. Especially the downregulated tubulin transcripts could be confirmed also by qPCR suggesting an important role for tubulin transcripts in axon growth and establishment. This becomes even more interesting regarding the fact that a knockdown of Tdp-43 also downregulates histone deacetylase 6 (HDAC6) (Fiesel et al., 2010), a solely cytoplasmic α-tubulin deacetylase (Hubbert et al., 2002). In the cytoplasm, HDAC6 associates with microtubules, as well as the microtubule motor complex p150^{glued} (Smith et al., 2000), mediating the deacetylation of polymerized microtubules

(Hubbert et al., 2002). Furthermore, HDAC6 seems to be in close association with neurodegeneration and histone deacetylase inhibitors are already discussed as therapeutic tools (Rivieccio et al., 2009, Dietz and Casaccia 2010, d'Ydewalle et al., 2012).

Although Smn itself is not a RNA binding protein but is part of RNP complexes, we also performed RNA-Seq on Smn knockdown cultures and subsequent analysis of these data revealed interesting results. First, GOterm analysis of transcripts downregulated in the axonal compartment upon Smn depletion showed a high enrichment for GOterms associated with actin cytoskeleton and actin binding. This is in line with previous studies suggesting a relationship between SMA and actin dynamics (van Bergeijk et al., 2006, Bowerman et al., 2007, van Bergeijk et al., 2007, Bowerman et al., 2009, Nolle et al., 2011). Interestingly, Plastin 3 is often discussed as additional modifier (Oprea et al., 2008). The validation of distinct transcripts by qPCR showed a downregulation of the *Plastin 3* transcript in the axons of Smn knockdown motoneurons. Although a decrease in *Plastin 3* transcript levels specifically in axons upon Smn knockdown has not been described before, a correlation between *Plastin 3* expression and the severity of SMA has been reported in patients (Oprea et al., 2008). Another observation that is in line with our GOterm results is the recently published enhanced activation of RhoA and ROCK in the spinal cord of a SMA mouse model (Coque et al., 2014). Both small GTPase RhoA and its major downstream effector Rho kinase (ROCK) are key players in cytoskeletal organization and are suggested to contribute to the pathology of motoneuron diseases. Therefore, an inhibition of ROCK as a therapy for SMA is widely discussed (Bowerman et al., 2010, Nolle et al., 2011, Bowerman et al., 2012, Hensel et al., 2014).

In our studies, we only did a comparison of microarray and RNA-Seq results for our whole transcriptome amplification method, but not for all the knockdown experiments. Nevertheless, we obtained data suggesting that RNA-Seq performs better in gene detection and differential gene expression analysis. This is also in line with several studies comparing microarray and RNA-seq results (Marioni et al., 2008, Guo et al., 2013, Xu et al., 2013, Mantione et al., 2014, Wang et al., 2014, Zhao et al., 2014)

revealing especially a higher specificity for RNA-Seq for the detection of low abundant genes. Although microarrays are a widely used tool in transcriptome studies there are still some disadvantages compared to RNA-Seq. The most important disadvantages of microarrays are the possibility of crosshybridization as well as the occurrence of non-specific background noise (Zhao et al., 2014), two problems not occurring with RNA-Seq. But even the genomic ranges covered by both approaches differs significantly (Xu et al., 2013). Additionally, RNA-Seq discovers expressed transcripts in an unbiased manner and is therefore independent of probe design turning it into a highly promising method in future. Nevertheless, all studies comparing microarray profiling with RNA-seq are still showing a high overlap between both approaches suggesting both methods as useful tools for transcriptome studies.

4.3 Outlook

In this thesis I have obtained unbiased data regarding the axonal transcriptome of motoneurons from control and disease-related conditions. Bioinformatical analysis of the data gives us a global overview and therefore a first hint of what is going on with respect to altered axonal RNA metabolism, pathing a direction which appears worthwhile to go further. Nevertheless, although the validation of individual candidates already narrows down the analysis, the search for key players in these processes should be followed up in more detail. To do this many questions should be answered and many experiments could be suggested or thought of.

One of the first questions could be the effect of mutations in RNA-binding proteins onto the transcriptome. Especially for TDP-43 many mutations have been discovered so far (Scotter et al., 2015). Until now 38 mutations have been identified in the *TARDBP* gene clustering prominently in the region encoding the C-terminus. The same as in wildtype proteinopathy, also mutant TDP-43 proteinopathy exhibits cytoplasmic accumulations as aggregated and insoluble deposits (Rutherford et al., 2008, Van Deerlin et al., 2008). Furthermore, nuclear clearing in a subset of motoneurons (Rutherford et al., 2008) as well as C-terminal fragmentation could be observed (Yokoseki et al., 2008). As some studies reported that cytoplasmic TDP-43 aggregates colocalize with stress granule markers (Colombrita et al., 2009, Liu-

Yesucevitz et al., 2010, Dewey et al., 2011, McDonald et al., 2011, Wolozin 2012) two different models of TDP-43 aggregate formation could be proposed (Dewey et al., 2012). One model supposes that an aggregation of TDP-43 is independent of stress granules whereas the other model follows the idea that stress granule formation contributes to TDP-43 aggregation implying that chronic stress leads to concentration-dependent TDP-43 aggregation. Nevertheless, the association of TDP-43 with cytoplasmic stress granules seems to be a reversible process in healthy conditions becoming severly disturbed in pathological conditions. (Liu-Yesucevitz et al., 2010, Li et al., 2013). These results are basis for the assumption that mutant TDP-43 proteinopathy and TDP-43 knockdown conditions are similar in their effects leading to disturbed axonal RNA metabolism. As TDP-43 knockdown leads to massive changes of especially the axonal transcriptome it would be interesting to even investigate the transcriptome in both compartments of compartmentalized motoneurons when TDP-43 is mutated rather than knocked down.

In line with this is the question if the transcriptome changes upon knockdown of the RNA-binding proteins TDP-43 or hnRNP R are direct or indirect consequences. So far, our results just give a global impression of the transcriptome changes but we do not know which altered transcripts are directly bound by the RNA-binding proteins and which are not. To answer this question a first approach could be to do iCLIP of the specific proteins and compare the results with the already obtained RNA-Seq data. This procedure has already been described in the result section in the case of hnRNP R. For TDP-43 (i)CLIP experiments have been done by two independent groups so far (Polymenidou et al., 2011, Tollervey et al., 2011). As both of them used brain samples, either mouse or human to identify direct RNA targets, no experiments with primary motoneurons have been done so far. Therefore, it would be interesting to do iCLIP of TDP-43 in motoneurons and compare the identified RNA targets with the transcriptome changes upon TDP-43 knockdown.

As the knockdown of Smn shows the biggest transcriptome alterations in our studies compared to the Tdp-43 and the hnRNP R knockdown, and taking into account that SMN itself is not a RNA-binding protein, this leads to the hypothesis that SMN is part of many different RNP transport complexes mediating RNA transport. Therefore, one interesting idea would be to try immunoprecipitation of the whole SMN complex to

investigate the transcriptome alterations upon SMN deficiency in more detail. Admittedly, one problem here will still be that we are not able to distinguish the different SMN containing complexes and just precipitate all of them at the same time. But one idea could be to repeat as a subsequent step the immunoprecipitation experiments of the SMN complexes under knockdown conditions of individual RNA-binding proteins. As it is already known that SMN interacts with TDP-43 (Wang et al., 2002, Tsuiji et al., 2013), hnRNP R (Rossoll et al., 2002) and FUS (Yamazaki et al., 2012) all three of them would be possible candidates. Furthermore, it would be even more interesting to do these immunoprecipitation experiments only from the axonal compartment. Although this will be highly challenging due to the very low amounts of RNA and protein on the axonal side this would give us a specific insight into the composition of RNP transport complexes in the axons of motoneurons. Additionally, it could be even worth thinking to try the immunoprecipitation the other way around namely with a specific RNA. Via this method one would be able to have a closer look on a distinct RNA and to resolve the RNP transport complex(es) specifically for this individual RNA.

Another quite interesting question is whether the detected transcriptome alterations upon knockdown of any of the proteins are also reflected in the proteome. Therefore, it would be important to first determine the proteome in the somatodendritic and the axonal compartment of compartmentalized wildtype motoneurons and to compare the resulting levels of protein abundance with the RNA abundance. Subsequently, these experiments could then be repeated with knockdown cultures. Again, one limiting factor will be the low amount of protein in the axonal compartment as here amplification is not possible making these experiments quite challenging. In line with this idea is the establishment of a ribosome-profiling technique suitable for motoneuron cultures in general and for compartmentalized motoneuron cultures in particular. With this method it could be possible to directly monitor which mRNAs are translated at the moment of cell lysis. Ribosome profiling has been described before with different modifications (Arava et al., 2003, Ingolia et al., 2009, Heiman et al., 2014, Jan et al., 2014, Williams et al., 2014). So far, two main protocols are available. The first is based on gradient centrifugation (Arava et al., 2003), the second one on

immunoprecipitation of purified ribosomes (Heiman et al., 2014, Jan et al., 2014, Williams et al., 2014).

To overcome the problem of the low amounts of RNA or protein in the axonal compartment another idea would be to make use of either ES cell- or iPS cell derived motoneurons. So far these cells are widely used and seem to resemble primary mouse motoneurons (Wichterle et al., 2002, Su et al., 2013, Toma et al., 2015). Because this method is not limited in producing huge amounts of motoneurons experiments could be repeated with higher numbers of cells. As it is even possible to differentiate motoneurons out of hiPS cells it would be also interesting to use hiPS cell lines from patients presenting neurodegenerative diseases to investigate the underlying mechanisms in more detail.

So far, virtually all experiments are done *in vitro*. Therefore, it would also be quite important to investigate the *in vivo* situation. We could isolate distinct nerves from early postnatal or even adult mice (wildtype mice or mouse models for neurodegenerative diseases) and compare the axonal transcriptome as well as the axonal proteome from our *in vitro* experiments with the transcriptome obtained from the isolated nerves. As the nerves only contain axons and no cell bodies the results from both experiments should be comparable. One example are the *Smn-/-;SMN2tg* mice or the *Smn-/-;SMN2;SMNΔ7* mice, both mouse models for SMA. As the *Smn-/-;SMN2tg* mice die normally latest two days after birth it will be quite difficult to isolate nerves. Hence, it would be a good idea to start with the *Smn-/-;SMN2;SMNΔ7* mouse model and dissect nerves from P1 or P6 pups. But still one problem could be the contamination of the axonal transcriptome with surrounding Schwann cells. Normally the development of Schwann cells starts around birth, but to be sure to obtain a pure axonal transcriptome different markers like myelin protein zero (P0) or myelin basic protein (Mbp) could be used to exclude any contamination for both transcriptome as well as proteome analysis.

In conclusion, this study has revealed a broad spectrum of novel data on the axonal transcriptome of primary mouse motoneurons in general as well as transcript level changes of multiple specific RNAs under disease-resembling knockdown conditions.

The presented results here already point to interesting candidates and therefore provide a good starting point for subsequent experiments for further elucidation of the mechanisms underlying neurodegenerative diseases like ALS and SMA.

5 List of figures

6 List of tables

7 References

Agnes, F. and M. Perron (2004). RNA-binding proteins and neural development: a matter of targets and complexes. Neuroreport **15**(17): 2567-2570.

Andersen, P. M. and A. Al-Chalabi (2011). Clinical genetics of amyotrophic lateral sclerosis: what do we really know? Nat Rev Neurol **7**(11): 603-615.

Andreassi, C., et al. (2010). An NGF-responsive element targets myo-inositol monophosphatase-1 mRNA to sympathetic neuron axons. Nat Neurosci **13**(3): 291-301.

Antar, L. N., et al. (2005). Localization of FMRP-associated mRNA granules and requirement of microtubules for activity-dependent trafficking in hippocampal neurons. Genes Brain Behav **4**(6): 350-359.

Arava, Y., et al. (2003). Genome-wide analysis of mRNA translation profiles in Saccharomyces cerevisiae. Proc Natl Acad Sci U S A **100**(7): 3889-3894.

Atlas, R., et al. (2007). Dynamic association with polysomes during P19 neuronal differentiation and an untranslated-region-dependent translation regulation of the tau mRNA by the tau mRNA-associated proteins IMP1, HuD, and G3BP1. J Neurosci Res **85**(1): 173-183.

Barrandon, C., et al. (2007). The transcription-dependent dissociation of P-TEFb-HEXIM1-7SK RNA relies upon formation of hnRNP-7SK RNA complexes. Mol Cell Biol **27**(20): 6996-7006.

Barrandon, C., et al. (2008). Non-coding RNAs regulating the transcriptional machinery. Biol Cell **100**(2): 83-95.

Barry, J., et al. (2014). Ankyrin-G directly binds to kinesin-1 to transport voltage-gated Na+ channels into axons. Dev Cell **28**(2): 117-131.

Battle, D. J., et al. (2006). The SMN complex: an assembly machine for RNPs. Cold Spring Harb Symp Quant Biol **71**: 313-320.

Baumer, D., et al. (2009). Alternative splicing events are a late feature of pathology in a mouse model of spinal muscular atrophy. PLoS Genet **5**(12): e1000773.

Ben-Yaakov, K., et al. (2012). Axonal transcription factors signal retrogradely in lesioned peripheral nerve. EMBO J **31**(6): 1350-1363.

Bi, J., et al. (2007). Copb1-facilitated axonal transport and translation of kappa opioid-receptor mRNA. Proc Natl Acad Sci U S A **104**(34): 13810-13815.

Bolstad, B. M., et al. (2003). A comparison of normalization methods for high density oligonucleotide array data based on variance and bias. Bioinformatics **19**(2): 185-193.

Boulanger, L. M. and C. J. Shatz (2004). Immune signalling in neural development, synaptic plasticity and disease. Nat Rev Neurosci **5**(7): 521-531.

Bowerman, M., et al. (2009). SMN, profilin IIa and plastin 3: a link between the deregulation of actin dynamics and SMA pathogenesis. Mol Cell Neurosci **42**(1): 66-74.

Bowerman, M., et al. (2010). Rho-kinase inactivation prolongs survival of an intermediate SMA mouse model. Hum Mol Genet **19**(8): 1468-1478.

Bowerman, M., et al. (2012). Fasudil improves survival and promotes skeletal muscle development in a mouse model of spinal muscular atrophy. BMC Med **10**: 24.

Bowerman, M., et al. (2007). Smn depletion alters profilin II expression and leads to upregulation of the RhoA/ROCK pathway and defects in neuronal integrity. J Mol Neurosci **32**(2): 120-131.

Brittis, P. A., et al. (2002). Axonal protein synthesis provides a mechanism for localized regulation at an intermediate target. Cell **110**(2): 223-235.

Buckley, P. T., et al. (2014). Cytoplasmic intron retention, function, splicing, and the sentinel RNA hypothesis. Wiley Interdiscip Rev RNA **5**(2): 223-230.

Buratti, E. and F. Baralle (2010). The multiple roles of TDP-43 in pre-mRNA processing and gene expression regulation. RNA Biol **7**: 420 - 429.

Buratti, E. and F. E. Baralle (2008). Multiple roles of TDP-43 in gene expression, splicing regulation, and human disease. Front Biosci **13**: 867-878.

Buratti, E., et al. (2010). Nuclear factor TDP-43 can affect selected microRNA levels. Febs j **277**(10): 2268-2281.

Buratti, E., et al. (2001). Nuclear factor TDP-43 and SR proteins promote in vitro and in vivo CFTR exon 9 skipping. EMBO J **20**(7): 1774-1784.

Burghes, A. H. and C. E. Beattie (2009). Spinal muscular atrophy: why do low levels of survival motor neuron protein make motor neurons sick? Nat Rev Neurosci **10**(8): 597-609.

Castelo-Branco, G., et al. (2013). The non-coding snRNA 7SK controls transcriptional termination, poising, and bidirectionality in embryonic stem cells. Genome Biol **14**(9): R98.

Chari, A., et al. (2008). An assembly chaperone collaborates with the SMN complex to generate spliceosomal SnRNPs. Cell **135**(3): 497-509.

Chazal, P. E., et al. (2013). EJC core component MLN51 interacts with eIF3 and activates translation. Proc Natl Acad Sci U S A **110**(15): 5903-5908.

Chen, S., et al. (2013). Genetics of amyotrophic lateral sclerosis: an update. Molecular Neurodegeneration **8**(1): 28.

Chen, Y., et al. (2011). Adenomatous polyposis coli regulates axon arborization and cytoskeleton organization via its N-terminus. PLoS One **6**(9): e24335.

Cho, S. and G. Dreyfuss (2010). A degron created by SMN2 exon 7 skipping is a principal contributor to spinal muscular atrophy severity. Genes Dev **24**(5): 438-442.

Clement, A. M., et al. (2003). Wild-type nonneuronal cells extend survival of SOD1 mutant motor neurons in ALS mice. Science **302**(5642): 113-117.

Colombrita, C., et al. (2012). TDP-43 and FUS RNA-binding Proteins Bind Distinct Sets of Cytoplasmic Messenger RNAs and Differently Regulate Their Post-transcriptional Fate in Motoneuron-like Cells. Journal of Biological Chemistry **287**(19): 15635-15647.

Colombrita, C., et al. (2009). TDP-43 is recruited to stress granules in conditions of oxidative insult. J Neurochem **111**(4): 1051-1061.

Coque, E., et al. (2014). ROCK inhibition as a therapy for spinal muscular atrophy: understanding the repercussions on multiple cellular targets. Front Neurosci **8**: 271.

Corriveau, R. A., et al. (1998). Regulation of Class I MHC Gene Expression in the Developing and Mature CNS by Neural Activity. Neuron **21**(3): 505-520.

Crawford, T. O. and C. A. Pardo (1996). The neurobiology of childhood spinal muscular atrophy. Neurobiol Dis **3**(2): 97-110.

Crosio, C., et al. (2000). La protein has a positive effect on the translation of TOP mRNAs in vivo. Nucleic Acids Res **28**(15): 2927-2934.

d'Ydewalle, C., et al. (2012). HDAC6 at the Intersection of Neuroprotection and Neurodegeneration. Traffic **13**(6): 771-779.

Damiano, M., et al. (2006). Neural mitochondrial Ca2+ capacity impairment precedes the onset of motor symptoms in G93A Cu/Zn-superoxide dismutase mutant mice. J Neurochem **96**(5): 1349-1361.

Darnell, J. C., et al. (2011). FMRP stalls ribosomal translocation on mRNAs linked to synaptic function and autism. Cell **146**(2): 247-261.

De Vos, K. J., et al. (2007). Familial amyotrophic lateral sclerosis-linked SOD1 mutants perturb fast axonal transport to reduce axonal mitochondria content. Hum Mol Genet **16**(22): 2720-2728.

Deglincerti, A. and S. R. Jaffrey (2012). Insights into the roles of local translation from the axonal transcriptome. Open Biology **2**(6).

Deuel, T. A., et al. (2006). Genetic interactions between doublecortin and doublecortin-like kinase in neuronal migration and axon outgrowth. Neuron **49**(1): 41-53.

Dewey, C. M., et al. (2011). TDP-43 is directed to stress granules by sorbitol, a novel physiological osmotic and oxidative stressor. Mol Cell Biol **31**(5): 1098-1108.

Dewey, C. M., et al. (2012). TDP-43 aggregation in neurodegeneration: are stress granules the key? Brain Res **1462**: 16-25.

Di Giorgio, F. P., et al. (2008). Human embryonic stem cell-derived motor neurons are sensitive to the toxic effect of glial cells carrying an ALS-causing mutation. Cell Stem Cell **3**(6): 637-648.

Dietz, K. C. and P. Casaccia (2010). HDAC inhibitors and neurodegeneration: at the edge between protection and damage. Pharmacol Res **62**(1): 11-17.

DiGiacomo, V. and D. Meruelo (2015). Looking into laminin receptor: critical discussion regarding the non-integrin 37/67-kDa laminin receptor/RPSA protein. Biol Rev Camb Philos Soc.

Dombert, B., et al. (2014). Presynaptic Localization of Smn and hnRNP R in Axon Terminals of Embryonic and Postnatal Mouse Motoneurons. PLoS One **9**(10): e110846.

Donnelly, C. J., et al. (2011). Limited availability of ZBP1 restricts axonal mRNA localization and nerve regeneration capacity. EMBO J **30**(22): 4665-4677.

DuBridge, R. B., et al. (1987). Analysis of mutation in human cells by using an Epstein-Barr virus shuttle system. Mol Cell Biol **7**(1): 379-387.

Dull, T., et al. (1998). A third-generation lentivirus vector with a conditional packaging system. J Virol **72**(11): 8463-8471.

Edgar, R., et al. (2002). Gene Expression Omnibus: NCBI gene expression and hybridization array data repository. Nucleic Acids Res **30**(1): 207-210.

Fadrosh, D. W., et al. (2014). An improved dual-indexing approach for multiplexed 16S rRNA gene sequencing on the Illumina MiSeq platform. Microbiome **2**(1): 6.

Fallini, C., et al. (2012). The ALS disease protein TDP-43 is actively transported in motor neuron axons and regulates axon outgrowth. Hum Mol Genet **21**(16): 3703-3718.

Fallini, C., et al. (2014). Dynamics of survival of motor neuron (SMN) protein interaction with the mRNA-binding protein IMP1 facilitates its trafficking into motor neuron axons. Dev Neurobiol **74**(3): 319-332.

Fallini, C., et al. (2011). The Survival of Motor Neuron (SMN) Protein Interacts with the mRNA-Binding Protein HuD and Regulates Localization of Poly(A) mRNA in Primary Motor Neuron Axons. The Journal of Neuroscience **31**(10): 3914-3925.

Feiguin, F., et al. (2009). Depletion of TDP-43 affects Drosophila motoneurons terminal synapsis and locomotive behavior. FEBS Lett **583**(10): 1586-1592.

Feng, J., et al. (2002). Regulation of neurotransmitter release by synapsin III. J Neurosci **22**(11): 4372-4380.

Fiesel, F. C., et al. (2011). TDP-43 knockdown impairs neurite outgrowth dependent on its target histone deacetylase 6. Mol Neurodegener **6**: 64.

Fiesel, F. C., et al. (2010). Knockdown of transactive response DNA-binding protein (TDP-43) downregulates histone deacetylase 6. EMBO J **29**(1): 209-221.

Fischer, U., et al. (1997). The SMN-SIP1 complex has an essential role in spliceosomal snRNP biogenesis. Cell **90**(6): 1023-1029.

Frank, C. L. and L. H. Tsai (2009). Alternative functions of core cell cycle regulators in neuronal migration, neuronal maturation, and synaptic plasticity. Neuron **62**(3): 312-326.

Froussard, P. (1992). A random-PCR method (rPCR) to construct whole cDNA library from low amounts of RNA. Nucleic Acids Res **20**(11): 2900.

Fu, X., et al. (2013). Doublecortin (Dcx) family proteins regulate filamentous actin structure in developing neurons. J Neurosci **33**(2): 709-721.

Gabanella, F., et al. (2007). Ribonucleoprotein assembly defects correlate with spinal muscular atrophy severity and preferentially affect a subset of spliceosomal snRNPs. PLoS One **2**(9): e921.

Garcia, E. L., et al. (2013). Developmental arrest of Drosophila survival motor neuron (Smn) mutants accounts for differences in expression of minor intron-containing genes. RNA **19**(11): 1510-1516.

Glinka, M., et al. (2010). The heterogeneous nuclear ribonucleoprotein-R is necessary for axonal β-actin mRNA translocation in spinal motor neurons. Human Molecular Genetics **19**(10): 1951-1966.

Glisovic, T., et al. (2008). RNA-binding proteins and post-transcriptional gene regulation. FEBS Lett **582**(14): 1977-1986.

Grosskreutz, J., et al. (2010). Calcium dysregulation in amyotrophic lateral sclerosis. Cell Calcium **47**(2): 165-174.

Gumy, L. F., et al. (2011). Transcriptome analysis of embryonic and adult sensory axons reveals changes in mRNA repertoire localization. RNA **17**(1): 85-98.

Guo, Y., et al. (2013). Large Scale Comparison of Gene Expression Levels by Microarrays and RNAseq Using TCGA Data. PLoS One **8**(8): e71462.

Gurney, M. E., et al. (1994). Motor neuron degeneration in mice that express a human Cu,Zn superoxide dismutase mutation. Science **264**(5166): 1772-1775.

Harraz, M. M., et al. (2008). SOD1 mutations disrupt redox-sensitive Rac regulation of NADPH oxidase in a familial ALS model. J Clin Invest **118**(2): 659-670.

Hassfeld, W., et al. (1998). Molecular definition of heterogeneous nuclear ribonucleoprotein R (hnRNP R) using autoimmune antibody: immunological relationship with hnRNP P. Nucleic Acids Res **26**(2): 439-445.

Heiman, M., et al. (2014). Cell type-specific mRNA purification by translating ribosome affinity purification (TRAP). Nat Protoc **9**(6): 1282-1291.

Hensel, N., et al. (2014). Bilateral crosstalk of rho- and extracellular-signal-regulated-kinase (ERK) pathways is confined to an unidirectional mode in spinal muscular atrophy (SMA). Cell Signal **26**(3): 540-548.

Higashi, S., et al. (2007). Concurrence of TDP-43, tau and alpha-synuclein pathology in brains of Alzheimer's disease and dementia with Lewy bodies. Brain Res **1184**: 284-294.

Hogg, J. R. and K. Collins (2007). RNA-based affinity purification reveals 7SK RNPs with distinct composition and regulation. RNA **13**(6): 868-880.

Hong, Y., et al. (2012). SRPK2 phosphorylates tau and mediates the cognitive defects in Alzheimer's disease. J Neurosci **32**(48): 17262-17272.

Huang da, W., et al. (2009). Systematic and integrative analysis of large gene lists using DAVID bioinformatics resources. Nat Protoc **4**(1): 44-57.

Hubbert, C., et al. (2002). HDAC6 is a microtubule-associated deacetylase. Nature **417**(6887): 455-458.

Huh, G. S., et al. (2000). Functional requirement for class I MHC in CNS development and plasticity. Science **290**(5499): 2155-2159.

Ingolia, N. T., et al. (2009). Genome-wide analysis in vivo of translation with nucleotide resolution using ribosome profiling. Science **324**(5924): 218-223.

Jablonka, S., et al. (2007). Defective Ca2+ channel clustering in axon terminals disturbs excitability in motoneurons in spinal muscular atrophy. J Cell Biol **179**(1): 139-149.

Jan, C. H., et al. (2014). Principles of ER cotranslational translocation revealed by proximity-specific ribosome profiling. Science **346**(6210): 1257521.

Ji, X., et al. (2013). SR proteins collaborate with 7SK and promoter-associated nascent RNA to release paused polymerase. Cell **153**(4): 855-868.

Jonson, L., et al. (2007). Molecular composition of IMP1 ribonucleoprotein granules. Mol Cell Proteomics **6**(5): 798-811.

Jung, H., et al. (2012). Axonal mRNA localization and local protein synthesis in nervous system assembly, maintenance and repair. Nat Rev Neurosci **13**(5): 308-324.

Kar, A. N., et al. (2013). Intra-axonal synthesis of eukaryotic translation initiation factors regulates local protein synthesis and axon growth in rat sympathetic neurons. J Neurosci **33**(17): 7165-7174.

Kariya, S., et al. (2008). Reduced SMN protein impairs maturation of the neuromuscular junctions in mouse models of spinal muscular atrophy. Hum Mol Genet **17**(16): 2552-2569.

Kim, T. H., et al. (2014). Ribosomal proteins as unrevealed caretakers for cellular stress and genomic instability. Oncotarget **5**(4): 860-871.

Kohtz, J. D., et al. (1994). Protein-protein interactions and 5'-splice-site recognition in mammalian mRNA precursors. Nature **368**(6467): 119-124.

Koizumi, J., et al. (1999). The subcellular localization of SF2/ASF is regulated by direct interaction with SR protein kinases (SRPKs). J Biol Chem **274**(16): 11125-11131.

Kolb, S. J., et al. (2007). Molecular functions of the SMN complex. J Child Neurol **22**(8): 990-994.

Kong, L., et al. (2009). Impaired synaptic vesicle release and immaturity of neuromuscular junctions in spinal muscular atrophy mice. J Neurosci **29**(3): 842-851.

Krecic, A. M. and M. S. Swanson (1999). hnRNP complexes: composition, structure, and function. Curr Opin Cell Biol **11**(3): 363-371.

Kundel, M., et al. (2009). Cytoplasmic polyadenylation element-binding protein regulates neurotrophin-3-dependent beta-catenin mRNA translation in developing hippocampal neurons. J Neurosci **29**(43): 13630-13639.

Laurie, G. W., et al. (1991). Elevated 32-kDa LBP and low laminin mRNA expression in developing mouse cerebrum. Differentiation **46**(3): 173-179.

Le Hir, H., et al. (2000). The spliceosome deposits multiple proteins 20-24 nucleotides upstream of mRNA exon-exon junctions. EMBO J **19**(24): 6860-6869.

Le Hir, H., et al. (2000). Pre-mRNA splicing alters mRNP composition: evidence for stable association of proteins at exon-exon junctions. Genes Dev **14**(9): 1098-1108.

Lefebvre, S., et al. (1995). Identification and characterization of a spinal muscular atrophy-determining gene. Cell **80**: 155 - 165.

Li, D. K., et al. (2014). SMN control of RNP assembly: from post-transcriptional gene regulation to motor neuron disease. Semin Cell Dev Biol **32**: 22-29.

Li, Y. R., et al. (2013). Stress granules as crucibles of ALS pathogenesis. J Cell Biol **201**(3): 361-372.

Liu-Yesucevitz, L., et al. (2011). Local RNA translation at the synapse and in disease. J Neurosci **31**(45): 16086-16093.

Liu-Yesucevitz, L., et al. (2010). Tar DNA binding protein-43 (TDP-43) associates with stress granules: analysis of cultured cells and pathological brain tissue. PLoS One **5**(10): e13250.

Liu, Q., et al. (1997). The spinal muscular atrophy disease gene product, SMN, and its associated protein SIP1 are in a complex with spliceosomal snRNP proteins. Cell **90**(6): 1013-1021.

Lotti, F., et al. (2012). An SMN-dependent U12 splicing event essential for motor circuit function. Cell **151**(2): 440-454.

Mackenzie, I. R., et al. (2010). TDP-43 and FUS in amyotrophic lateral sclerosis and frontotemporal dementia. Lancet Neurol **9**(10): 995-1007.

Maekawa, S., et al. (2009). TDP-43 is consistently co-localized with ubiquitinated inclusions in sporadic and Guam amyotrophic lateral sclerosis but not in familial amyotrophic lateral sclerosis with and without SOD1 mutations. Neuropathology **29**(6): 672-683.

Maher-Laporte, M. and L. DesGroseillers (2010). Genome wide identification of Staufen2-bound mRNAs in embryonic rat brains. BMB Rep **43**(5): 344-348.

Mancuso, R. and X. Navarro (2015). Amyotrophic lateral sclerosis: Current perspectives from basic research to the clinic. Prog Neurobiol.

Mantione, K. J., et al. (2014). Comparing bioinformatic gene expression profiling methods: microarray and RNA-Seq. Med Sci Monit Basic Res **20**: 138-142.

Marioni, J. C., et al. (2008). RNA-seq: An assessment of technical reproducibility and comparison with gene expression arrays. Genome Research **18**(9): 1509-1517.

Maris, C., et al. (2005). The RNA recognition motif, a plastic RNA-binding platform to regulate post-transcriptional gene expression. Febs j **272**(9): 2118-2131.

Martin, K. C. and A. Ephrussi (2009). mRNA localization: gene expression in the spatial dimension. Cell **136**(4): 719-730.

Mathew, R., et al. (2008). Phosphorylation of human PRP28 by SRPK2 is required for integration of the U4/U6-U5 tri-snRNP into the spliceosome. Nat Struct Mol Biol **15**(5): 435-443.

McDonald, K. K., et al. (2011). TAR DNA-binding protein 43 (TDP-43) regulates stress granule dynamics via differential regulation of G3BP and TIA-1. Hum Mol Genet **20**(7): 1400-1410.

McGovern, V. L., et al. (2008). Embryonic motor axon development in the severe SMA mouse. Hum Mol Genet **17**(18): 2900-2909.

McWhorter, M., et al. (2003). Knockdown of the survival motor neuron (Smn) protein in zebrafish causes defects in motor axon outgrowth and pathfinding. J Cell Biol **162**: 919 - 931.

Merianda, T. and J. Twiss (2013). Peripheral nerve axons contain machinery for co-translational secretion of axonally-generated proteins. Neurosci Bull **29**(4): 493-500.

Merianda, T. T., et al. (2013). Axonal localization of neuritin/CPG15 mRNA in neuronal populations through distinct 5' and 3' UTR elements. J Neurosci **33**(34): 13735-13742.

Merianda, T. T., et al. (2013). Axonal transport of neural membrane protein 35 mRNA increases axon growth. J Cell Sci **126**(Pt 1): 90-102.

Mili, S. and J. A. Steitz (2004). Evidence for reassociation of RNA-binding proteins after cell lysis: implications for the interpretation of immunoprecipitation analyses. RNA **10**(11): 1692-1694.

Mishra, V. N., et al. (2004). A clinical and genetic study of spinal muscular atrophy. Electromyogr Clin Neurophysiol **44**(5): 307-312.

Mizutani, A., et al. (2000). SYNCRIP, a Cytoplasmic Counterpart of Heterogeneous Nuclear Ribonucleoprotein R, Interacts with Ubiquitous Synaptotagmin Isoforms. Journal of Biological Chemistry **275**(13): 9823-9831.

Monani, U. R., et al. (1999). A single nucleotide difference that alters splicing patterns distinguishes the SMA gene SMN1 from the copy gene SMN2. Hum Mol Genet **8**(7): 1177-1183.

Monani, U. R., et al. (2000). The human centromeric survival motor neuron gene (SMN2) rescues embryonic lethality in Smn(-/-) mice and results in a mouse with spinal muscular atrophy. Hum Mol Genet **9**(3): 333-339.

Mourelatos, Z., et al. (2001). SMN interacts with a novel family of hnRNP and spliceosomal proteins. EMBO J **20**(19): 5443-5452.

Murray, L. M., et al. (2008). Selective vulnerability of motor neurons and dissociation of pre- and post-synaptic pathology at the neuromuscular junction in mouse models of spinal muscular atrophy. Hum Mol Genet **17**(7): 949-962.

Murray, L. M., et al. (2010). Pre-symptomatic development of lower motor neuron connectivity in a mouse model of severe spinal muscular atrophy. Hum Mol Genet **19**(3): 420-433.

Nagai, M., et al. (2007). Astrocytes expressing ALS-linked mutated SOD1 release factors selectively toxic to motor neurons. Nat Neurosci **10**(5): 615-622.

Nardo, G., et al. (2013). Transcriptomic indices of fast and slow disease progression in two mouse models of amyotrophic lateral sclerosis. Brain **136**(11): 3305-3332.

Neumann, H., et al. (1995). Induction of MHC class I genes in neurons. Science **269**(5223): 549-552.

Neumann, M., et al. (2006). Ubiquitinated TDP-43 in Frontotemporal Lobar Degeneration and Amyotrophic Lateral Sclerosis. Science **314**(5796): 130-133.

Ng, S. Y., et al. (2013). The long noncoding RNA RMST interacts with SOX2 to regulate neurogenesis. Mol Cell **51**(3): 349-359.

Nguyen, V. T., et al. (2001). 7SK small nuclear RNA binds to and inhibits the activity of CDK9/cyclin T complexes. Nature **414**(6861): 322-325.

Nielsen, J., et al. (2004). Sequential dimerization of human zipcode-binding protein IMP1 on RNA: a cooperative mechanism providing RNP stability. Nucleic Acids Res **32**(14): 4368-4376.

Nolle, A., et al. (2011). The spinal muscular atrophy disease protein SMN is linked to the Rho-kinase pathway via profilin. Hum Mol Genet **20**(24): 4865-4878.

Oliveira, A. L., et al. (2004). A role for MHC class I molecules in synaptic plasticity and regeneration of neurons after axotomy. Proc Natl Acad Sci U S A **101**(51): 17843-17848.

Oprea, G. E., et al. (2008). Plastin 3 is a protective modifier of autosomal recessive spinal muscular atrophy. Science **320**(5875): 524-527.

Pak, C. W., et al. (2008). Actin-binding proteins take the reins in growth cones. Nat Rev Neurosci **9**(2): 136-147.

Pan, X., et al. (2013). Two methods for full-length RNA sequencing for low quantities of cells and single cells. Proc Natl Acad Sci U S A **110**(2): 594-599.

Pesiridis, G. S., et al. (2009). Mutations in TDP-43 link glycine-rich domain functions to amyotrophic lateral sclerosis. Hum Mol Genet **18**(R2): R156-162.

Pesiridis, G. S., et al. (2011). A "two-hit" hypothesis for inclusion formation by carboxyl-terminal fragments of TDP-43 protein linked to RNA depletion and impaired microtubule-dependent transport. J Biol Chem **286**(21): 18845-18855.

Piazzon, N., et al. (2008). In vitro and in cellulo evidences for association of the survival of motor neuron complex with the fragile X mental retardation protein. J Biol Chem **283**(9): 5598-5610.

Polymenidou, M., et al. (2011). Long pre-mRNA depletion and RNA missplicing contribute to neuronal vulnerability from loss of TDP-43. Nat Neurosci **14**: 459 - 468.

Praveen, K., et al. (2012). A Drosophila model of spinal muscular atrophy uncouples snRNP biogenesis functions of survival motor neuron from locomotion and viability defects. Cell Rep **1**(6): 624-631.

Reaume, A. G., et al. (1996). Motor neurons in Cu/Zn superoxide dismutase-deficient mice develop normally but exhibit enhanced cell death after axonal injury. Nat Genet **13**(1): 43-47.

Rivieccio, M. A., et al. (2009). HDAC6 is a target for protection and regeneration following injury in the nervous system. Proc Natl Acad Sci U S A **106**(46): 19599-19604.

Rosen, D. R., et al. (1993). Mutations in Cu/Zn superoxide dismutase gene are associated with familial amyotrophic lateral sclerosis. Nature **362**(6415): 59-62.

Ross, A. F., et al. (1997). Characterization of a beta-actin mRNA zipcode-binding protein. Mol Cell Biol **17**(4): 2158-2165.

Rossoll, W., et al. (2003). Smn, the spinal muscular atrophy–determining gene product, modulates axon growth and localization of β-actin mRNA in growth cones of motoneurons. The Journal of Cell Biology **163**(4): 801-812.

Rossoll, W., et al. (2003). Smn, the spinal muscular atrophy-determining gene product, modulates axon growth and localization of beta-actin mRNA in growth cones of motorneurons. J Cell Biol **163**: 801 - 812.

Rossoll, W., et al. (2002). Specific interaction of Smn, the spinal muscular atrophy determining gene product, with hnRNP-R and gry-rbp/hnRNP-Q: a role for Smn in RNA processing in motor axons? Human Molecular Genetics **11**(1): 93-105.

Ruiz, R., et al. (2010). Altered intracellular Ca2+ homeostasis in nerve terminals of severe spinal muscular atrophy mice. J Neurosci **30**(3): 849-857.

Rutherford, N. J., et al. (2008). Novel Mutations in <italic>TARDBP</italic> (TDP-43) in Patients with Familial Amyotrophic Lateral Sclerosis. PLoS Genet **4**(9): e1000193.

Rutherford, N. J., et al. (2008). Novel mutations in TARDBP (TDP-43) in patients with familial amyotrophic lateral sclerosis. PLoS Genet **4**(9): e1000193.

Saal, L., et al. (2014). Subcellular transcriptome alterations in a cell culture model of spinal muscular atrophy point to widespread defects in axonal growth and presynaptic differentiation. RNA.

Saliba, A. E., et al. (2014). Single-cell RNA-seq: advances and future challenges. Nucleic Acids Res **42**(14): 8845-8860.

Schrank, B., et al. (1997). Inactivation of the survival motor neuron gene, a candidate gene for human spinal muscular atrophy, leads to massive cell death in early mouse embryos. Proc Natl Acad Sci U S A **94**(18): 9920-9925.

Schwab, C., et al. (2008). Colocalization of transactivation-responsive DNA-binding protein 43 and huntingtin in inclusions of Huntington disease. J Neuropathol Exp Neurol **67**(12): 1159-1165.

Scotter, E. L., et al. (2015). TDP-43 Proteinopathy and ALS: Insights into Disease Mechanisms and Therapeutic Targets. Neurotherapeutics **12**(2): 352-363.

Sendtner, M. (2014). Motoneuron disease. Handb Exp Pharmacol **220**: 411-441.

Sephton, C. F., et al. (2011). Identification of neuronal RNA targets of TDP-43-containing ribonucleoprotein complexes. J Biol Chem **286**(2): 1204-1215.

Shatz, C. J. (2009). MHC class I: an unexpected role in neuronal plasticity. Neuron **64**(1): 40-45.

Simpson, E. P., et al. (2004). Increased lipid peroxidation in sera of ALS patients: a potential biomarker of disease burden. Neurology **62**(10): 1758-1765.

Smith, D. S., et al. (2000). Regulation of cytoplasmic dynein behaviour and microtubule organization by mammalian Lis1. Nat Cell Biol **2**(11): 767-775.

Smith, R. G., et al. (1998). Presence of 4-hydroxynonenal in cerebrospinal fluid of patients with sporadic amyotrophic lateral sclerosis. Ann Neurol **44**(4): 696-699.

Snee, M., et al. (2002). RNA trafficking and stabilization elements associate with multiple brain proteins. J Cell Sci **115**(Pt 23): 4661-4669.

Sotelo-Silveira, J., et al. (2008). Myelinated axons contain beta-actin mRNA and ZBP-1 in periaxoplasmic ribosomal plaques and depend on cyclic AMP and F-actin integrity for in vitro translation. J Neurochem **104**(2): 545-557.

St Laurent, G., 3rd, et al. (2009). Non-coding RNA transcripts: sensors of neuronal stress, modulators of synaptic plasticity, and agents of change in the onset of Alzheimer's disease. Neurosci Lett **466**(2): 81-88.

St Laurent, G., et al. (2012). Intronic RNAs constitute the major fraction of the non-coding RNA in mammalian cells. BMC genomics **13**: 504.

Steward, O. and W. B. Levy (1982). Preferential localization of polyribosomes under the base of dendritic spines in granule cells of the dentate gyrus. J Neurosci **2**(3): 284-291.

Strong, M. J., et al. (2007). TDP43 is a human low molecular weight neurofilament (hNFL) mRNA-binding protein. Mol Cell Neurosci **35**(2): 320-327.

Su, H., et al. (2013). Transplanted motoneurons derived from human induced pluripotent stem cells form functional connections with target muscle. Stem Cell Research **11**(1): 529-539.

Swoboda, K., et al. (2005). Natural history of denervation in SMA: Relation to age, SMN2 copy number, and function. Ann Neurol **57**: 704 - 712.

Tal, T. L. and R. L. Tanguay (2012). Non-coding RNAs--novel targets in neurotoxicity. Neurotoxicology **33**(3): 530-544.

Taylor, A. M., et al. (2009). Axonal mRNA in Uninjured and Regenerating Cortical Mammalian Axons. The Journal of Neuroscience **29**(15): 4697-4707.

Taylor, A. M., et al. (2009). Axonal mRNA in uninjured and regenerating cortical mammalian axons. J Neurosci **29**(15): 4697-4707.

Thams, S., et al. (2009). Classical Major Histocompatibility Complex Class I Molecules in Motoneurons: New Actors at the Neuromuscular Junction. The Journal of Neuroscience **29**(43): 13503-13515.

Tollervey, J., et al. (2011). Characterizing the RNA targets and position-dependent splicing regulation by TDP-43. Nat Neurosci **14**: 452 - 458.

Toma, J. S., et al. (2015). Motoneurons Derived from Induced Pluripotent Stem Cells Develop Mature Phenotypes Typical of Endogenous Spinal Motoneurons. The Journal of Neuroscience **35**(3): 1291-1306.

Tsai, N. P., et al. (2007). The adaptor Grb7 links netrin-1 signaling to regulation of mRNA translation. EMBO J **26**(6): 1522-1531.

Tsuiji, H., et al. (2013). Spliceosome integrity is defective in the motor neuron diseases ALS and SMA. EMBO Mol Med **5**(2): 221-234.

Twiss, J. L. and M. Fainzilber (2009). Ribosomes in axons--scrounging from the neighbors? Trends Cell Biol **19**(5): 236-243.

Twiss, J. L. and J. van Minnen (2006). New insights into neuronal regeneration: the role of axonal protein synthesis in pathfinding and axonal extension. J Neurotrauma **23**(3-4): 295-308.

Ulitsky, I. and D. P. Bartel (2013). lincRNAs: genomics, evolution, and mechanisms. Cell **154**(1): 26-46.

Urushitani, M., et al. (2006). Chromogranin-mediated secretion of mutant superoxide dismutase proteins linked to amyotrophic lateral sclerosis. Nat Neurosci **9**(1): 108-118.

van Bergeijk, J., et al. (2006). Valproic acid promotes neurite outgrowth in PC12 cells independent from regulation of the survival of motoneuron protein. Chem Biol Drug Des **67**(3): 244-247.

van Bergeijk, J., et al. (2007). The spinal muscular atrophy gene product regulates neurite outgrowth: importance of the C terminus. Faseb j **21**(7): 1492-1502.

Van Deerlin, V. M., et al. (2008). TARDBP mutations in amyotrophic lateral sclerosis with TDP-43 neuropathology: a genetic and histopathological analysis. Lancet Neurol **7**(5): 409-416.

Van Epps, H., et al. (2010). Nuclear pre-mRNA 3'-end processing regulates synapse and axon development in C. elegans. Development **137**(13): 2237-2250.

Van Herreweghe, E., et al. (2007). Dynamic remodelling of human 7SK snRNP controls the nuclear level of active P-TEFb. EMBO J **26**(15): 3570-3580.

van Niekerk, E. A., et al. (2007). Sumoylation in axons triggers retrograde transport of the RNA-binding protein La. Proc Natl Acad Sci U S A **104**(31): 12913-12918.

Venticinque, L., et al. (2011). Interactions between laminin receptor and the cytoskeleton during translation and cell motility. PLoS One **6**(1): e15895.

Wade, R. H. (2009). On and around microtubules: an overview. Mol Biotechnol **43**(2): 177-191.

Wahl, M. C., et al. (2009). The spliceosome: design principles of a dynamic RNP machine. Cell **136**(4): 701-718.

Walker, B. A., et al. (2012). Reprogramming axonal behavior by axon-specific viral transduction. Gene Ther **19**(9): 947-955.

Wang, C., et al. (2014). The concordance between RNA-seq and microarray data depends on chemical treatment and transcript abundance. Nat Biotechnol **32**(9): 926-932.

Wang, H. Y., et al. (1998). SRPK2: a differentially expressed SR protein-specific kinase involved in mediating the interaction and localization of pre-mRNA splicing factors in mammalian cells. J Cell Biol **140**(4): 737-750.

Wang, I. F., et al. (2002). Higher order arrangement of the eukaryotic nuclear bodies. Proc Natl Acad Sci U S A **99**(21): 13583-13588.

Wang, Z., et al. (2009). RNA-Seq: a revolutionary tool for transcriptomics. Nat Rev Genet **10**(1): 57-63.

Weidensdorfer, D., et al. (2009). Control of c-myc mRNA stability by IGF2BP1-associated cytoplasmic RNPs. RNA **15**(1): 104-115.

Wichterle, H., et al. (2002). Directed differentiation of embryonic stem cells into motor neurons. Cell **110**(3): 385-397.

Wiese, S., et al. (2010). Isolation and enrichment of embryonic mouse motoneurons from the lumbar spinal cord of individual mouse embryos. Nat Protoc **5**(1): 31-38.

Williams, C. C., et al. (2014). Targeting and plasticity of mitochondrial proteins revealed by proximity-specific ribosome profiling. Science **346**(6210): 748-751.

Willis, D. E., et al. (2007). Extracellular stimuli specifically regulate localized levels of individual neuronal mRNAs. J Cell Biol **178**(6): 965-980.

Willis, D. E., et al. (2011). Axonal Localization of transgene mRNA in mature PNS and CNS neurons. J Neurosci **31**(41): 14481-14487.

Wirth, B. (2000). An update of the mutation spectrum of the survival motor neuron gene (SMN1) in autosomal recessive spinal muscular atrophy (SMA). Hum Mutat **15**(3): 228-237.

Wolozin, B. (2012). Regulated protein aggregation: stress granules and neurodegeneration. Mol Neurodegener **7**: 56.

Xing, L., et al. (2012). Negative regulation of RhoA translation and signaling by hnRNP-Q1 affects cellular morphogenesis. Mol Biol Cell **23**(8): 1500-1509.

Xu, X., et al. (2013). Parallel comparison of Illumina RNA-Seq and Affymetrix microarray platforms on transcriptomic profiles generated from 5-aza-deoxy-cytidine treated HT-29 colon cancer cells and simulated datasets. BMC Bioinformatics **14**(Suppl 9): S1.

Yamazaki, T., et al. (2012). FUS-SMN protein interactions link the motor neuron diseases ALS and SMA. Cell Rep **2**(4): 799-806.

Yang, Z., et al. (2001). The 7SK small nuclear RNA inhibits the CDK9/cyclin T1 kinase to control transcription. Nature **414**(6861): 317-322.

Yokoseki, A., et al. (2008). TDP-43 mutation in familial amyotrophic lateral sclerosis. Ann Neurol **63**(4): 538-542.

Yoo, S., et al. (2013). A HuD-ZBP1 ribonucleoprotein complex localizes GAP-43 mRNA into axons through its 3' untranslated region AU-rich regulatory element. J Neurochem **126**(6): 792-804.

Zhang, H., et al. (2003). Active transport of the survival motor neuron protein and the role of exon-7 in cytoplasmic localization. J Neurosci **23**: 6627 - 6637.

Zhang, H. L., et al. (2001). Neurotrophin-induced transport of a beta-actin mRNP complex increases beta-actin levels and stimulates growth cone motility. Neuron **31**(2): 261-275.

Zhang, Z., et al. (2008). SMN deficiency causes tissue-specific perturbations in the repertoire of snRNAs and widespread defects in splicing. Cell **133**(4): 585-600.

Zhang, Z., et al. (2013). Dysregulation of synaptogenesis genes antecedes motor neuron pathology in spinal muscular atrophy. Proceedings of the National Academy of Sciences **110**(48): 19348-19353.

Zhao, S., et al. (2014). Comparison of RNA-Seq and Microarray in Transcriptome Profiling of Activated T Cells. PLoS One **9**(1): e78644.

Zhou, Q., et al. (2012). RNA polymerase II elongation control. Annu Rev Biochem **81**: 119-143.

Zivraj, K. H., et al. (2010). Subcellular profiling reveals distinct and developmentally regulated repertoire of growth cone mRNAs. J Neurosci **30**(46): 15464-15478.

Zong, C., et al. (2012). Genome-Wide Detection of Single-Nucleotide and Copy-Number Variations of a Single Human Cell. Science **338**(6114): 1622-1626.

Zufferey, R., et al. (1998). Self-inactivating lentivirus vector for safe and efficient in vivo gene delivery. J Virol **72**(12): 9873-9880.

8 Appendix

8.1 Supplementary Figure 1
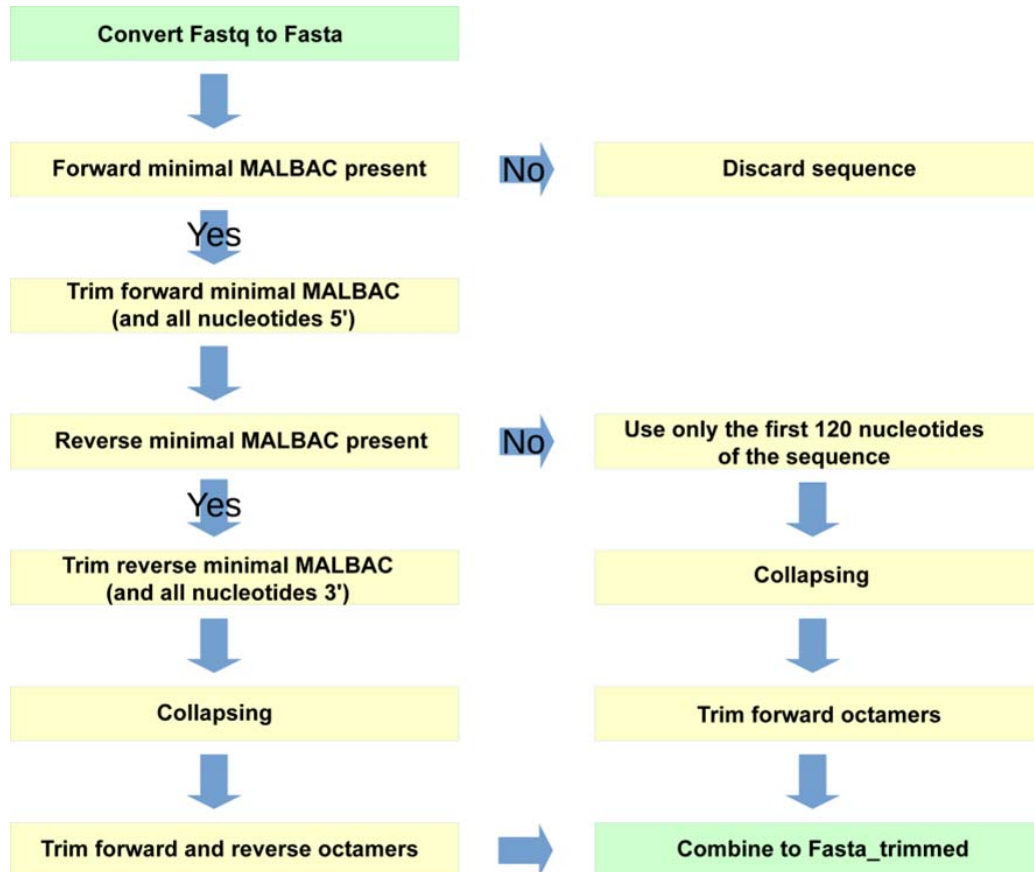
Supplementary Figure S1: Schematic outline of read processing using inhouse script. Reads are scanned for presence of forward and reverse minimal MALBAC sequence. MALBAC sequence is removed and duplicate reads are deleted (collapsing). Octamers originating from the ransom region of MALBAC primer are removed.

Affidavit

I hereby confirm that my thesis entitled "Whole transcriptome profiling of compartmentalized motoneurons" is the result of my own work. I did not receive any help or support from commercial consultants. All sources and/or materials applied are listed and specified in the thesis.

Furthermore, I confirm that this thesis has not yet been submitted as part of another examination process neither in identical nor in similar form.

Place, Date   Signature

Eidesstattliche Erklärung

Hiermit erkläre ich an Eides statt, die Dissertation mit dem Titel „Globale Transkriptomanalyse von kompartimentierten Motoneuronen" eigenständig, d.h. insbesondere selbstständig und ohne Hilfe eines kommerziellen Promotionsberaters, angefertigt und keine anderen als die von mir angegebenen Quellen und Hilfsmittel verwendet zu haben.

Ich erkläre außerdem, dass die Dissertation weder in gleicher noch in ähnlicher Form bereits in einem anderen Prüfungsverfahren vorgelegen hat.

Ort, Datum   Unterschrift

Curriculum Vitae

Personal Details

Name:	Lena Saal
Date of Birth:	01.06.1985
Place of Birth:	Schweinfurt
Nationality:	German

Education

2011 – present	Clinical University of Würzburg
	Institute for Clinical Neurobiology PhD student
2010 – 2011	Diploma thesis, Institute for Clinical Neurobiology (Chairman: Prof. Dr. Sendtner), Clinical University of Würzburg
	Title: Characterisation of a UbP-mTDP43M337V transgenic mouse line and Cloning of the RNA/DNA binding protein FUS in an expression vector (1,0)
2010	Diploma examination
	Neurobiology (main subject) Biochemistry (minor subject) Virology and Immunobiology (minor subject)
2007 – 2011	Advanced courses in Biology
2007	Intermediate Examination
2005	Commencement of studies in Biology at the Julius-Maximilians-University of Würzburg
2004 – 2005	Study in Pharmaceutics at the University of Regensburg
1995 – 2004	Johann-Philipp-von-Schönborn Gymnasium, Münnerstadt Advanced courses: Biology and German
1992 – 1995	Grundschule Rothhausen (elementary school), Rothhausen

Professional Experiences

2009   University of Würzburg,
F2 advanced practical course at the Institute for Clinical Neurobiology
Title: Examination of hNRNP R splice isoforms in motoneurons

2008   University of Würzburg
F1 practical course at the Institute for Virology and Immunobiology

2008   Biocenter, University of Würzburg
F1 practical course in the department of Genetics and Neurobiology

Working Experience

2007   University of Würzburg
Advisor

2009   Clinical University of Würzburg
Institute for Clinical Neurobiology

Skills

Languages   German (native speaker)
English (fluent)

Publication list

1. **Saal, L.,** Briese, M., Kneitz, S., Glinka, M. and Sendtner, M. (2014) Subcellular transcriptome alterations in a cell culture model of spinal muscular atrophy point to widespread defects in axonal growth and presynaptic differentiation. *RNA.*, **20**, 1789-1802.
2. Briese, M., **Saal, L.**, Appenzeller, S., Moradi, M., Baluapuri, A. and Sendtner, M. (2015) Whole transcriptome profiling reveals the RNA content of motor axons. *Nucleic Acids Research*, **29**;44(4):e33

Poster presentation

1. SFB 487 symposium, July 2011, Wuerzburg
"Compartmentalized cultures of motoneurons for studying axonal mRNA"
2. NGF meeting , June 2012, Wuerzburg
"Compartmentalized cultures of motoneurons for studying axonal mRNA"
3. SfN conference, November 2013, San Diego
"Compartmentalized motoneuron cultures reveal alterations in axonal mRNAs after TDP-43 depletion"
4. EMBO conference RNA localization and local translation, June/July 2015, Crete
"Compartmentalized motoneuron cultures reveal alterations in axonal mRNAs after Smn depletion"

Acknowledgements

As a thesis like the one presented here is always the result of many years of hard work and undoubtedly not possible without the help of many people, I will now take the opportunity to thank all the people which went this long way together with me.

First of all I want to place my sincere gratitude to my supervisor Prof. Dr. Michael Sendtner. Thank you for giving me the opportunity to pursue doctoral dissertation under your guidance and for keeping faith in me to perform such a challenging scientific project. Thank you for your never-ending encouragement, support, advice and help. Furthermore, thank you for your understanding, patience and your never-ending support during the time of my disease. It meant a lot to me and was a big help! Thank you!

I also want to thank Prof. Dr. Erich Buchner for your support and encouragement as one of my supervisors and your always open-standing door for all of us.

Likewise I want to thank Prof. Dr. Utz Fischer for your support as my supervisor and the evaluation of my thesis.

Prof. Dr. Paul Pauli I want to thank for taking over the job of the chairperson during my defense.

One of my biggest thanks goes to Dr. Michael Briese. Thank you for your decision to join this lab three years ago. Thank you for all your help, your support and your supervision during this time. But I also want to thank you for all the fun in the lab and during the conferences we attended together, for all the discussions but also the silent times and last but not least thank you for not just being the best colleague I could imagine but also for becoming a very good friend!

Furthermore I want to thank Dr. Silke Appenzeller and Dr. Susanne Kneitz for all your work and help and the great collaborations.

Likewise I am thankful to all my current colleagues who supported me during all these years and which are still a great help. Special thanks to PD Dr. Sibylle Jablonka, PD Dr. Robert Blum, PD Dr. Rudolf Götz, Prof. Dr. Anna Maria Musti, Prof. Dr. Carmen Villmann, Dr. Stefanie Rauskolb, Dr. Britta Wachter, Dr. Natascha Schäfer, Thomas Andreska, Mehri Moradi, Michael Skoruppa, Verena Surrey, Dr. Georg Langlhofer, Sinem Atak, Corinna Martin, Manju Sasi, Cora Rüdt von Collenberg, Nicole Elflein, Katrin Walter, Christian Mehling, Hildegard Troll, Gudrun Schell and Toni. It is always a pleasure to work with all of you!

In line with this I also want to thank all the other people which already left the lab but crossed my way in the last years. Thank you to Dr. Dirk Pühringer, Dr. Frank Krieger, Dr. Christian Simon and Dr. Beatriz Blanco (I wish you both all the best) Dr. Andrea Wetzel, Dr. Samira Samtleben, Dr. Reena Rathod, Dr. Narayan Subramanian, Dr. Chandrankanth Reddy, Dr. Lidia Albanito, Elke Spirk, Manuela Kohles, Dominique Schmitt and Kerstin Müller.

I gratefully appreciate the financial support of the Deutsche Forschungsgemeinschaft, the Hermann and Lilly Schilling Stiftung im Stifterverband der deutschen Industrie, the European Community's Health Seventh Framework Programme, the German Government (BMBF) funded Motoneuron Disease Network, The Sobek Foundation, and the Bayerischer Forschungsverbund Induzierte Pluripotente Stammzellen. Furthermore I want to thank the University Hospital of Würzburg and the Graduate School of Life Sciences, University Würzburg that made it possible to complete my thesis.

Last, but not least I want to thank all my other friends but especially my family.
Danke Mama und Papa für eure immerwährende Unterstützung und eueren Glauben an mich. Danke, dass ihr mich immer meine Entscheidungen selber habt treffen lassen und ich somit immer meinen eigenen Weg gehen durfte. Danke!
Danke auch an meinen Bruder Hannes. Wer hätte vor 30 Jahren gedacht, dass wir beruflich ähnliche Wege einschlagen und tatsächlich mal im gleichen Bereich enden werden? Und auch wenn ich dich immer wieder gerne in Chicago besucht habe und oft an unseren gemeinsamen Urlaub entlang der Westküste der USA nach der SfN